POLITECNICO DI MILANO
Scuola di Ingegneria Industriale e dell'Informazione
Corso di Laurea Magistrale in Engineering Physics

Out of Equilibrium Monte Carlo Simulations for the Ising Model

Advisor: Prof. Paolo Biscari
Co-advisor: Prof. Andrea Tosin

Author:
Federico Ettori
matr. 946346

Academic Year 2020-2021

Acknowledgements

Vorrei ringraziare sentitamente il Professore Paolo Biscari per avermi accompagnato durante la stesura di questo lavoro e per avermi fatto appassionare all'argomento. La sua costante presenza durante tutto il percorso, la disponibilità per incontrarci per discutere degli aspetti più complessi e i suoi suggerimenti sono stati fondamentali per la realizzazione di questa tesi. Ringrazio anche il Professore Andrea Tosin del Politecnico di Torino per la disponibilità mostrata e per avermi fornito materiale per ampliare lo spettro di interesse di questa tesi.

Vorrei ringraziare tutta la mia famiglia, in particolare i miei genitori Ivan e Stefania e le mie sorelle Arianna e Sara, non solo per avermi supportato durante tutto il periodo di preparazione di questa tesi, ma per avermi anche accompagnato durante tutto questo lungo percorso di studi come meglio possibile. L'amore e l'aiuto che mi hanno dimostrato sono stati fondamentali perché potessi ottenere questi risultati.

Ringrazio anche tutte le persone a me care, fra cui Anna (Girl), Marco (Rocco), Melissa (Meluz), Alberto (Masso), Emanuele (Ema) e Silvia (Zinzi), per il tempo che mi hanno dedicato nei vari anni di questo percorso e per i bei momenti che, insieme, abbiamo costruito. Infine, vorrei anche ringraziare le persone che hanno permesso che io coltivassi la passione per le materie scientifiche durante gli anni del Liceo, in particolare le Professoresse Maria Bresciani e Laura Ziche.

Grazie.

Sommario

Per simulare al calcolatore il comportamento di materiali magnetici l'approccio solitamente considerato utilizza simulazioni con metodo Monte Carlo su modello di Ising con dinamica alla Glauber. Il tutto viene solitamente implementato grazie all'algoritmo Metropolis. Lo scopo di questa tesi è quello di utilizzare un algoritmo alternativo (algoritmo di Lebowitz) con dinamica alla Glauber per descrivere il sistema fuori dall'equilibrio. Questo metodo alternativo permette, soprattutto in caso di sistemi a basse temperature, di ridurre i tempi di esecuzione della simulazione. Inoltre, permette di seguire con maggiore accuratezza il percorso fuori equilibrio del sistema, tenendo conto della differente velocità con cui il sistema approccia l'equilibrio quando si trova in differenti condizioni fuori equilibrio. Tramite comparazione dei risultati con quelli noti da studi teorici e altre simulazioni con algoritmo Metropolis, è possibile concludere che il modello sviluppato riproduce correttamente il comportamento dei sistemi magnetici sia all'equilibrio che non. Viene inoltre esplorata la possibilità di applicare il modello sviluppato alla sfera della socio-fisica, in particolare al fine di descrivere la formazione di opinioni nelle società, in sostituzione al modello Sznajd. I medesimi risultati di equilibrio vengono ottenuti, validando l'approccio considerato. In più, la presenza di un'Hamiltoniana (invece assente nel modello di Sznajd) permette di considerare a tutti gli effetti simulazioni Monte Carlo per analizzare anche il transitorio all'equilibrio.

Parole Chiave: Modello di Ising, Metodo Monte Carlo, algoritmo di Lebowitz, Dinamica alla Glauber, Transizione di Fase, Transizione di Fase Dinamica, Reticoli con Difetti, Rumore di Barkhausen, Modello di Sznajd.

Abstract

In order to investigate the magnetic materials behaviour, the common approach relies on Monte Carlo simulations on Ising system with Glauber dynamics. The implemented algorithm usually exploited for this investigation is the Metropolis algorithm. The aim of this work is to present an alternative algorithm (Lebowitz algorithm) with Glauber dynamics, especially designed to describe out of equilibrium magnetic systems. This alternative approach allows to reduce the execution time for the simulation, especially while simulating over low temperature systems. Moreover, the developed system approximates better the real behaviour of magnetic materials in out-of-equilibrium conditions. It takes into account how far from equilibrium the system is and allows the system to proceed with different velocities to equilibrium, something that is not explicitly considered in the Metropolis algorithm. Through comparison with known theoretical results and simulations with Metropolis algorithm, we are able to conclude that the developed approach reproduces well the behaviour in and out of equilibrium of magnetic systems. Moreover, we explore also the possibility to apply the developed approach into the sociophysic realm, in particular with the aim to describe opinion formation in human society, in substitution to the Sznajd model. The same equilibrium results are obtained, validating the considered approach. Additionally, the presence of a Hamiltonian (not present in the Sznajd model) allows to consider Monte Carlo simulations and to properly analyse also the transition toward equilibrium.

Keywords: Ising Model, Monte Carlo Method, Lebowitz Algorithm, Glauber Dynamics, Phase Transition, Dynamic Phase Transition, Lattice with Defects, Barkhausen noise, Sznajd Model.

Contents

List of Figures

List of Tables

Chapter 1

Introduction

Magnetic materials can be encountered in the everyday life of each one of us: from the materials constituting the memory of technological devices to the core of Magnetic Resonance Imaging scanning devices. Due to a high range of applicability, we can understand why studying and trying to predict the behaviour of magnetic materials is of extreme interest. New technologies can be devised considering new configurations or types of materials.
This work can be collocated in this framework. Gaining more insight and discussing a possible model for the prediction of the behaviour of real systems is its main focus. The more common approach found in literature regards the study of the equilibrium properties of magnetic systems through Monte Carlo simulations over the Ising model. This latter embeds all the basic characteristics of magnetic systems and allows to replicate the behavior of ferromagnets with good agreement. In this work, an alternative and efficient computational algorithm is presented and developed in order to describe bi-dimensional (or multi-dimensional) systems moving out of equilibrium while subjected to time-varying parameters. In particular, this approach relies on the Lebowitz algorithm [1] with Glauber dynamics [2]. The possibility to describe out of equilibrium systems is of major importance since, in real applications, we are not always able to assure the equilibrium conditions. With the developed approach, we are now able to say something on what to expect from magnetic systems when the external parameters such as temperature and magnetic field are modified.

This thesis begins with a brief introduction in chapter 2 about the phenomenological aspects regarding magnetic materials and proceeds with the deepening of a specific subgroup: the ferromagnetic materials. In chapter 3, basic information about the Ising model and what it means to perform simulations are illustrated. The algorithm used for the simulations is also explained. In the subsequent chapters, 4 and 5, we reproduce the behaviour of magnetic systems in equilibrium conditions and while a time-varying magnetic field is applied. In chapter 6, we break the assumption of ideal material, with the introduction of defects in the structure which allow adapting our simulations to describe a wider spectrum of magnetic materials and properties (such as spin-glasses). Finally, in chapter 7, we explore the possibility of applying the same methodologies to interacting systems aimed at modelling the human and/or sociological behaviour. More precisely, we apply the Ising model to describe opinion formation in society, as a practical example of how the Ising model and the simulation approach could be extended further.
The main conclusion deriving from this work is that the developed algorithm is equivalent to the ones usually implemented when we want to study the equilibrium properties of magnetic systems, but it allows also to replicate the out of equilibrium dynamics. Moreover, the new approach for the simulation of defects in magnetic materials gives reliable results while tracking the characteristics of real systems.

Chapter 2

Magnetic systems

We start now by familiarising with magnetic materials, considering their main properties and the different categories in which they can be divided. This brief introduction has the scope to review important aspects that will be resumed later on in this work.

2.1 First hints on magnetic materials

Considering a classical approach, we can look at each atom composing matter as constituted by electrons orbiting around the nucleus. Since we are dealing with charged particles, we can associate to their motion a current. In this framework, by considering Ampere's law, we can define a magnetic moment "replacing"each atom:

$$\vec{\mu} = \vec{A}I \tag{2.1}$$

where $\vec{A}$ is a vector which has modulus equal to the area of the loop made by the electron and I is the current we have associated with the electron. To each atom, therefore, we can associate a magnetic moment. In reality, things are more complex. The structure of molecules and the material came into play and modify this single-atom basic description. Moreover, the classical approach is not proper for the description of magnetic phenomena in condensed matter. A more rigorous quantum approach would be required. But

still, we can associate to every atom a proper magnetic moment.
When we switch on a magnetic field in presence of a magnetic moment, we introduce an energy term of the form:

$$E = -\vec{\mu} \cdot \vec{B} \tag{2.2}$$

If the system is isolated and no other energy terms come into play, a preferred direction for the magnetic moment will be set: the energy will be minimised only if the magnetic moment and the external field share the same orientation.
Since we are mainly interested in magnetic materials, a large ensemble of magnetic moments, we can rely on physical variables more adequate for the description of magnetic properties of the whole material. We consider the magnetization of the solid defined as the magnetic moment per unit volume:

$$\vec{M} = \frac{d\vec{\mu}}{dV} \tag{2.3}$$

If all the atoms are equivalent and we can associate to them the same magnetic moment, we will have:

$$\vec{M} = n\vec{\mu} \tag{2.4}$$

in which n is the atomic density of the material. As we have seen, the application of an external field B will cause an effect on the magnetic moments in the structure. Therefore, also the magnetization will be affected by the application of B. Equation (2.2) refers to the case of a single magnetic moment. In reality, this is not the only energy term influencing the orientation of magnetic moments. As an example, the periodic positioning of nucleus in the structure of the magnetic material could perturb the magnetic moments, causing an additional energy term. Moreover, the magnetization itself could induce a field that superimposes to B. As to take into account all these modifications, we will rely on a different quantity H describing the external magnetic field.
Now, we can define the magnetic susceptibility which represents the proportionality coefficient between the field and the response generated inside the material for vanishing magnetic field:

$$\chi_M = \left.\frac{\partial M}{\partial H}\right|_{H=0} \tag{2.5}$$

In the most simple case, where the magnetization orients in the same direction of the magnetic field (linear materials), we can therefore write the following relation between these two quantities:

$$\vec{M} = \chi_M \vec{H} \tag{2.6}$$

We can then start to look into magnetic materials by considering their response strength to an externally applied field. In particular, we can categorise magnetic materials into subgroups:

- Diamagnetic materials show a weak magnetization, with opposite directions to the external field. The magnetic susceptibility is therefore negative. This repulsive characteristic can be found, to some degree, in all the materials. If a material is not diamagnetic is only because a stronger effect is superimposed [3].
- Paramagnetic materials show a weak magnetization in the same direction of the field so that χ_M is positive.
- Ferromagnet materials show a non-linear reaction to a magnetic field. χ_M has a non-constant value and generally takes a positive value much stronger than the paramagnetic case.
- There are other types of materials, such as antiferromagnets and spin glass that show more complex behaviour and require a further deepening of the magnetic properties of matter. The latter ones will be resumed later in this work, at the beginning of chapter 6.

Interestingly, the materials can belong to different subgroups, depending on the value of the external parameters such as temperature and magnetic field. Indeed, the ones presented above are just different phases in which a magnetic material can be found. The transition from one phase to the other will be investigated later on. Table 2.1 shows some materials for the phases (at ambient temperature and in absence of an external field), with their magnetic susceptibility experimentally determined.

Material	**State**	$\chi_M/10^{-6}$
water	diamagnetic	-90
benzene	diamagnetic	-7.2
NaCl	diamagnetic	-13.9
$CuSO_4 \cdot 5H_2O$	paramagnetic	176
Al	paramagnetic	22
Na	paramagnetic	7.3

Table 2.1: Magnetic susceptibilities for the different magnetic materials. Source [3].

For diamagnetic and paramagnetic materials, a semi-classical approach can be applied, as to derive their described behaviour. Instead, for ferromagnets things are more complex. The classical interaction between magnetic moments alone is not enough to explain the nature of such response. A different approach is needed, which will require us to consider a quantum mechanics approach.

2.2 Ferromagnetic materials

We can now dive a little more into the realm of ferromagnetic materials. This fascinating category includes all the materials that show a strong interaction with an external magnetic field. But ferromagnets are commonly known for other important characteristics. On top of them, they present a critical temperature T_c below which a spontaneous magnetization manifests (i.e. in absence of an external magnetic field the system remains magnetized). If we increase the temperature above this limit instead, the system behaves as a paramagnet, and the magnetization is proportional to the magnetic field. This behaviour is represented in fig. 2.1, which shows the residual magnetization function of temperature after the magnetic field is switched off. We can observe that the absolute value of the residual magnetization depends on the temperature. Its sign, instead, depends on the direction of the previously applied field, since it induces the magnetization to share the same direction with itself.

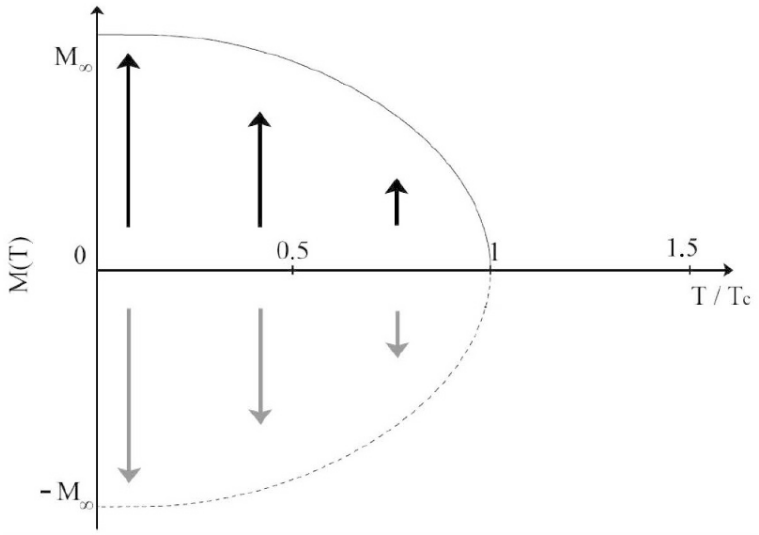

Figure 2.1: Residual magnetization of a ferromagnet M function of temperature. Source [4].

Another important characteristic of the system is the presence of hysteresis. If we track the response of our system to an applied magnetic field B, we can derive the plot shown in fig. 2.2. By starting from a disordered ferromagnetic material, with a null average magnetization, we can draw the first magnetization curve by increasing B. Here, M is not linear with B, and it reaches a maximum value which cannot be modified by further increasing the field. If we proceed with the inversion of the applied field, the magnetization starts to decrease not following backward the first magnetization line: after a specific value of B, it drifts away from it. This causes the residual magnetization phenomenon: when B returns to be null, the system presents a spontaneous magnetization M_0. To obtain null magnetization, B must be of a specific intensity B_c. This value is called coercive field. A complete cycle of B back and forth produces a symmetric S-shaped curve, called hysteresis loop. We can notice that $M(B)$ is a double-valued function: in order to derive the magnetization value, we have to know the history of the sample in addition to the value of the magnetic field.

This complex behaviour was found by Weiss [5] to be due to the presence of clusters made of magnetic moments with same orientation, composing the ferromagnet. These clusters are known as "Weiss domains"and are able to

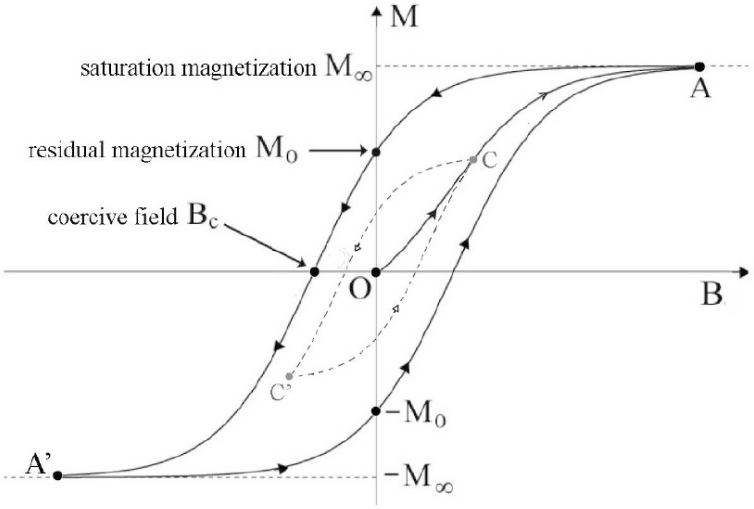

Figure 2.2: Hysteresis loop. Magnetization of a ferromagnet M function of the external magnetic field B. Source [4].

shrinks, enlarge and rotate over the effect of the external field.
By looking more closely to the magnetization along the cycle it is possible to observe that $M(B)$ is not "smooth". Indeed, if we look closely enough, we can found that the cycle is made of little jumps in the magnetization as represented in fig. 2.3. This behaviour is known as Barkhausen noise, from the name of its discoverer [6], and it is essentially due to presence of defects in the ferromagnetic structure that causes the pinning of the growing regions. The unpinning can derive only if the magnetic field is increased enough, when the electrostatic energy overcomes the pinning energy.

All these phenomenological aspects will be resumed later in this work, when we will try to reproduce them with our model.

2.3 Exchange interaction

By coming back to the quantistic approach for ferromagnetism, we can derive all the macroscopic properties above mentioned through the introduction of the "exchange interaction ". This type of interaction has no classical

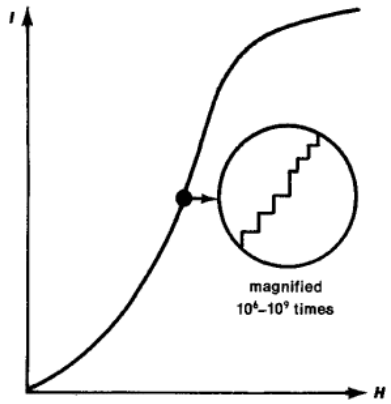

Figure 2.3: Magnetization jumps shown along the hysteresis loop, known as Barkhausen noise. On the x axis, the magnetic field, on the y axis, the magnetization. Source [7].

analogous, since it derives from the symmetry properties of the particles in quantum mechanics.
To derive the exchange interaction, we can rely on a simplified model: consider two electrons, from two distinct atoms in position r_1 and r_2 and with spin respectiely s_1 and s_2, independently represented by the wavefunctions $\Psi_\alpha(r_1, s_1)$ and $\Psi_\beta(r_2, s_2)$. Once we allow the interaction between the two electrons, we have to write the joint wavefunction. A first attempt could be considering:

$$\Psi(r_1, r_2, s_1, s_2) = \Psi_\alpha(r_1, s_1)\Psi_\beta(r_2, s_2) \tag{2.7}$$

But, this definition does not satisfy the exchange symmetry of quantum mechanics. Indeed, since we are dealing with fermions, the global wavefunction must by antisymmetric upon the exchange of the involved electrons. Since:

$$\Psi_\alpha(r_1, s_1)\Psi_\beta(r_2, s_2) \neq -\Psi_\alpha(r_2, s_2)\Psi_\beta(r_1, s_1) \tag{2.8}$$

this cannot be considered the joint wavefunction.
A step further can be made if we consider the structure of the single electron wavefunction $\Psi_\alpha(r_1, s_1)$. Since the spin value s_1 does not influence the energy of the system, unlike the position r_1, we can factorise the global wavefunction in two parts, one which refers to the spatial coordinate $\phi_\alpha(r_1)$ and the other which refers to the spin coordinate $\chi_\alpha(s_1)$:

$$\Psi_\alpha(r_1, s_1) = \phi_\alpha(r_1)\chi_\alpha(s_1) \tag{2.9}$$

The same consideration applies to the other single electron wavefunction $\Psi_\beta(r_2, s_2)$ and to the global wavefunction of the two electrons:

$$\Psi(r_1, r_2, s_1, s_2) = \phi(r_1, r_2)\chi(s_1, s_2) \tag{2.10}$$

Moreover, since the spin and the spatial coordinate cannot mix, $\phi(r_1, r_2)$ and $\chi(s_1, s_2)$ will be linear combinations of respectively the single electron spatial and spin parts. Since we have to obey the antisymmetric property of the global wavefunction, one between the spatial part $\phi(r_1, r_2)$ and the spin part $\chi(s_1, s_2)$ has to satisfy the antisymmetric property. The other one must be symmetric.
We can derive two possible solutions:

- Singlet state: $\phi(r_1, r_2)$ is symmetric and $\chi(s_1, s_2)$ is antisymmetric. The spin part is written as $\chi_S(s_1, s_2)$:

  $$\Psi_S(r_1, r_2, s_1, s_2) = \frac{1}{\sqrt{2}}[\phi_\alpha(r_1)\phi_\beta(r_2) + \phi_\alpha(r_2)\phi_\beta(r_1)]\chi_S(s_1, s_2) \tag{2.11}$$

  The total spin associated to this state is $S = 0$.

- Triplet state: $\phi(r_1, r_2)$ is antisymmetric and $\chi(s_1, s_2)$ is symmetric. The spin part is written as $\chi_T(s_1, s_2)$:

  $$\Psi_T(r_1, r_2, s_1, s_2) = \frac{1}{\sqrt{2}}[\phi_\alpha(r_1)\phi_\beta(r_2) - \phi_\alpha(r_2)\phi_\beta(r_1)]\chi_T(s_1, s_2) \tag{2.12}$$

  The total spin associated to this state is $S = 1$.

To each state is associated an energy E_S and E_T. Through classical considerations we can derive quite easily that these energy states will be different. Consider the triplet state. The spatial part is such that $\phi(r_1, r_2) = 0$ when $r_1 = r_2$. The two electrons will generally stay one far from the other. In the single state, instead, the electrons will enjoy stay closer. By considering the Coulombic interaction, we can understand that charged particles with the same sign will require more energy to stay closer. Therefore we expect $E_S > E_T$.

From a more rigorous approach, we can derive the Heisenberg interaction, describing the energy levels associated to a system made of two interacting

electrons with spins $\boldsymbol{S_1}$ and $\boldsymbol{S_2}$.

$$H^{ex} = -J\boldsymbol{S_1} \cdot \boldsymbol{S_1} \tag{2.13}$$

Here, J is called exchange interaction and represent the difference in the energy between the singlet and the triplet state $J = E_S - E_T$. This expression satisfy the previous considerations. If two electrons are in the triplet state, then $\boldsymbol{S_1}$ and $\boldsymbol{S_2}$ will have the same eigenvalues and their scalar product will be positive. Therefore, the energy is negative. Conversely, if the electrons are in the singlet state, the energy will be positive and therefore higher.
In reality, things are more complex. Indeed, the nice picture we have here considered, by assuming two electrons to be non interacting with the environment, is not always representative. Anyway, the Heisenberg Hamiltonian is still able to reproduce well all the properties seen for a ferromagnet. In particular, we can conclude that the (short range) interaction between neighbouring magnetic moments is able to induce order in the system. This will be our starting point. As we will see, this simple model embeds all the characteristics that we need to simulate the real behaviour of ferromagnetic systems.

Chapter 3

Out of Equilibrium Simulations for the Ising Model

In this chapter, the methods adopted in this work are presented and discussed. In particular, a brief overview of the Ising model, statistical mechanics and Monte Carlo simulations are first presented, continuing with an explanation of the core algorithm used for all the simulations in the following chapters.

3.1 The Ising model

Every model tries to emulate how a specific real system behaves and to make predictions on its future evolution. Moreover, a model can reveal the essential characteristics regulating a specific phenomenon: starting from few rules, if it is able to replicate with a good agreement the real behaviour, it means that we have grasped the key components of the phenomenon.

As an example, we may consider a ferromagnetic system. As already said, it has a rather complex behaviour, showing overall magnetization in particular temperature conditions. This system has been described by the Ising model, developed in 1925 by Ernst Ising in his doctoral thesis [8]. It has

a very simple structure which, however, entails all the basics characteristics that allow reproducing the order-disorder phase transition. The Ising model accounts for a lattice of N points. The lattice geometry can be chosen freely, considering different shapes (square; hexagonal) and various dimensionalities (2D and 3D usually). In it, to each lattice point is associated a spin, schematised as a scalar, which can only take two values: ± 1. A spin with value $+1$ (-1) represents a magnetic moment with up (down) orientation. Each spin interacts with its neighbours through exchange interaction J and feel the effect of an external field H. Overall, to the whole system is associated a Hamiltonian of the type:

$$\mathcal{H} = -J \sum_{\langle i,j \rangle} s_i s_j - \mu_0 H \sum_i s_i \tag{3.1}$$

in which $\langle i, j \rangle$ indicates that site i and j that appear in the sum are nearest neighbours. There is also the possibility to extend the sum over the second neighbours. In this case, the derived model will be called second-neighbours Ising model. In all our simulations we will apply periodic boundary conditions: the lattice can be imagined as folded to avoid presence of borders. Considering for example a 1D chain with periodic boundary conditions, the last spin in the structure will interact with the first one. In this way we are able to minimise the finite-size effects, accounting for spins that do not interact with the same number of neighbours as all the others.
In this work, we consider a 2D Ising model with only the first nearest-neighbour interaction, if not differently specified, with periodic boundary conditions. This is a convenient choice since it is possible to derive exactly the equilibrium configuration, as it derived by Onsager in 1944 [9]. Therefore, we are able to compare some of our results with the theoretical known values.
Now, a few definitions. To describe the Ising model properties, we can rely on some physical quantities such as the magnetization of the system:

$$M = \sum_{i=1}^{N} s_i; \tag{3.2}$$

and the magnetic susceptibility:

$$\chi_M = \frac{\partial M}{\partial H} \tag{3.3}$$

We can consider an easier way to derive the magnetic susceptibility without the necessity to consider numerical derivatives. We will use the following relation (its derivation can be found in [10]):

$$\chi_M = \beta(\langle M^2 \rangle - \langle M \rangle^2) \tag{3.4}$$

moreover, since the magnetization of the sample depends on the number of lattice points and we want to be able to compare the results coming from systems with different N, we will rely on the magnetization per site, defined as:

$$m = \frac{1}{N} \sum_{i=1}^{N} s_i; \tag{3.5}$$

These quantities (and others defined later on) depend on external parameters, such as temperature and the magnetic field. Understanding their dependence allows us to enrich our knowledge of magnetic systems and, possibly, to predict their behaviour.

We can now make few more observations. In general, the Hamiltonian (3.1) allows to retrieve the energy of the system (E) associated with a given disposition of the spins inside the lattice. As known from statistical mechanics, the equilibrium properties depend on the temperature of the system. Indeed, the thermodynamic potential that governs the behaviour of the system is the Helmholtz free energy, defined as:

$$F = E - TS \tag{3.6}$$

in which S represents the entropy of the system and T its temperature. Under prescribed temperature and volume the equilibrium configuration can be determined by minimising F.

Formula (3.6) shows the presence of two competing phenomena: on one side the spins would like to share the same direction, decreasing as much as possible the energy term related to the exchange interaction; on the other, temperature brings disorder, favouring configurations that have as much state as possible and hence a high entropy value. Therefore, by playing with the temperature, we are able to induce the exchange interaction to overcome the temperature effect and vice-versa. This allows us to reproduce the thermodynamical phase transition and to study its characteristics.

3.2 Probability distribution in the canonical ensemble

Statistical mechanics deals in general with a probabilistic approach describing the properties of systems with a large number of degrees of freedom.. This approach was developed to allow investigation over particularly large systems, in which an exact solution of the dynamics of each component is not only difficult (or impossible) to derive, but it is also useless, as the macroscopic properties we are interested in depend only on the average properties of the system, rather than on the detailed description of the state of each element. These systems are more common than one may expect. A common example regards an ideal gas inside a chamber. The number of particles fluctuating in it is of the order of the Avogadro constant (10^{23}). Considering all the particles and their possible behaviour with respect to each one of the others requires an incredible effort. Statistical mechanics avoids solving all the complex dynamic equations that can be derived and, instead, considers a probabilistic approach.

The basic idea behind statistical mechanics relies on the presence of a Hamiltonian H which describes the studied system and defines a set of "states"in which we can find it. With every state i of the system is associated an energy level E_i. The transition from one state to the others is allowed by the presence of a thermal reservoir, which can add or extract energy to/from the system. The transition is characterised by a certain rate $R(\mu \longrightarrow \nu)$, which describe the probability per unit time that the system in state μ and energy E_μ will make a transition into state ν with associated energy E_ν. Here, we assume transition rates to be time-independent. If we define with $w_\mu(t)$ the probability that the system is found in state μ at time t we can derive the following equation, defined as master equation, representing the time evolution of w_μ:

$$\frac{dw_\mu(t)}{dt} = \sum_\nu \left[w_\nu R(\nu \longrightarrow \mu) - w_\mu R(\mu \longrightarrow \nu)\right] \tag{3.7}$$

The first term in the sum represents the rate with which a system coming from state ν falls in μ; the second term takes into account the inverse process, considering the probability that a system exits from μ. If one solves the system of differential equations (for all possible μ) and provides the nor-

malisation condition of the probabilities w, one can find how w_ν varies in time. The importance of such dependency is embedded in the probabilistic approach. Once we know the probabilities that the system can be found in all the different states at a given time, we can compute the expected values of the physical quantities attached to the system as follows:

$$\langle Q \rangle = \sum_\mu w_\mu Q_\mu \tag{3.8}$$

where Q_μ represents the value of the physical quantity Q when the system is in state μ.
But what it means to substitute Q with $\langle Q \rangle$? The latter one can be interpreted as the average value of the physical quantity Q measured over multiple systems all prepared with the same initial conditions and then left free to evolve freely. Another interpretation, although a little more delicate, can be considered by making multiple measurements over the same system but at different times. Obviously, in this case, we must be sure not to change the conditions in which we are running the experiment. The equivalence of both experiments (averaging over many samples vs averaging one system over many times) is ensured when the system is ergodic. It can be proven that a Hamiltonian system kept at constant (finite) volume and (non-zero) temperature is ergodic.
This clarifies in which sense we are considering a probabilistic approach when we rely on statistical mechanics.

An equilibrium state is defined as the state in which all the dw_μ/dt become null. In this case, the probabilities w_μ will not change in time, as all the physical quantities related to the system. Therefore, if the transition rates assume values in which the right hand side of equation (3.7) is always null, we can say that the system is in equilibrium. This could happen in the long run. Therefore, In this case, we can write:

$$p_\mu = \lim_{t \to \infty} w_\mu \tag{3.9}$$

Moreover, we know that in a system in equilibrium with a thermal reservoir, the occupation probability p_μ related to a state with energy E_μ satisfies the following condition:

$$p_\mu = \lim_{t \to \infty} w_\mu = \frac{1}{Z} e^{-\beta E_\mu} \tag{3.10}$$

where $\beta = 1/k_B T$ ($k_B \approx 1.38 \cdot 10^{-}23 J K^{-1}$, the Boltzmann constant), and Z is a normalisation constant, called partition function.
The partition function is more than just a normalisation constant. Indeed, it allows deriving all sorts of properties of the system. As an example, if we know the expression of Z for a particular system, we can derive directly the average energy of the system $\langle E \rangle$ as:

$$\langle E \rangle = -\frac{1}{Z}\frac{\partial Z}{\partial \beta} \tag{3.11}$$

What presented thus far gives an idea of how powerful Statistical Mechanics is. The main issue with all of this is that most of the time, in real cases, to derive the partition function is quite a nightmare, if not impossible. In this case, we have to rely on a different approach. This is the case of numerical simulations, as the Monte Carlo that we now present.

3.3 Monte Carlo simulations

Monte Carlo simulations are a computational method developed to derive estimations of quantitative characteristics related to Statistical Physics problems. If one considers some practical examples, one can understand why the exact values cannot be easily derived. We have, therefore, to rely on estimations. Consider, for example, a $L \times L$ bi-dimensional Ising system. Its characteristics can be completely derived from the partition function:

$$Z = \sum_{\{s_i\}} e^{-\beta H} \tag{3.12}$$

where $\{s_i\}$ indicates the sum over all the possible orientation of the spins inside the lattice. If we chose $N = 10$, we end up doing a sum over 2^{10} terms, each of which requires the calculation of the system Hamiltonian (almost 2^6 operations) and of an exponential. Its derivation requires high computational power. Furthermore, if N increases, the required calculations increase exponentially. This cannot be considered as a feasible way of deriving information over the system. A different way must be pursued.
In our help comes all the numerical methods and, specifically in this work,

the Monte Carlo simulation. Indeed, in just a few words, the Monte Carlo simulation creates a fictitious replica of a real system and a chain of states through which the replica evolves as to emulate the behaviour of a real system. By numerous samplings of the physical quantities of such fictitious system, an estimate of the real ones can be derived.
Let us now look a little more closely at the problem of deriving estimations of the system's properties. Ideally, we would like to consider the following estimator related to the physical quantity Q:

$$\langle Q \rangle = \frac{\sum_\mu Q_{\mu_i} e^{-\beta E_{\mu_i}}}{\sum_\mu e^{-\beta E_{\mu_i}}} \tag{3.13}$$

where we consider a sum over all the states μ. In reality, in large systems, due to the enormous number of available states, we can only sample a "small"number of them. We will choose them following a particular probability distribution p_{μ_i} which depends on the states μ_i. Therefore:

$$Q_M = \frac{\sum_{i=1}^{M} Q_{\mu_i} p_{\mu_i}^{-1} e^{-\beta E_{\mu_i}}}{\sum_{i=1}^{M} p_{\mu_i}^{-1} e^{-\beta E_{\mu_i}}} \tag{3.14}$$

Now, it is important to select the appropriate values for p_μ. As an example, if we chose $p_\mu = 1$, we end up with a truncated version of the estimator Q. Because M must be finite, we will have to avoid some states and it may happen that we left out some important ones (in terms of weights in the sum). In this case, the estimation would be worse. The real problem, then, concerns deriving the appropriate p_μ as to pick more frequently the most important state (to still have a good estimation of Q) but as to reduce as much as possible the number of states required to sample. This technique takes the name of importance sampling and requires a brief discussion.

3.3.1 Importance sampling

A possible choice for p_{μ_i} can be to consider the Boltzmann probabilities: $p_{\mu_i} = 1/Ze^{-\beta E_i}$. In this case, we will simply obtain:

$$Q_M = \frac{1}{M} \sum_{i=1}^{M} Q_{\mu_i} \tag{3.15}$$

which corresponds to the mean of all the measured M values. To understand why this choice of p_{μ_i}, we can consider the case in which the system is in a low temperature and occupies one of the lowest-lying energy levels. The states where the system can be found and, therefore, that will characterise the value of Q are the same ones that we will sample more often. Our estimation will be a reliable estimate of the real measured quantity.
But, how do we pick the states proportional to the Boltzmann statistic? The Monte Carlo simulation solves this problem by building an appropriate chain of states defined as "Markov chain"which will give a density of states that follows the Boltzmann probability.

3.3.2 Markov chain

A Markov chain is the result of a Markov process. This process starts from a state μ and derives a new one (ν) following specific criteria. In particular, it links the two states by a certain probability, $P(\mu \longrightarrow \nu)$, that is such to verify the following properties:

- Time independence.
- It depends only on the properties of state μ and state ν.
- Normalisation condition: $\sum_\nu P(\mu \longrightarrow \nu) = 1$.

Nothing is said about $P(\mu \longrightarrow \mu)$ (probability to remain in the same state) which can be taken also different from 0. As we will see, in the Metropolis algorithm, this feature will be used consistently. The system will be allowed to remain in the same state for as long as needed. The Markov chain is designed to give, in the long run, states that appear with probability equal to the Boltzmann statistics. In this way, considering all the states after a certain point in the chain and evaluating them, we will obtain the desired p_{μ_i} and therefore a good estimation of Q.
The Markov chain must also satisfy two additional conditions that now we present.

Ergodicity

Ergodicity requires that every possible state could be, sooner or later, considered in the Markov chain and therefore not excluded a-priori. This is a crucial requirement. Imagine not to satisfy the ergodicity condition and therefore to have two different groups of states that are not linked. Now, if we start the Markov chain in one of the two groups of states, we would miss the chance of obtaining one of the states from the other group. This would mean that, depending on the starting condition, we will probably miss sampling important states with consistent p_μ.

Detailed balance

Detailed balance, instead, is a more subtle condition. Practically, it requires that the probabilities of moving into or out from the state μ must be equal:

$$p_\mu P(\mu \longrightarrow \nu) = p_\nu P(\nu \longrightarrow \mu) \tag{3.16}$$

This condition provides that the Markov process will generate states with probability following the Boltzmann distribution, at equilibrium. Moreover, it also eliminates the possibility that the Markov chain ends up locked inside a loop of states but instead reaches a dynamic equilibrium. Both of these consequences are not trivial and are further explained in [10].

Thus far, we have always spoken about equilibrium conditions, even though we may also be interested in the out-of-equilibrium properties of the system. In particular, all the Markov process has been found to give a reliable succession of states provided that we are in equilibrium, but nothing is said before the equilibrium is reached. Or not?
The condition of detailed balance is more general. If we want the Boltzmann statistics at equilibrium then we simply impose:

$$\frac{P(\mu \longrightarrow \nu)}{P(\nu \longrightarrow \mu)} = \frac{p_\nu}{p_\mu} = e^{-\beta(E_\nu - E_\mu)} \tag{3.17}$$

But if we chose a different statistic for p_μ then the chain will satisfy a different statistic. This may become helpful in case we want to say something in the out-of-equilibrium dynamics, as we will see.

Nevertheless, detailed balance does not completely settle the problem. Indeed, only the ratio between the transition probabilities has been fixed, nothing is constrained regarding their single value. This gap becomes quite useful. In particular, we can decompose each transition probability in two distinct terms: acceptance ratio $A(\mu \longrightarrow \nu)$ and selection probability $g(\mu \longrightarrow \nu)$, as follows:

$$P(\mu \longrightarrow \nu) = g(\mu \longrightarrow \nu)A(\mu \longrightarrow \nu) \tag{3.18}$$

The selection probability represents the probability that from a state μ the Markov process will generate the state ν; the acceptance ratio, instead, deals with the probability that the generated state will be effectively chosen as to be the next one in the chain. In a certain way, we have that g deals with the a-priori probability to find a new state, A with the a-posteriori probability, once the state has been generated/investigated and we have the correct understanding as to refuse it or not (depending on if we are going towards equilibrium, as to obtain the Boltzmann statistics or not).
We have many choices. As an example, we can consider the Metropolis approach: a certain number K of states ν are identified as "first neighbours"of the present μ. These "first neighbours"could be all the states ν that differ from μ only in the state of one of its elements. Then it is chosen:

$$g(\mu \longrightarrow \nu) = \begin{cases} \frac{1}{K}, & \text{if } \nu \text{ is a "first neighbour"} \\ 0, & \text{otherwise} \end{cases} \tag{3.19}$$

Every "first neighbour"state has the same probability to be selected as the next one. But it is not guaranteed to be the next one in the Markov chain since there is the possibility that it may be rejected. This type of approach will be called "a-priori". Instead, in "a-posteriori"approach, the acceptance ratios are always equal to 1. The new state will be accepted no matter what, reducing the number of attempts required before a new state is found. In this case, the real problem comes from the selection ratios. They must embed information on the state that will be generated and sets their values consequently. This requires a-priori knowledge, which is something not easy to derive.

In the following paragraphs, we will deal with all of these approaches. First, we consider the most famous a-posteriori approach, the Metropolis algorithm. Afterwards, we will present, instead, a-priori approach: the Lebowitz algorithm.

3.4 Metropolis algorithm

The Metropolis algorithm allows to perform simulations over the Ising system, characterised by the Hamiltonian:

$$H = -J \sum_{\langle i,j \rangle} s_i s_j - \mu_0 H \sum_i s_i \tag{3.20}$$

First, we have to define how the new state ν is generated starting from μ. The Metropolis algorithm is devised to consider a single spin-flip dynamics, in which the new state is generated from the old one by inversion of a single spin in the whole structure. This means that starting from μ we will have N possible next states. Then, it considers for simplicity:

$$g(\mu \longrightarrow \nu) = \frac{1}{N} \tag{3.21}$$

independently from the final state ν. All the possible states have the same probability to be selected. From this, it is quite simple to demonstrate that the ergodicity property is verified: any state can be reached from any other state, in a finite number of steps. If we want to preserve the condition of detailed balance, the acceptance ratios must satisfy the condition:

$$\frac{A(\mu \longrightarrow \nu)}{A(\nu \longrightarrow \mu)} = e^{-\beta(E_\nu - E_\mu)} \tag{3.22}$$

As to increase the efficiency of the algorithm, we want to have as high as possible acceptance ratios. For this reason, the Metropolis algorithm considers:

$$A(\mu \longrightarrow \nu) = \begin{cases} e^{-\beta(E_\nu - E_\nu)}, & \text{if } E_\nu - E_\nu > 0 \\ 1, & \text{otherwise} \end{cases} \tag{3.23}$$

Every "move"that brings the system in a lower energy state is accepted. In case the energy has to increase, the algorithm has a certain probability to reject the "move".
The core of the simulation requires the following steps:

1. With equal probability, a spin in the lattice is chosen to be reversed.
2. The ΔE deriving from the inversion of that spin is calculated.

3. If $\Delta E \leq 0$, lowering the system total energy, the move is accepted. If $\Delta E < 0$ then we have a probability equal to $e^{-\beta(E_\nu - E_\nu)}$ to proceed in the flipping. A random number r is generated in the interval $[0, 1)$. If $r < e^{-\beta(E_\nu - E_\nu)}$ then the move is accepted; otherwise, the move is rejected and the system remains in the same state.

4. If the spin is flipped, then energy and magnetization of the system are updated.

Within this algorithm is embedded the choice: $P(\mu \longrightarrow \mu) \neq 0$.

Now we have to deal with an important aspect, which regards all the simulations. What do we choose as the initial configuration for the lattice? Theoretically, every possible state for the system, i.e. arrangement of the spins inside the structure, would not make any difference at all. But we can still choose an initial configuration to allow the system to proceed more quickly towards equilibrium. Indeed, as already said, a real ferromagnetic system will tend for $T \to 0$ to a completely magnetized configuration. Indeed, for $T = 0$, the equilibrium configurations are the ones in which the system has all spins equally oriented and $|m| = 1$. If we increase the temperature, some spins will gain energy due to thermal fluctuation and the equilibrium will start to drift from the one completely magnetized. At finite T, but still lower than T_c, the system will exhibit $|m| > 0$. For $T \to \infty$ thermal fluctuation completely overcomes the interaction energy and each spin orients independently from its neighbours. At equilibrium, in this conditions, the magnetization oscillates around 0 and the lattice has randomly oriented spins. Therefore we can define two main equilibrium conditions: completely magnetized and completely random configurations, respectively for $T \to 0$ and $T \to \infty$. They will be considered as a starting point for our simulation. Generally, if we simulate $T > T_c$ we will start with a system with random orientation of the spins. Otherwise, we will start from a configuration completely magnetized ($m = +1$ or $m = -1$).

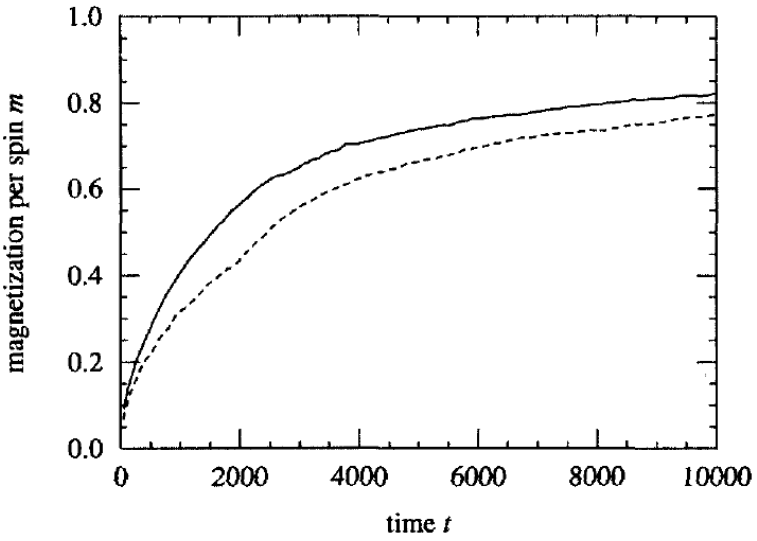

Figure 3.1: Average magnetization (over 200 runs) followed by different algorithm (Metropolis in solid line, heat-bath in dotted line) for $T = 2.1 < T_c$. Source [10].

3.5 Out-of-equilibrium dynamics

The Metropolis algorithm can reproduce the main characteristics of a magnetic system, showing a phase transition between order and disorder for a finite value of the temperature. But, one of the drawbacks is related to the fact that this model can reproduce only the equilibrium properties of the system. The simulation does not give reliable information concerning how a system goes to equilibrium. Indeed, if one considers a different algorithm for the Monte Carlo simulation of the same magnetic system, the system properties follow different dynamical behaviours as shown in fig. 3.1.

Which one is the more reliable? The answer is no one of them. All the equilibrium algorithms are thought to derive the correct equilibrium behaviour, rather than the transient regimes. The same problem applies when, in a system in equilibrium, we decide to change the parameters in time as the magnetic field or the temperature. In this case, the system may fail to reproduce the correct behaviour of the physical parameters such as magnetization or magnetic susceptibility. For this reason, a different approach must be con-

sidered. This is the aim of the following paragraph, where a now dynamical approach is considered.

3.6 Glauber dynamics

A time-dependent approach was developed by Glauber [2] as to follow the time-dependent properties of the system. The model allows to determine a new expression for the transition probabilities $P(\mu \longrightarrow \nu)$, different from what is assumed in the Metropolis algorithm. As we saw, we have a certain degree of freedom in the selection of $P(\mu \longrightarrow \nu)$ and the detailed balance condition does not give any constrain over the single value, just over the ratio between it and the inverse transition.

The procedure for the transition probability determination now follows, as presented in [11]. We indicate with $w_j(s_1, \ldots, s_j, \ldots, s_N)$ the transition probability per unit time for the j-th spin, i.e the probability that spin s_j will be inverted, for a give configuration of the lattice $\{s_1, \ldots, s_N\}$. For simplicity, we will shorten the notation as $w_j(s_1, \ldots, s_j, \ldots, s_N) = w_j(s_j)$ We also identify with $p(s_1, \ldots, s_j, \ldots, s_N, t)$ the probability that, at time t, the system is in state $\{s_1, \ldots, s_N\}$. We can write the following master equation (more precisely a set of 2^N differential equations, on for all the possible states) representing the variation of the probability with time.

$$\frac{d}{dt}p(s_1, \ldots, s_j, \ldots, s_N, t) = -\sum_{j=1}^{N} w_j(s_j)p(s_1, \ldots, s_j, \ldots, s_N, t) + \sum_{j=1}^{N} w_j(-s_j)p(s_1, \ldots, -s_j, \ldots, s_N, t) \quad (3.24)$$

in which the first term in the right hand side represents the transition rate out from the considered state to any possible one (in the single spin-flip dynamics) and the second term the transition rate into it. In the equilibrium

condition $\frac{d}{dt}p(s_1, \ldots, s_j, \ldots, s_N, t) = 0$ and therefore:

$$\sum_{j=1}^{N} w_j(s_j)p(s_1, \ldots, s_j, \ldots, s_N, t) = \sum_{j=1}^{N} w_j(-s_j)p(s_1, \ldots, -s_j, \ldots, s_N, t) \tag{3.25}$$

in reality, detailed balance sets an even stronger condition. Indeed, we will have

$$w_j(s_j)p_0(s_1, \ldots, s_j, \ldots, s_N, t) = w_j(-s_j)p_0(s_1, \ldots, -s_j, \ldots, s_N, t) \tag{3.26}$$

in which p_0 denotes that we are considering the probabilities of finding the system in the considered state at time t in equilibrium condition. Finally, since the equilibrium probabilities are proportional to the Boltzmann factors $e^{-\beta H}$ we derive:

$$\frac{w_j(s_j)}{w_j(-s_j)} = \frac{1 - s_j \tanh(\beta E_j)}{1 + s_j \tanh(\beta E_j)} \tag{3.27}$$

where, given $J_{k,j}$ equal to the interaction energy between spin j and spin k,

$$E_j = \mu H + \sum_{k=1}^{N} J_{k,j} s_k \tag{3.28}$$

where μ indicates the magnetic permeability, such that: $\mu H = B$. We chose as single transition probability the ones of the form:

$$w_j(s_j) = \frac{1}{2\alpha}(1 - s_j \tanh(\beta E_j)) \tag{3.29}$$

Here, α is expressed in seconds, since $w_j(s_j)$ is expressed by the inverse of a time. We can think of it as a measurement of the time frame of the system. Since we are not considering simulations reproducing behaviours of real systems and we can take arbitrary the unit time, we consider $\alpha = 1s$. In future works, a better choice for the constant α could be considered to match the behaviour observed in real materials. We expect a lower-valued time constant since a transition rate of one inversion per second would require a consistent amount of seconds (of the order of the atoms in the materials) to allow the system to reach equilibrium.
With these new transition probabilities, we are able to describe the time-varying conditions of our system. In particular, the magnetic field time

dependence is considered implicitly in the expression of the state energy E_j. in our case, we extend this assumption to the case in which also the temperature change in time, by considering β as the time-varying parameter.

In this work, considering the Glauber dynamics is our first choice. The second one is related to the implemented algorithm. As said in the previous paragraph, the Metropolis algorithm, especially near equilibrium, has many steps that are rejected. This causes the algorithm to run slowly, especially at low temperatures. We present now an a-priori type of algorithm which, in exchange for little complexity in the algorithm is able to always accept the inversion of the spin.

3.7 Lebowitz algorithm

In this work, instead of relying on the standard Metropolis algorithm, we have decided to consider a different approach for the Monte Carlo simulation. As seen, the Metropolis algorithm has a quite simple structure that relies on the probability of spin-flip depending on the energy that the reversal would bring into the system. Being a posteriori approach, the spin-flip event is questioned afterwards the spin has been chosen. But, what does it happen if we instead chose the spin with a criterion? In particular, with an energy criterion? We should immediately address the problem of whether to flip it or not. Even better, if we chose the spin depending on its energy (not anymore at random between all the N spins in the structure), we can stop interrogating if it must flip or not since it will be flipped no matter what. This is what we aim to do and what is allowed considering the Lebowitz algorithm [1].

As mentioned before, the a priori approach allows saving a great quantity of computational time. Indeed, think at an Ising system in the condition $T < T_c$ and near-equilibrium (almost completely ordered). The Metropolis algorithm picks a spin at random and, since most of the spins are equally oriented, it is more likely that the chosen spin will have the same orientation as the neighbours and no energy gain will be associated with its reversal. This means that we have a small probability to flip it and its reversal will be rejected. The rejection goes on and on until suddenly or a spin that has the opposite direction of its neighbours is chosen, or the random generation

number will give a positive result. In the case of the Lebowitz algorithm, instead, no matter how near we are to equilibrium, a spin is inverted at each step. Therefore, we have a faster algorithm (10 times faster when $T \approx 0.5 \cdot T_c$). What the Lebowitz algorithm does, is just a reorganisation of the Metropolis algorithm.

What we have to keep in mind is that the simulation steps will not be comparable. This is a problem for the Lebowitz algorithm since it is quite clear that if a system is in an equilibrium condition, spin-flip events must happen at a lower rate. The Metropolis algorithm has simulation steps that allow following the time evolution. The Lebowitz algorithm, instead, has to rely on a different time concept which will be explained later in paragraph 3.8.

3.7.1 Structure of the Lebowitz algorithm: Ten-Fold Way

As said before, the most important difference with respect to the Metropolis algorithm is that now we want to chose with a certain probability the next state to invert ($g(\nu \longrightarrow \mu) \neq const$), as to retain always the acceptance ratio equal to one. This can be achieved only by considering a priori the energy variation that a spin-flip event could induce in the system. Is this meaning that we have to track all the N possible energy variation that all N possible spin-flip events can bring? Fortunately not. We can divide all the spins in the structure in different classes, depending on the value of the energy variation that their flipping would bring into the system. Now, how many classes do we need? The answer can be obtained by considering the Ising Hamiltonian, equation (3.20) and focusing the attention over a single spin s_j: its flipping can change the energy in the system due to change in the reciprocal orientation with neighbouring spins and with the external field. We consider now a bi-dimensional system in which every spin has four neighbours, even though the extension to higher order can be easily achieved. In case of a null magnetic field, since all the exchange interactions are equals and independent from the magnetic moment position $J_{i,j} = J \; \forall i, j$, a spin-flip event can change the system energy by $-4J; -2J; 0; 2J; 4J$. Therefore, in this case, only 5 classes would be required, depending on the reciprocal orientation with the neighbouring spins. What if, instead, we were to consider also a

Classes of a 10-Fold Way			
Class	spin orientation	Number of nearest neighbours spin up	ΔE
1	+1	4	+4
2	+1	3	+2
3	+1	2	0
4	+1	1	-2
5	+1	0	-4
6	−1	4	-4
7	−1	3	-2
8	−1	2	0
9	−1	1	+2
10	−1	0	+4

Table 3.1: Table with the main characteristics of the classes related to the 10 Fold Way algorithm for a square lattice.

magnetic field? In this case, also the reciprocal orientation with the magnetic field would matter. The number of classes would double, considering also spin oriented "up"or "down". Table 3.1 contains the information about all the classes and their characteristics.

From a practical point of view, to guide us in the selection of the spin to invert at each step of the simulation, we will have a variable that keeps track of the class of each spin in the structure. This variable is called CLASS. In particular, it is a matrix with ten rows and a certain number of columns. In the k-th row are contained all the spins in the lattice in the k-th class. Saved in each cell there are the coordinates of the spin inside the lattice.
Now, upon a flip inversion, the class of the chosen spin will change by ± 5, since the orientation of the neighbours will remain the same. But it is not the only one to change class. Also, all its neighbours experience a modification: indeed, their number of neighbours with spin up will change by -1 if the selected spin is flipped in the state up; will change by $+1$ if the selected spin is flipped in the state down.
We have therefore the need to quickly retrieve the neighbours of the selected spin inside the matrix CLASS to modify their position in it. For this task, we use an additional $(L \times L)$ matrix that we call "LOCATION".

To sum up, we will use in the algorithm 3 auxiliary matrices (or arrays, if one prefers):

- LATTICE: is the matrix with the spins schematised as $+1$ (-1) if have an up (down) orientation.
- CLASS: contains a number of row equal to the number of total classes. In each row are listed the position in LATTICE (row and column) of the spins in that particular class indicated by the row.
- LOCATION: required to find the address of each spin inside the matrix CLASS and therefore retrieve its class. This matrix allows one-to-one correspondence among the matrices LOCATION and CLASS.

Other auxiliary vectors, allowing a faster or more readable code are:

- N-ARRAY: array of 10 cells. The i-th cell contains the number of spins in the i-th class.
- M-ARRAY: array of 10 cells. The i-th cell contains the number of spins in the previous classes:

$$\text{M-ARRAY}(i) = \sum_{i=1}^{10} \text{N-ARRAY}(i) \tag{3.30}$$

- Q-ARRAY: is defined as follows:

$$\text{Q-ARRAY}(i) = \sum_{i=1}^{10} \text{N-ARRAY}(i) \cdot P(i) \tag{3.31}$$

  where $P(i)$ is the transition probability for a spin flip in the i-th class. This array is used for the determination of the spin to invert every step.

Fig. 3.2 shows the structure of the Matrices after some steps of simulation, starting from a completely random orientation of spins inside the lattice.

Now it follows the procedure adopted in the Lebowitz algorithm. It can be divided into 4 sub-parts: initialisation of the variables; spin selection; update of the variables; measurement of physical variables. Let us start with the first one, initialisation:

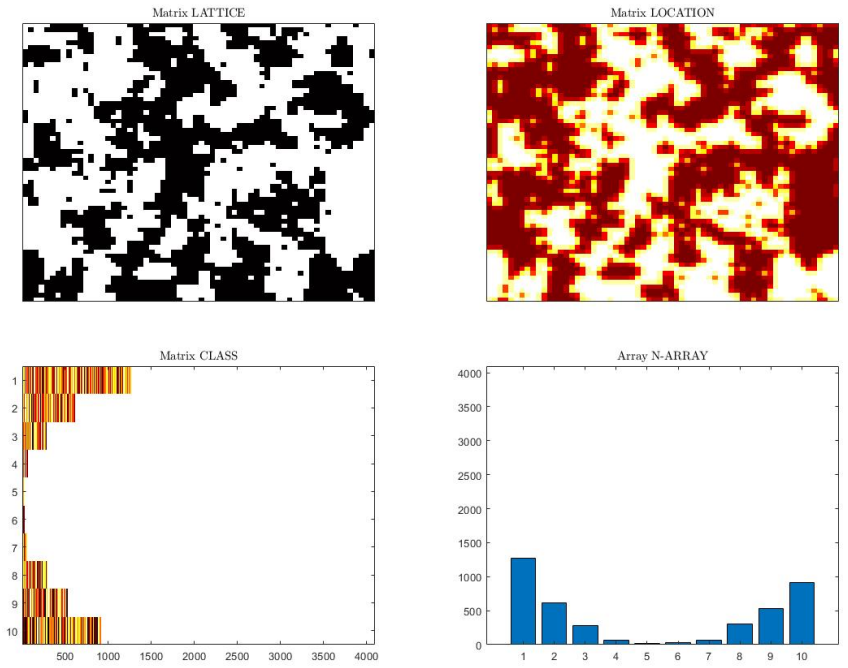

Figure 3.2: Graphical representation of the matrices. In the first figure, the lattice, with spin up white and spin down black. In the second figure, the matrix LOCATION that maps every spin in matrix CLASS; here the colours indicate the class, the position in the row is not represented here. In the third, the matrix CLASS; each colour indicates a different couple of coordinates. In the last, the vector N-ARRAY, which simply counts the number of spins inside every class.

1. At the beginning, the lattice is scanned: for each spin, the number of neighbouring spin up is counted and its class is determined.

2. The spin position is added in the matrix CLASS, in the specific row, in the empty cell with lower possible index.

3. After all the spins have been scanned, matrix CLASS is considered. Reading from each occupied cell of CLASS, the coordinates inside LOCATION are found and we access to it. The cell in LOCATION that we have found stores now the coordinate of the cell CLASS. This allow a one-to-one correspondence between the matrices.

4. N-ARRAY is updated at the end of the process, taking in k cell the number of elements in the k row of CLASS.

5. M-ARRAY is simply taken as:

$$\text{M-ARRAY}(k) = \sum_{i=0}^{k} \text{N-ARRAY}(i) \tag{3.32}$$

After the initialisation, we can start with the proper simulation. At each step, a spin is selected with a proper procedure that now follows:

1. Allowing the possibility of time-dependency, external physical variables (magnetic field or temperature) are updated. After their modification, also the transition probabilities from Glauber dynamics are accordingly modified, following equations (3.29).

2. The vector Q-ARRAY is updated following definition (3.31).

3. A random number R is chosen wit uniform probability inside the interval $[0, \text{Q-ARRAY}(10))$.

4. The class of the spin to invert (k) is selected such that:

$$\text{Q-ARRAY}(k-1) \leq R < \text{Q-ARRAY}(k) \tag{3.33}$$

5. The spin is chosen with uniform probability inside the class k. It is generated an integer random number R^* in the interval $[0, \text{N-ARRAY}]$ and the spin that will be flipped can be found in $\text{CLASS}(k, R^*)$.

Notice that is not possible to pick an empty class, since in that case the related Q-ARRAY value will be equal to the precedent class.
We now consider the algorithm for the variable update part:

1. The spin that must be inverted now changes position in CLASS. Its class change by $+5$ if it was in spin up or -5 if it was spin down before the reversal. Matrix LOCATION is consequently updated, as N-ARRAY and M-ARRAY for both the classes that have lost/gained a spin.

2. The neighbouring spins are now considered. For each one of them, the position in CLASS (accessed considering the matrix LOCATION) is changed by $+1$ row if the inverted spin was down, -1 row if the inverted spin was up before the inversion. As before, the spin position is added inside CLASS as to occupy the empty cell with lower possible index. LOCATION is then updated, followed by both N-ARRAY and M-ARRAY.

Finally, the physical variables are measured. It is done by considering the value at the precedent step and then considering the update coming from the reversal. The magnetization changes of $\Delta m = +2$ (-2) if $k \leq 5$ (> 5). The energy changes of an amount indicated by the class of the spin that has been flipped: $E_{t+ti} = E_t + \Delta E(k)$. For our simulations, most of the time, not all the series of values for all the physical properties were considered instead, only one every fixed number of simulations steps (usually measured in Monte Carlo single steps, *MCSS*, which corresponds to N number of simulation steps) or, even better, every Δt. Indeed, we have to recall that the *MCSS* for the Lebowitz algorithm is not reliable in describing the evolution of the simulation since, at every step, a spin is inverted. Instead, we would rely on a different physical variable that could take into account the fact that a *MCSS* weights differently if we are near or far from equilibrium.

3.7.2 Time evolution

To every step of the simulation, we can assign a time variable representing how fast the system leaves a state. This is achieved by considering the following formula for time increment:

$$\Delta t = \frac{\tau}{\text{Q-ARRAY(10)}} \ln R \tag{3.34}$$

where τ represents a time constant for the system (in our case, fixed to 1) and R is a random number uniformly chosen in the interval $(0, 1)$.
The expectation value for Δt is proportional to Q-ARRAY$(10)^{-1}$. Since Q-ARRAY(10) is equivalent to the number of spins multiplied by the average probability that an attempt will produce a spin-flip event, Δt is proportional

to the number of attempts per site. Moreover, this definition of the physical-time embeds the choice of the Glauber dynamic. Indeed, while deriving Q-ARRAY(10) we use the transition probabilities defined by relation (3.29) obtained following the Glauber dynamics. For this reason, the physical-time allows following the time evolution of out of equilibrium systems.

3.8 The concept of time

Now, we have to look a little closer to the problem of time. As previously anticipated while dealing with Glauber dynamics, we will consider time-varying parameters. Therefore, we have to specify which time we use as a reference. Thus far, two times have been considered (other than the computational time, which does not have any proper meaning for the simulation):

- The *MCSS* in the Lebowitz algorithm.
- The physical-time calculated at each step of the simulation.

The *MCSS* in the Lebowitz algorithm follows the succession of the states in the Markov chain, even if it does not consider the possibility that between two states the time for the transition could vary. Indeed, because the acceptance ratio is always equal to 1, between a state and the following there will be always one simulation step. This does not sound physical. Consider the case in which the system is magnetized, with $T \to 0$: the inversion of a spin in the opposite direction to the overall magnetization will require a certain amount of time, being a thermal fluctuation. The inverse process, instead, will happen statistically speaking more quickly since also the exchange interaction cooperates to have all the spins magnetized. For this reason, we consider the physical-time to change the external parameters. Since *MCSS* and physical-time are not linearly correlated, it could be interesting to derive their relative dependency. This will be investigated in the following chapters, in different conditions.
In the Metropolis algorithm, instead, the *MCSS* resembles more the physical-time condition, since $P(\mu \longrightarrow \mu) \neq 0$: at each simulation step does not correspond the creation of a new state and for "moves"that brings the system

far from equilibrium, more simulation steps are required, since more steps will be discarded.
An important difference between the Glauber physical-time and the Metropolis *MCSS* is now considered. In the latter case, all the moves toward states with lower energy have the same transition probabilities associated, since the acceptance ratio is always equal to one if $\Delta E \leq 0$. In the former case, instead, spin-flip events with $\Delta E = -4J$ and $\Delta E = -2$ have different transition probabilities. This is a better representation of a real system. As an example, consider a ramp with a fixed length and a disc. The time required before the disc reaches the end of the ramp depends on the angle θ between the ramp and the ground: when θ increases, the disc velocity increases, and less time is required before equilibrium is reached. This is what we simulate with Glauber dynamics applied in the Lebowitz algorithm by considering different transition probabilities.

In the following part of the work, whenever we will speak of *MCSS* we implicitly refer to the ones of the Lebowitz algorithm, if not otherwise specified.

Chapter 4

Defect-Free Bi-dimensional System

The main focus of this chapter is to discuss the validity of the results obtained considering the Lebowitz algorithm with Glauber dynamics applied to a bi-dimensional square lattice through critical temperature measurements and their comparison to the theoretical value. A first investigation of what means consider the physical-time is presented, followed by a discussion concerning the most widely used methodology for the critical temperature determination and a new technique, based on the peculiarity of the algorithm employed.

4.1 Physical-time

As already mentioned, the introduction of a physical-time, implicitly considering the easiness with which a state towards equilibrium happens, allows to detach the variation of time-dependent parameters from the simulation steps, which in the Lebowitz algorithm has poor physical meaning. This detachment becomes relevant only if the *MCSS* of the simulation and the physical-time are not linearly correlated, otherwise the only difference between the results with the two different methods would be merely a proportionality factor.

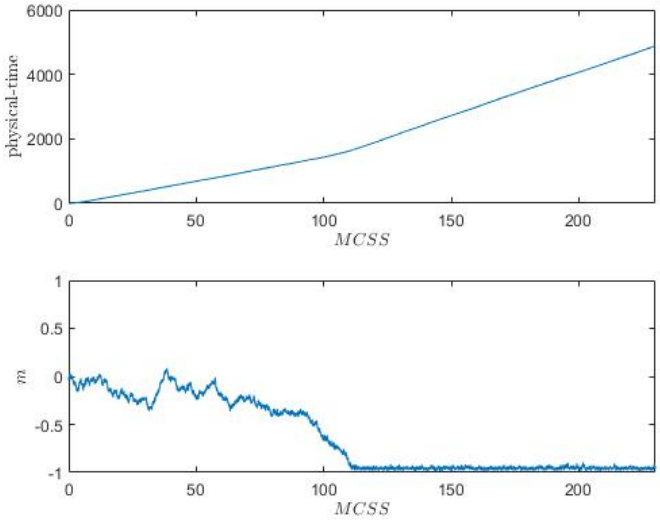

Figure 4.1: The first panel shows the relation between physical-time and MCSS. The second panel shows the related magnetization of the lattice function of the MCSS.

In order to investigate this aspect, the following simulation is devised: a square lattice ($L = 40$) is prepared with random orientation of the spins and then it is left free to evolve. The temperature (always expressed in unit of J/k, J exchange constant and K Boltzmann constant) is fixed below the critical one, as to induce the system to show an overall magnetization (in particular, the temperature is fixed: $T = 1.5$). Therefore, we are able to track down the relation physical-time versus *MCSS* in both the conditions "far from equilibrium"(at beginning of the simulation) and "near equilibrium"(at the end of simulation). Fig. 4.1 shows the results of the simulation.

It is possible to notice two different regions:

- Far equilibrium: the magnetization fluctuates while proceeding towards the equilibrium state. The relation physical-time versus *MCSS* is linear with a shallow angle.
- Near equilibrium: the magnetization fluctuates around the equilibrium value (in this case ≈ -1). The relation physical-time versus *MCSS* is

linear with a steep angle.

Actually, this behaviour is rather intuitive. In the "near"equilibrium condition the algorithm has the lowest energetic classes almost completely filled. Therefore, Q-ARRAY(10), defined in the previous chapter, has the lowest possible value and remains constant through time.
By considering the formula linking Q-ARRAY(10) and Δt:

$$\Delta t = -\frac{1}{\text{Q-ARRAY(10)}} \ln(R) \tag{4.1}$$

we can notice that also the expected value for Δt remains constant and has the highest possible value. For this reason, in the near equilibrium condition, the dependence physical-time vs *MCSS* is linear with steeper angle.
The measurements show that the variation in the proportionality coefficient linking *MCSS* with physical-time tends to change by almost a factor of 10 depending on how far from equilibrium we are. This feature would not be considered if we were relating time-varying variables to the *MCSS*: nothing would change if the system was "far"or "near"equilibrium.

As to derive the relation with the initialisation parameters, simulations for different system sizes and temperatures are considered and the coefficients representing the proportionality constant between *MCSS* and physical-time t are derived:

$$t = K_{near/far} \times MCSS \tag{4.2}$$

The results are shown in fig. 4.2 and 4.3.

Considering fig. 4.2, it can be noted that the "near equilibrium"coefficient does not depend on the particular choice of the lattice size L. Instead, the "far equilibrium"coefficient is influenced by L. The difference between the two coefficients, for a fixed choice of L and T, is in accordance with what can be observed in fig. 4.1, giving an higher value for the "near equilibrium"one.

By looking at fig. 4.3, it can be observed that both near and far from equilibrium coefficients are influenced by the temperature. An important observation now follows. While decreasing the temperature, the "near equilibrium"coefficient increases substantially. One *MCSS* correspond to almost

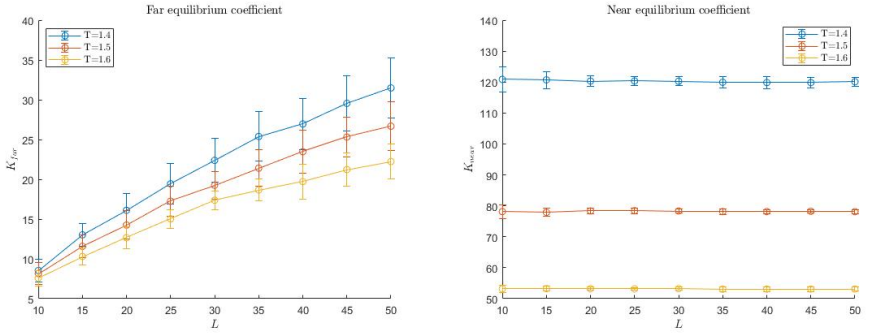

Figure 4.2: T fixed. In the left panel "far equilibrium"coefficient; in the right panel "near equilibrium"coefficient for different values of the lattice lateral size.

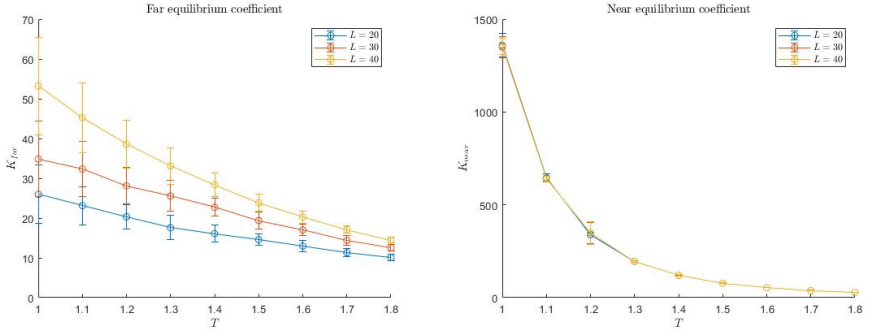

Figure 4.3: L fixed. In the left panel "far equilibrium"coefficient; in the right panel "near equilibrium"coefficient for different values of the Temperature.

10^3 physical-time units. Therefore, while considering a time-varying parameter (which could be the magnetic field or the temperature), one should consider choosing a time dependence that allows the system a sufficient amount of steps (fraction of the *MCSS*) to adapt to the external variation. This problem is not crucial in the case the system moves far from equilibrium. In case it moves near equilibrium, the temperature limit must be checked. As a rule of thumb, simulations with $T < 1$ are not considered.

4.2 Critical temperature investigation

The classical bi-dimensional Ising Model has been demonstrated by Onsager [9] to possess a critical temperature separating the ordered (ferromagnetic) phase from the disordered (paramagnetic) phase. The exact value was shown to be (in units of J/K):

$$T_c = \frac{2}{\ln\left(1+\sqrt{2}\right)} \approx 2.26918531421\ldots \tag{4.3}$$

If the system is left free to behave with $T > T_c$ then it will reach an equilibrium where every spin has, on average, a random orientation with respect to the neighbours. On the contrary, if the temperature is fixed $T < T_c$ the system will reach an equilibrium where a preferential direction for the orientation of the spins is present. This dependence on the temperature of the system is represented in fig. 4.4, where the magnetization (m) is used in order to describe order ($m = 1$) and disordered phase ($m = 0$).

Now, we are interested in deriving an estimate for the value of the critical temperature from our simulations. In the bi-dimensional model, the exact value of the critical temperature is known. This is a particular condition since for other systems (3D Ising model, Ising model with "defects"as defined in chapter 6, ...) no exact value is available. Right now we aim to verify the ability of our system to match the known value, since sooner or later we may be interested in calculating the critical temperature for different systems. From fig. 4.4 a first estimation of the critical temperature can be derived, even though more reliable procedures are usually used for its determination. In the following paragraphs, different methods are presented.

4.2.1 Magnetic susceptibility

The traditional and more accurate way of experimentally determining the value of T_c relies on the magnetic susceptibility of the system, defined by the relation (3.4) which we report here for convenience:

$$\chi_M = \beta N(\langle m^2\rangle - \langle m\rangle^2) \tag{4.4}$$

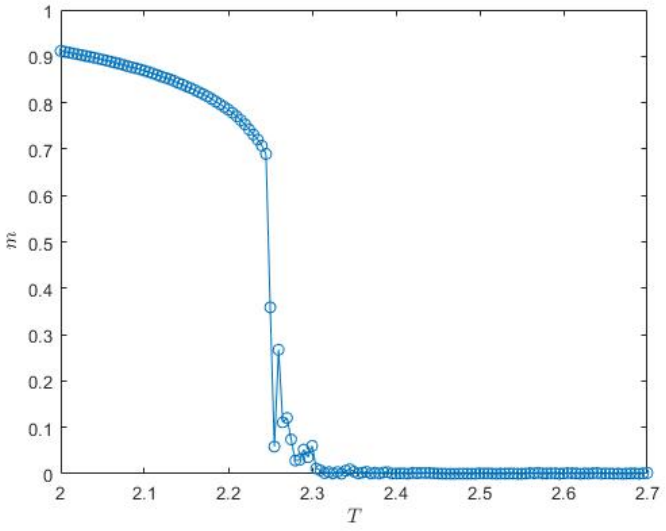

Figure 4.4: Magnetization function of the temperature applied. Simulation done for a system with lateral size $L = 128$.

where N represents the total number of spins in the structure. The procedure adopted for the derivation of χ_M is the following:

1. Temperature is fixed and the square lattice is prepared with random orientation of the spins.
2. After waiting for a specific amount of time, in which the system reaches equilibrium, the magnetization is sampled every Δt fixed. As to decide if equilibrium condition was reached, we have considered the magnetization autocorrelation function: it shows a plateau when the system reaches equilibrium.
3. The value of χ_M is computed.
4. Steps 1-2-3 are repeated several times for different values of the temperature.

A plot representing the dependence $\chi_M(T)$ can be derived from this simulation. Where the magnetic susceptibility shows a maximum, the system

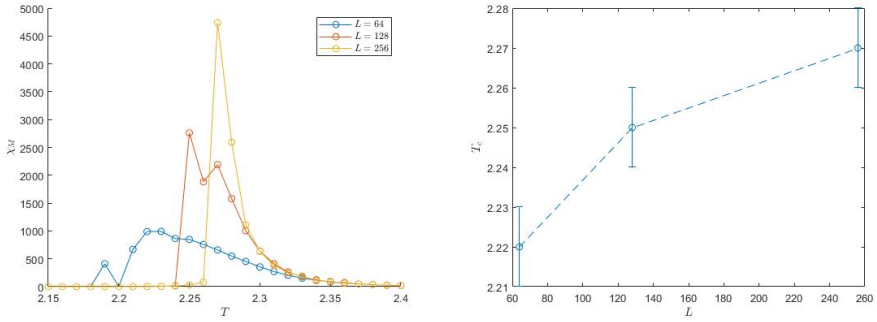

Figure 4.5: On the left panel, the magnetic susceptibility; on the right panel, the derived critical temperature for different dimensions of the lateral size $L = 64; 128; 256$.

exhibits a phase transition and the related temperature value can be considered to be the critical temperature. Results of the simulation are shown in fig. 4.5, for different lateral size L of the square lattice. Table 4.1 reports the derived critical temperatures.

Critical temperature		
$L = 64$	$L = 128$	$L = 256$
2.22 ± 0.01	2.25 ± 0.01	2.27 ± 0.01

Table 4.1: Table for equilibrium critical temperature.

The estimated values are in good agreement with the theoretical one and, while the lateral size increases, the estimate becomes more precise, as represented in fig. 4.5.

4.2.2 Temperature driven experiments

The conventional way for the determination of the critical temperature is the analysis of the Magnetic Susceptibility, as previously seen. Nevertheless, different methodologies can be devised in order to derive it. As an example, a first estimation of T_c can be obtained just from the plot of the magneti-

zation function of the temperature, by considering the point in which the magnetization crosses the 0.5 line.

In the following, a new technique is presented, which relies on the peculiarity of the algorithm considered: the out-of-equilibrium behaviour. The procedure is the following:

1. The starting temperature (T_i) is fixed and the system is prepared in the adequate equilibrium condition (if $T_i > T_c$ the system is prepared with random orientation of the spins; if $T_i < T_c$ the system is prepared completely magnetized).
2. In a fixed amount of physical-time (Δt), the temperature is changed from T_i to T_f and the magnetization is tracked.
3. The critical temperature is derived by considering the crossing of the 0.5 line.
4. The measurement is repeated several time, before changing Δt.
5. The critical temperature in the limit of infinite $\Delta t \to \infty$ (i.e. the case we move through equilibrium states), can be interpolated.

For the standard Metropolis algorithm, this procedure would be off-limits. We cannot rely on the system dynamics in out-of-equilibrium conditions. For the Lebowitz algorithm, instead, the dynamics has a physical meaning and the interpolation gives a reliable result.

Two separated experiments can be investigated: starting with $T_i < T_c$ and then "heating"the system (heating experiment), starting with $T_i > T_c$ and then "cooling"the system (cooling experiment). Typical simulations are the ones represented in fig. 4.6.

To provide a statistical analysis, many repetitions of the same experiment are considered. The critical temperature for a particular choice of Δt can be derived in different ways:

- T_{c1} as the mean value of the T_c coming from each repetition.

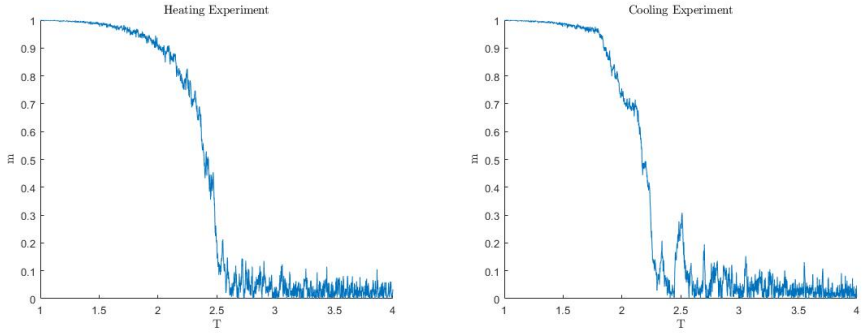

Figure 4.6: In the left panel, heating experiment, starting from a completely ordered condition (time elapses from left to right). In the right panel, cooling experiment, starting from a completely disordered condition (time elapses from right to left).

- T_{c2} as the T_c derived from the mean magnetization curve. The mean magnetization curve can be obtained by simply considering the mean of all the magnetization curve coming from the repetitions of the same heating/cooling experiment.

- T_{c3} as the T_c taken from the minimum magnetization curve. The minimum magnetization curve is obtained by superimposing all the curves coming from the repetitions of the same heating/cooling experiment and then interpolating the minimum magnetization for all the temperatures.

- T_{c4} as the T_c taken from the maximum magnetization curve. The maximum curve is obtained by superimposing all the curves coming from the repetitions of the same heating/cooling experiment and then interpolating the maximum magnetization for all the temperatures.

Generally, we expect T_{c1} and T_{c2} to be quite similar. Instead, due to presence of outliers, T_{c3} and T_{c4} could be less precise estimates. Fig. 4.7 shows the different curves introduced for the determination of T_c, for a particular choice of Δt. The graphics are obtained from the processing of 50 repetitions of the same experiments, considering only the curves able to reach the equilibrium condition ($|m| > 0.95$ for cooling experiment and $|m| < 0.05$ for heating experiment) at the end of the temperature sweep.

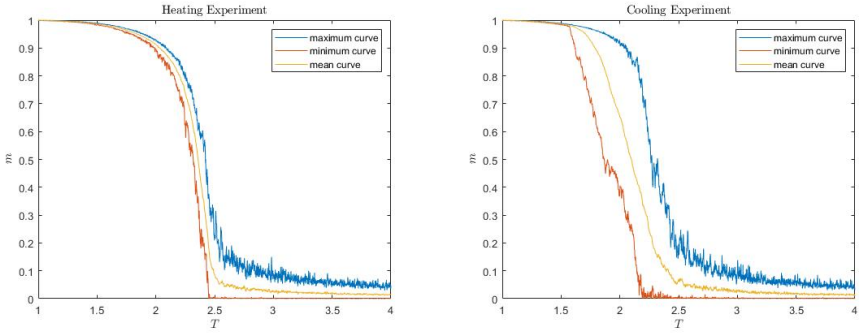

Figure 4.7: In the left panel, heating experiment, with minimum, mean and maximum curve. In the right panel, same for the cooling experiment. Experiments executed with the same value of Δt.

By looking at the two plots, it can be seen that, in the case of the cooling experiment, the minimum curve shows a slower transition if compared to all the other curves. This can be understood by considering that the complete magnetization of the sample requires the coordination of all the lattice sites, unlike the demagnetization in which the spins start to behave independently. Since the ordering process requires all the spins to cooperate and requires a certain amount of time between the nucleation of just few spins and the spreading to all the lattice, we expect the cooling experiment to have a slowest transition towards equilibrium if compared to the heating experiment. This tendency will be highlighted in the minimum curve, since it interpolates the slowest possible transition towards equilibrium. Another important difference between cooling and heating experiment comes from the presence of metastable states along the trajectory. Striped configurations of the lattice (as the one represented in fig. 4.8) can emerge while decreasing the temperature and do not allow the system to reach equilibrium. These metastable states appear only during the cooling experiment and leave the system with a total magnetization far from 1. In order to avoid considering the simulations that remain trapped in these striped configurations, a cut-off threshold for the magnetization has been set ($m_{thr} = 0.95$). This expedient does not filter out systems that remain trapped for a short amount of time in metastable states (and are able to reach equilibrium anyway before the end of the simulation) to be considered in the calculations. But, only few systems showed this behaviour in the simulations. The simulations not reaching the

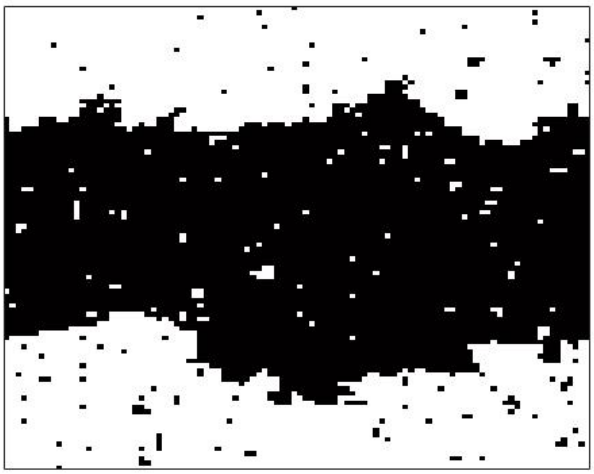

Figure 4.8: Example of striped configuration for a lattice white $L = 100$. The with colour refers to spin oriented up; the black colour to spin oriented down. This configuration is metastable: the system takes a considerable amount of time before escaping from it and reaching equilibrium.

threshold level have been counted as failed simulations. We have noticed that the failing rate tends to decrease while Δt increases. This is reasonable: if enough time is provided, the system is able to escape from a metastable state with higher probability and it will reach more likely the equilibrium condition.

Fig. 4.9 shows the results from heating and cooling experiments for different values of Δt. From the figure, it is possible to notice a tendency to converge for $\Delta t \to \infty$ to a value near 2.3, for all the different lateral size of the bi-dimensional system. Instead, while decreasing Δt, all the derived values for T_c tend to increase. In order to model this behaviour, we can consider the presence of an intrinsic response-time (t_{res}) showed by the system when an external stimulus is applied, which delays the crossing of the $m = 0.5$ line for a certain amount of time. It is possible to assume that this response-time depends on the value of Δt and on the specific experiment considered. Indeed, the system response-time is expected to be lower in case the stimulus applied varies rapidly. Moreover, in order to consider the presence of metastable

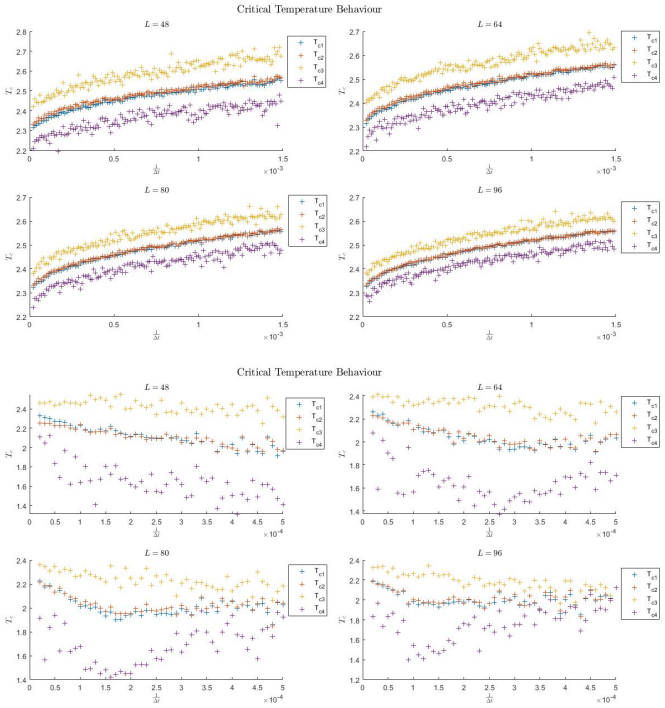

Figure 4.9: In the first figure, heating experiments; in the second figure, cooling experiments. The four critical temperatures are represented in the case of different choices of the system lateral size: $L = 64; 80; 96; 128$. The x-axis is chosen to be the inverse of Δt, to visualise better the limit for $\Delta t \to \infty$.

states along the cooling experiment, we must have:

$$t_{res}(cooling) > t_{res}(heating) \tag{4.5}$$

This time delay affects the measurement of the critical temperature. We can consider the following relation between the equilibrium value of T_c and the one measured $T_{c,Meas}$ at a specific Δt:

$$T_{c,Meas} = T_{c,Eq} + \Delta T \tag{4.6}$$

where

$$\Delta T = \Delta T(t_{res}) = \frac{t_{res}}{\Delta t}(T_f - T_i) \tag{4.7}$$

This justifies the different trend of $T_{c,Meas}$ experienced while decreasing Δt for the two experiments. In case of cooling experiment, $T_{c,Meas}$ decreases, for the heating experiment $T_{c,Meas}$ increases, as clearly showed in fig. 4.9. Moreover, we retrieve the condition in which, when $\Delta t \to \infty$, the critical temperature measured matches the equilibrium one.

The following paragraphs aim to estimate the equilibrium value of the critical temperature, in order to compare it to the one known (equation (4.3)).

Mean curve

If we neglect assumption (4.5), in order to simplify the calculations, we can assume:

$$t_{res}(cooling) = t_{res}(heating) = t_{res} \tag{4.8}$$

Thus

$$\Delta T(heating) = -\Delta T(cooling) \tag{4.9}$$

And

$$T_{c,Eq} = \frac{1}{2}[T_{c,heating} + T_{c,cooling}] \tag{4.10}$$

independently from the Δt considered.
Fig. 4.10 shows the trend of the critical temperature, derived considering the values of T_{c1} and T_{c2} separately. If the assumption (4.8) is reliable, $T_{c,Eq}$ should be constant over Δt. This is generally the condition, even if a

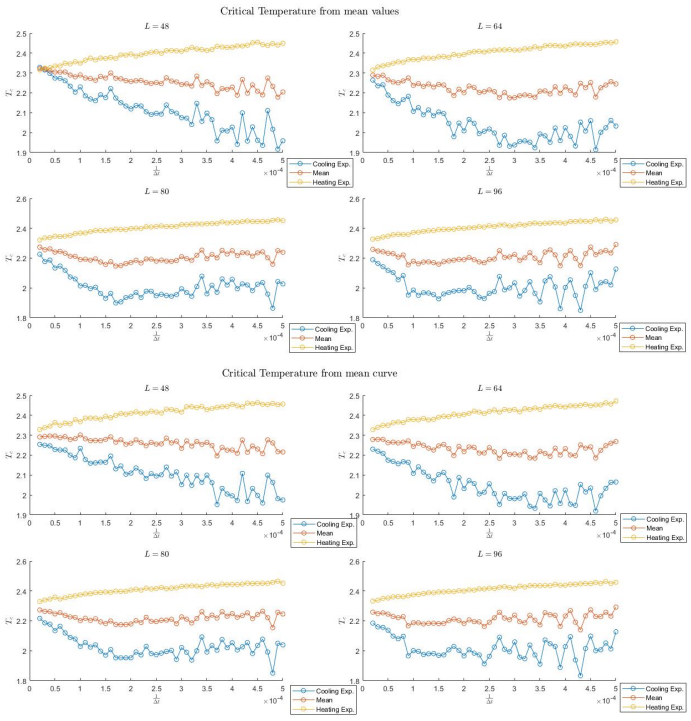

Figure 4.10: The top figure considers T_{c1}; the bottom figure considers T_{c2}. The critical temperature trend is represented, function of Δt, for different choices of the lateral size ($L = 64; 80; 96; 128$). The x-axis is chosen to be the inverse of Δt, as to derive more easily the limit for $\Delta t \to \infty$.

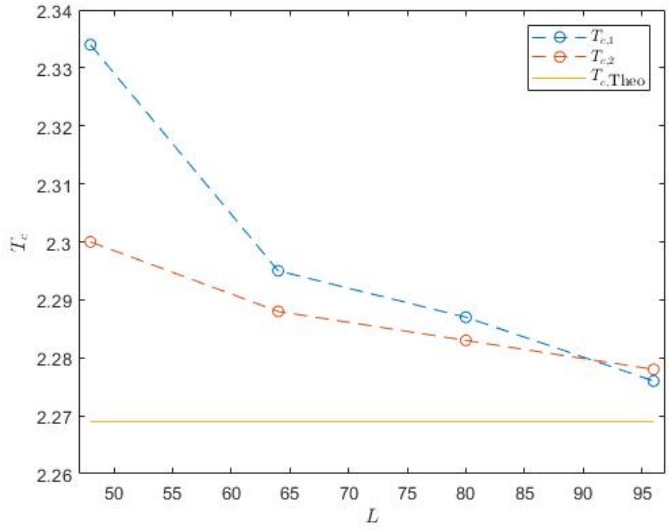

Figure 4.11: Equilibrium critical temperatures derived from the measured values T_{c1} and T_{c2}, for different lateral size of the system. For convenience, also the theoretical value is represented.

Critical temperature				
	$L = 48$	$L = 64$	$L = 80$	$L = 96$
$T_{c1,Eq}$	2.334	2.295	2.287	2.276
$T_{c2,Eq}$	2.300	2.288	2.283	2.278

Table 4.2: Table for equilibrium critical temperature

residual dependence emerges, mostly in the case of small lateral size of the bi-dimensional system. This could derive from the presence of a residual dependence of t_{res} from the type of experiment considered, as suggested by (4.5). Therefore, as final value for the equilibrium critical temperature, a linear regression over one decade of data is considered and $T_{c,Eq}$ is taken as the intercept with the y-axis. The equilibrium critical temperatures derived considering both T_{c1} or T_{c2} are reported in the table 4.2 and shown in fig. 4.11, for different lateral sizes of the system.

Good agreement with the theoretical value is shown. Moreover, while increasing the lateral size, the value of the critical temperature decreases, following

the relation suggested by Ferrenberg *et al.* [12]. The difference between the two values derived shrinks while increasing the lateral size.

Minimum and maximum curves

In the previous paragraph, we have considered the system response-time to be independent from the type of experiment, even if the considerations about the striped configurations clearly induce us to think at the opposite. In order to avoid the necessity of express such dependence we can try to minimise the system response time, and, if possible, delete it from the equation. The response time of the system is the consequence of the presence of metastable states, in which the system wonders for a certain amount of time before proceeding towards equilibrium. Therefore, to eliminate t_{res} from the equation, we can build a fictitious simulation in which metastable states are avoided. But, how do we devise such fictitious simulations? Instead of preparing a particular simulation, we can think about the possible outcome. If no metastable states are encountered, the system evolves in the fastest way possible. Therefore, the outcome from such simulations can be considered the minimum curve in the case of the heating experiment and the maximum curve for the cooling experiment, already introduced previously and showed in fig. 4.7. One of the possible strengths of this approach is the reliability of the measurements. By looking at fig. 4.9, we can see that the measurements coming from the maximum curve in the case of the cooling experiment is subjected to a lower variability. Finally, as to eliminate also the residual dependence from t_{res}, we can apply the same procedure presented in the previous paragraph, considering, therefore:

$$T_{c,Eq} = \frac{1}{2}[T_{c4,heating} + T_{c3,cooling}] \tag{4.11}$$

The interpolation considering the data with higher Δt gives an estimation for the equilibrium value of the critical temperature, which in the case of $L = 96$ is:

$$T_{c,Eq} = 2.307 \tag{4.12}$$

This value measured is similar to the results already obtained, even though the estimation error for the intercept is higher. This is consequence of the

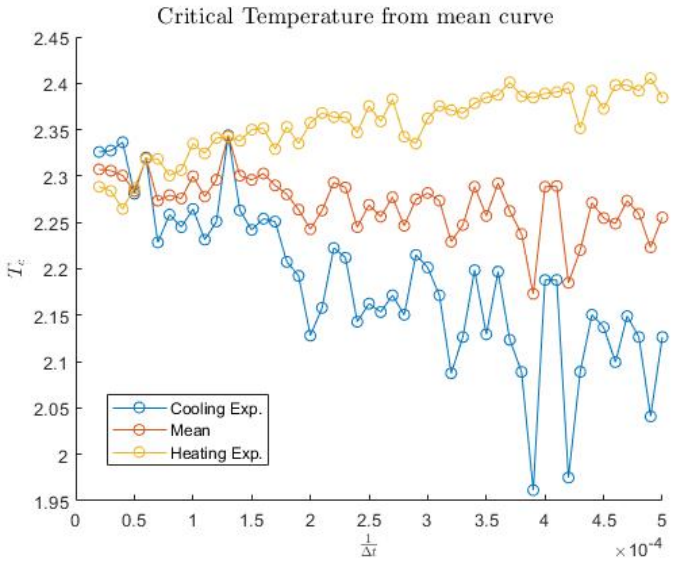

Figure 4.12: Critical temperature behaviour calculated from simulations on system with lateral size $L = 96$.

presence of outliers, as discussed before, that worsen the precision of T_{c3} and T_{c4}.

This chapter explains the potentiality of the Lebowitz algorithm. On one side is able to reproduce the same results obtained from the widely used Metropolis algorithm in equilibrium conditions. On the other side, it enables a new type of analysis that could drastically reduce the time required for a single simulation: moving through out-of-equilibrium states and interpolating the equilibrium behaviour allows quicker simulations. Another aspect relies on the possibility of tracking the system while subjected to time-varying external parameters, which will be the subject of the following chapter.

Chapter 5

Field-induced Dynamic Phase Transitions

As already said in chapter 3, simulations with the Metropolis algorithm, considering Boltzmann dynamics, allow the analysis of the system's equilibrium properties only. Therefore, as an example, the results obtained through Metropolis algorithms in the presence of oscillating external fields possess full physical meaning only if the oscillations period is assumed to be much longer than the relaxation time of the spin system so that the system is allowed to move adiabatically across equilibrium configurations.
With the Metropolis algorithm, a way to follow the evolution of the system while the magnetic field is varied could be done in steps, moving through equilibrium states:

1. The magnetic field is applied.
2. The simulation starts and the system is left free to reach equilibrium.
3. The physical parameters are determined once equilibrium has been reached.
4. The value of the field is changed.
5. Points 2, 3 and 4 are repeated for the entire range of values for the magnetic field we want to explore.

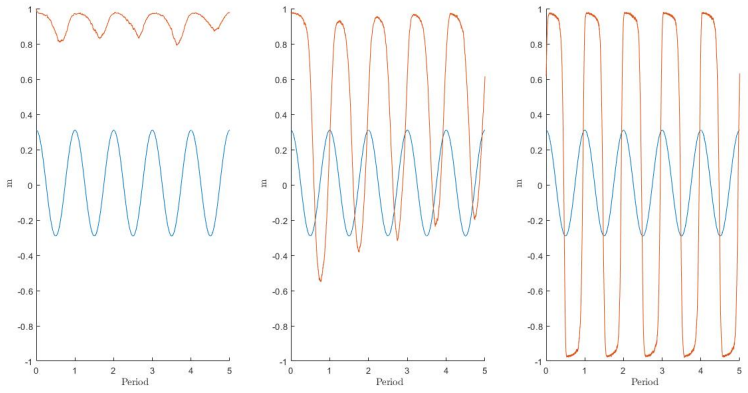

Figure 5.1: Magnetization (orange line) of the system following the oscillation of the magnetic field (blue line). Different conditions are represented, for different values of the oscillating period. From the left: $P = 100; 350; 1000$. Other parameters for the simulation: $H_0 = 0.3$; $H_b = 0.01$; $L = 128$.

This requires a consistent effort in terms of computational time and, in any case, leaves aside the possibility of analysing rapidly varying external fields.

An improvement can be made by considering, instead of the Boltzmann dynamics, the Glauber dynamics, as said in chapter 3. We only have to modify the expressions of the transition rates between states. Now we can follow the evolution between states while the magnetic field varies rapidly, giving physical meaning at the system transition while moving out of equilibrium.

We now consider the presence of a uniform (independent from the position) time-varying external field H applied to the lattice. We will express the field in units of J, exchange constant. Generally, we will consider a sinusoidal dependence:

$$H(t) = H_b + H_0 \sin\left(\frac{2\pi}{P}t\right) \tag{5.1}$$

Fig. 5.1 shows the possible scenarios for a magnetic system subjected to an oscillating field.

Since every spin will gain energy from being oriented in the same direction of the applied field, the lattice magnetization will try to follow as close as possible the field variation. If enough time is provided before the field changes its

sign, we will observe the magnetization following the same time behaviour (as happens in the third panel of fig. 5.1). If the field oscillates too quickly, instead, the system will not have enough time to adapt to the external stimulus: it will fluctuate near the equilibrium shown in the absence of the external magnetic field (as happens in the first panel of fig. 5.1). Different parameters influence which condition we will observe in the system: temperature, field strength and oscillation period on top of them.

The aim of this chapter is the characterisation of some of the properties related to this dynamic behaviour and a deep investigation of when and how the inversion of the magnetization happens. Before proceeding with this analysis, we have to consider problems deriving from the concept of time in the simulation.

5.1 Physical-time in presence of a time varying field

For the Metropolis algorithm, the time parameter regulating the change of the magnetic field can be only the simulation step, as it is the only parameter measuring the advance of time (the execution time of the algorithm cannot represent a reliable parameter, as it may depend on the simulating device and its computational power).
Attaching the *MCSS* in the Lebowitz algorithm would give incorrect results, for the reasons explained in 3.8. Therefore, the key parameter regulating the advance of time for time-varying parameters must be the physical-time.
A first investigation could be focused on the quantification of the relation between physical-time and *MCSS* for the Lebowitz algorithm, now that we add an oscillating field. We want to search for discrepancies with respect to the results found in section 4.1 and to derive information over the system equilibrium condition.

For this purpose, we simulate a period of oscillation of the magnetic field applied over a lattice with lateral size $L = 40$. Temperature is fixed below the critical one ($T = 1.5$), which would induce the unperturbed system in the magnetized equilibrium condition. We can now derive the relation physical-

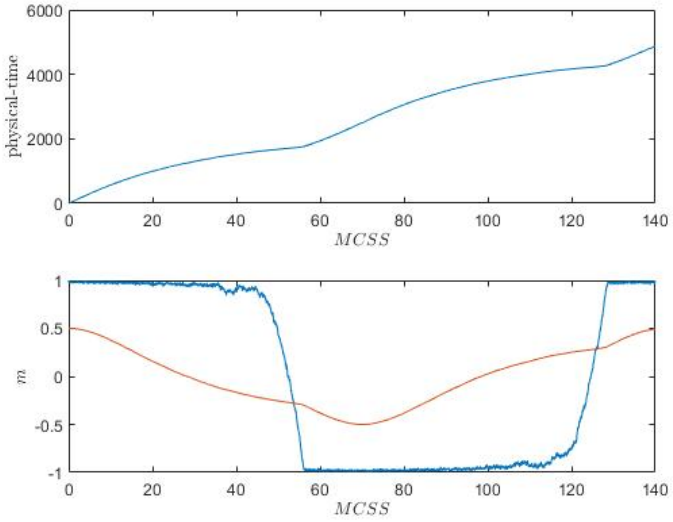

Figure 5.2: The first panel shows the relation physical-time versus *MCSS*. The second panel, how the magnetization (orange line) changes sign while following an oscillating magnetic field (blue line). The period of oscillation is chosen as the allow a complete inversion of the magnetization ($P = 5000$). Other parameters used in the simulation: $H_b = 0$; $H_0 = 0.5$.

time versus *MCSS* and compare it with fig. 4.1. Fig. 5.2 shows the result of the devised simulation. By looking at it, different observations are worth being listed.

- The relation physical-time versus *MCSS* is not linear. Instead, it is periodic with half the periodicity of the magnetic field.
- The tangent to the curve in the top panel has a steeper angle when the system is in the "near equilibrium"condition (i.e. when the magnetic field and the magnetization share the same orientation) and a shallower angle just before the magnetization inversion, where the system is in the "far equilibrium"condition (i.e. when magnetization and field have opposite signs).
- We want the magnetic field to have a sinusoidal time dependence with the physical-time. Since the x-axis is in *MCSS*, and the dependence

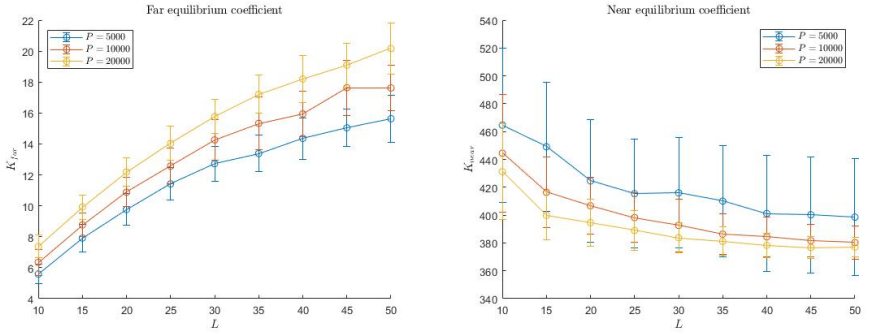

Figure 5.3: T fixed at 1.5. In the right panel "near equilibrium" coefficient; in the left panel "far equilibrium" coefficient for different values of the lattice lateral size. Simulations done for different values of the oscillation period.

physical-time versus *MCSS* is not linear, the magnetic field has a non-sinusoidal dependence with *MCSS*, as can be clearly seen in the first figure. This is emphasised during the inversion of the system's magnetization.

Simulations with variable lattice lateral size and temperature were devised. "Near equilibrium" and "far equilibrium" coefficients were defined as, respectively, maximum and minimum angular coefficient of the tangent to the curve physical-time versus *MCSS*.

From the comparison between fig. 4.2 and 4.3 with 5.3 and 5.4, it is possible to derive the following conclusions:

- Generally, the "far equilibrium" coefficient does not change consistently in presence or absence of an external magnetic field. Moreover, the mismatch between the coefficients reduces while increasing the period of oscillation, suggesting a similarity between the two out-of-equilibrium conditions in absence or presence of a magnetic field when we leave enough time to the system to adapt to the external stimulus.
- The "near equilibrium" coefficient, instead, has a factor of 2-3 of discrepancy. In particular, we have a coefficient with a lower value in the absence of the external magnetic field. In this condition, the transition towards equilibrium takes more steps when the system is near

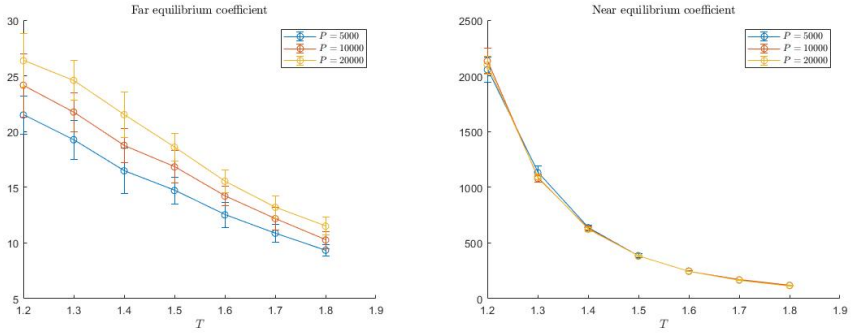

Figure 5.4: L fixed at 40. In the right panel, the "near equilibrium"coefficient; in the left panel, the "far equilibrium"coefficient for different values of the system temperature. Simulations executed for different values of the oscillation period: $P = 5000; 10000; 20000$.

to it. This makes perfect sense: the application of a magnetic field fights back the thermal fluctuations. This latter, near equilibrium, is the main element that slows down the transition toward equilibrium.

- The graph, independently from the presence or the absence of the magnetic field seems to show the same dependency from T and L.

As previously anticipated, particular attention is required when a simulation is devised: if not enough *MCSS* are provided before the conclusion of a period of the magnetic field, we could fail to simulate the correct behaviour of the system. This becomes a crucial aspect when considering Hysteresis Loops, something that will be studied more in-depth in one of the following chapters. As a safety rule, we can consider "reliable"the results coming from a simulation in which in a period of oscillation, at least one *MCSS* lasts. In order to understand the limits for the simulation parameters, fig. 5.5 should be considered, representing the number of *MCSS* per period for different choices of the simulation parameters. A shallow dependence from the system size is shown, which tends to set constant for high system size. The period of oscillation, as one can expect, influences heavily the outcome: if P decreases, also the number of *MCSS* decreases. The real problem emerges in the case of small periods and low T. This can lead us to the "danger zone".

Before any simulation, the "at least one *MCSS*"condition must be checked.

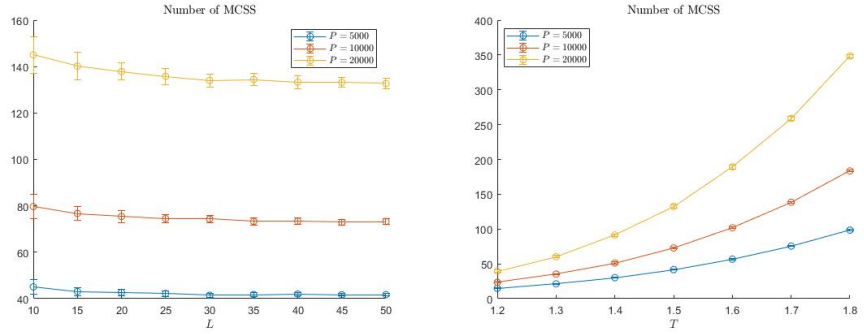

Figure 5.5: Plots of the number of *MCSS* per period for different system sizes and temperatures. Different curves refer to different periods of oscillation: $P = 5000; 10000; 20000$.

This is implicitly verified in the following simulations.

5.2 Magnetic systems in presence of an oscillating field

Once seen the general behaviour of the magnetization following a sinusoidal field and how the physical-time enters into play, we can deepen the analysis and try to derive and compare the results obtained from our algorithm with the ones from the standard Metropolis algorithm. Before proceeding, a brief review of the theoretical aspects related to the Ising model subjected to an oscillating field is presented.

5.2.1 Magnetization general behaviour

The two different behaviours illustrated in fig. 5.1 can be defined more precisely as follows:

- When the magnetization follows the magnetic field with only a time delay, the system is said to be in the Dynamic Disordered Phase (DDP).

In this regime, the magnetization function of time is such that

$$\langle m(t)\rangle = -\langle m(t + \frac{P}{2})\rangle \tag{5.2}$$

where P is the period of the field and $\langle m(t)\rangle$ indicates the ensemble average of the magnetization. Its behaviour is represented in the left panel of fig. 5.6. In this dynamic phase, the average magnetization per cycle defined as:

$$Q = \frac{1}{P}\int_0^P \langle m(t)\rangle dt \tag{5.3}$$

takes null value.

- When, instead, the magnetization remains trapped near one of the two equilibrium states and fluctuates around it, the system is said to be in the Dynamic Ordered Phase (DOP). The magnetization does not share the same property in equation (5.2). Instead, in the DDP, if we define as $m^+(t)$ the magnetization of the system fluctuating near the positive equilibrium state and as $m^-(t)$ the one fluctuating near the negative equilibrium state, it is verified:

$$\langle m(t)\rangle^+ = -\langle m(t + \frac{P}{2})\rangle^- \tag{5.4}$$

Its behaviour is represented in the right panel of fig. 5.6. Moreover, we have $Q \neq 0$.

To distinguish the two dynamical phases and study the phase transition, one can consider one of the two order parameters Q or $m_0(t) = \frac{1}{2}[m^+(t) + m^-(t + P/2)]$, both becoming null in the DDP and different from zero in the DOP. For practical simulations, a reliable way to determine which phase the system shows can be achieved by a histogram representation of a series of Q: in the DOP we expect two deltas (or even just one) peaked around the values ± 1, indicating that the system is trapped in one of the two magnetized equilibrium states; on the contrary, in the DDP we expect only one peak around the value 0. Fig. 5.7 shows the two expected behaviours.

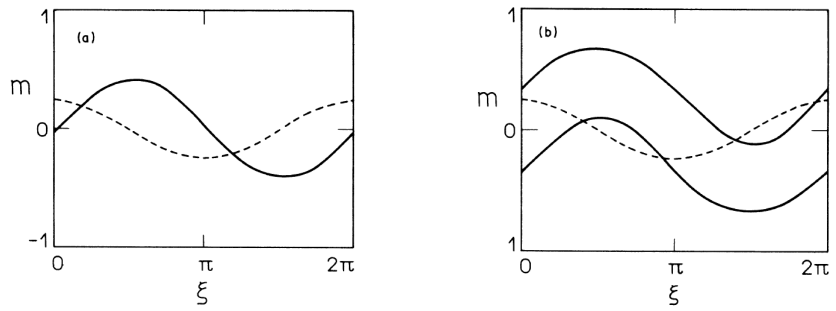

Figure 5.6: Plots of the magnetization function of time in both the DDP (left panel) and DOP (right panel) conditions. In the latter case, both $\langle m(t)\rangle^+$ and $\langle m(t)\rangle^-$ are shown. The dotted line represent the sinusoidal magnetic field; ξ is the time parameter. Source [13].

5.2.2 Dynamic Phase Transition

The transition between the two phases is regulated by the field strength H_0 and its period P, the temperature T and the system size L. The transition is of the second-order [14], in contrast with what has been predicted first and then observed in the earlier works on the topic. Indeed, it has been found that the order parameter Q varies with continuity from the two different values that it assumes in the ordered and disordered phases, as shown for a specific set of parameters in fig. 5.8. It must be noted that this type of transition is different from the ones usually considered for the equilibrium model since also the period of oscillation can induce the system to move from one phase to the other, not only temperature. The clues on the first-order transition were only due to the finite-size effect of the system, which becomes negligible when the size L of the system is sufficiently increased. Moreover, the second-order phase transition possesses the same exponent of the 2D equilibrium transition for a bi-dimensional Ising Model [15].

The most reliable way to determine the critical dynamical conditions derives from the analysis of the Binder cumulant [16], or fourth-order cumulant, defined as:

$$U = 1 - \frac{\langle Q^4 \rangle}{3\langle Q^2 \rangle^2} \tag{5.5}$$

Near the critical point, the Binder cumulant satisfies the finite-size scaling

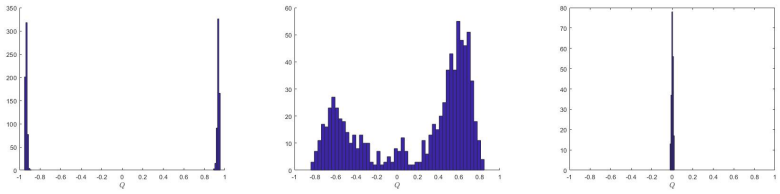

Figure 5.7: Histogram plots of the average magnetization per cycle Q, for different values of the oscillation period: $P = 50; 270; 400$. From left to right: DOP; transition between the two phases; DDP. The DOP was obtained by superimposing two simulations starting from different opposite magnetization conditions. The first 200 periods were discarded as to let the system reach steady-state condition. Other parameters for the simulation: $T = 0.8 \cdot T_c$, $L = 64$, $H_0 = 0.3$.

property [15]:

$$U(L, T) = b(\epsilon L^{\frac{1}{\nu}}) \tag{5.6}$$

where $\epsilon = (T - \theta_c)/(T)$ and $\nu = 1$ is a critical exponent dependent on the considered phenomena. Here, we define θ_c to be the dynamical critical temperature, in the same fashion as the thermodynamical critical temperature T_c, even though they represent different phenomena. We can consider the following parallelism: if $T < T_c$ the system favours the ordered phase (ferromagnetic); if $T > T_c$, the favoured phase is the disordered one (paramagnetic). Similarly, for a given couple (P, H_0), if $T < \theta_c$ the system favours the ordered dynamical phase (DOP); if $T > \theta_c$ the DDP is favoured. From now on, we will refer to T_c by the term "thermodynamical critical temperature"; to θ_c by the term "dynamical critical temperature". Moreover, we will refer to "Thermodynamical Phase Transition"(TPT) as the ferromagnetic-paramagnetic phase transition and to "Dynamical Phase Transition"(DPT) as the DOP-DDP phase transition.
Back to the Binder cumulant, by measuring the dependence of U from T for different values of L, it is possible to derive the dynamic critical temperature θ_c by interpolating the crossing point of all the curves. The Binder Cumulant method can also be rearranged in order to determine also the critical period P_c for fixed values of T and H_0, through simple interpolation.
Nevertheless, a different and more accessible way for a first estimation of the critical period involves a different property of the system: the metastable lifetime parameter τ. It is defined as the time required for a system completely

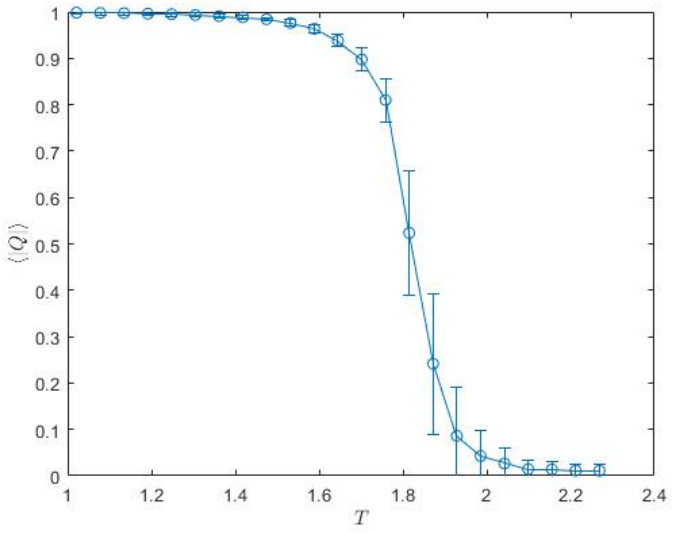

Figure 5.8: plot of the order parameter Q for different values of the temperature, obtained from simulations with Lebowitz algorithm. Simulations details: $L = 100$; $P = 258$; $H_0 = 0.3$; $H_b = 0$.

positively magnetized, subjected to a negative field, to invert the magnetization. Practically speaking, it is taken as the time which passes before the crossing of the $m = 0$ magnetization line. τ gives a clear indication of the intrinsic time possessed by the system. It is natural to relate the metastable life time with the field oscillating period P, or better, the semi-period $P_{1/2}$. If τ is larger than the semi-period, is impossible for the system to change the magnetization accordingly to the external field. Therefore, when $P_{1/2} < \tau$, the system is in the DDP. Vice versa, when $P_{1/2} > \tau$, the system reacts sufficiently fast as to follow adequately the inversion of the field. Therefore, it is reasonable to assume $P_c \approx 2\tau$.
It must be pointed out that this methodology gives just an estimation of P_c. Indeed, since the progression of the physical-time changes substantially depending on how much the system is out of equilibrium, applying an oscillating field has different effects if compared to a sudden reversal of the field.

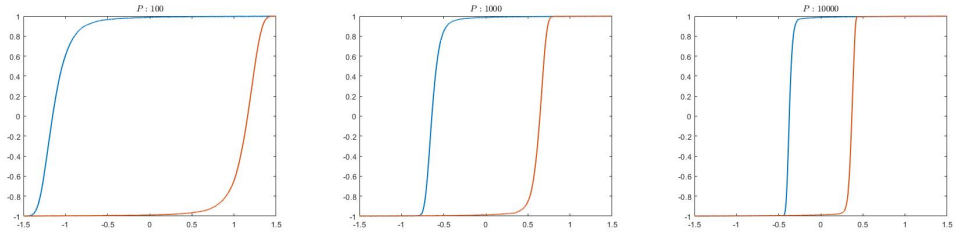

Figure 5.9: Plots of one hysteresis loops resulting from a simulation for a system with lateral size 100, averaged over 10 cycles, with period $P = 10; 100; 1000$. It can be noted that in these conditions the system is always in DDP since the magnetization changes from -1 to $+1$ and the cycle is centred in the origin ($\langle Q \rangle = 0$). The system is prepared completely negatively magnetized. A linear field is applied and the magnetization is tracked. The blue line represents the initial swept from -1.5 to 1-5, the orange line the conclusive swept from 1.5 to -1.5. Increasing the period means that the magnetization is able to follow more closely the magnetic field. As a consequence, the hysteresis loop shrinks. T fixed at $0.8 \cdot T_c$.

5.2.3 Hysteresis loop characterisation and properties

An interesting behaviour emerges if the magnetization is plotted against the applied magnetic field. What results is a hysteresis loop, coming from the presence of time lag between the two physical quantities, as represented in fig. 5.9.

The already introduced Q parameter here represents the "centre of the loop", indicating the centre of mass around which the magnetization oscillates.
Therefore, for what said above, while the system is in DDP, the hysteresis loop is expected to show a symmetric shape independently from the initial condition; if the system is in DOP, instead, the hysteresis loop becomes asymmetric and is centred in different positions depending on the initialisation condition.
The transition from DOP to DDP can be achieved simply by modifying the temperature of the system or the strength of the magnetic field. This also allows to modify the shape of the loop, its area and its orientation. These quantities can be derived from the simulations. The most studied property, also for its straightforward derivation, is the loop area, defined by the rela-

tion:

$$A = \int_0^P \langle m(t) \rangle dh(t) \tag{5.7}$$

The area allows a different way to estimate the dynamical critical temperature θ_c. Indeed, it shows finite-size scaling properties after $T = \theta_c$ and the temperature derivatives dA/dT has a minimum at $T = \theta_c$ [15].
The loop area has been extensively studied also from the point of view of the scaling behaviour with field (h_0), frequency ($\omega = 1/P$) and temperature (T). In particular, it has been derived the following relation [17]:

$$A \sim h_0^{\alpha} T^{-\beta} g(\frac{\omega}{h_0^{\gamma} T^{\delta}}) \tag{5.8}$$

where

$$g(x) = \frac{x^{\epsilon} e^{-x^2}}{\sigma} \tag{5.9}$$

with α, β, γ, δ, ϵ, critical exponents. In the limit of $\omega \to 0$, i.e. for high values of the period, the scaling relation reduces to a simple power-law:

$$A \sim h_0^a \omega^b T^{-c} \tag{5.10}$$

with $a = 0.70$, $b = 0.36$ and $c = 1.18$ for the bi-dimensional Ising model.
Other properties that allow us to derive information over the system, coming from the analysis of the hysteresis loop, are the coercive field and the DC magnetic susceptibility, defined as follows:

- Coercive field: value of the magnetic field when the magnetization crosses the $m = 0$ line.
- DC magnetic susceptibility: slope of the tangent to the hysteresis loop while the magnetization crosses the $m = 0$ line.

$$\chi = \left. \frac{\partial m}{\partial H} \right|_{H=0} \tag{5.11}$$

In particular, from the DC magnetic susceptibility, one can derive an estimation of the thermodynamical critical temperature T_c considering the Curie-Weiss law:

$$\chi = \frac{K}{T - T_c} \tag{5.12}$$

while sampling the tangent in the temperature range: $T > T_c$.

5.2.4 AC magnetic susceptibility

In the previous section, we have considered the DC magnetic susceptibility even if we are applying an oscillating magnetic field. This can be justified by the fact that, for $T > T_c$, the magnetization is able to follow the magnetic field without any time lag (the area of the loop shrinks to 0). In this condition, when the magnetization crosses the $m = 0$ line (i.e when $H = 0$), we reproduce the same condition as if the magnetic field was not oscillating. Therefore, by considering the derivative of the magnetization with respect to the field, we obtain the DC magnetic susceptibility.
Instead, when either the temperature or the period of oscillations decreases, the magnetization will lag behind the magnetic field but still producing a periodic function with the same period. The derivative does not give back the DC magnetic susceptibility since we cannot define it in these conditions. Fortunately, we can rely on something similar. From the analysis and comparison between the shapes of the two functions, it is possible to study the AC magnetic susceptibility defined as:

$$\chi_{AC} = \chi^{'} - i\chi^{''} \tag{5.13}$$

where

$$\chi^{'} = \frac{m_0}{h_0}\cos\left(\frac{2\pi}{P}\tau_{eff}\right) \tag{5.14}$$

$$\chi^{''} = \frac{m_0}{h_0}\sin\left(\frac{2\pi}{P}\tau_{eff}\right) \tag{5.15}$$

Here m_0 and h_0 represent the amplitudes of the magnetization and magnetic field, and τ_{eff} their phase lag. The temperature behaviour of these components allows retrieving the critical temperature for a fixed choice of h_0 and P. Indeed, as it happens for all the second-order phase transitions, the real and

imaginary parts of the susceptibility (in this case AC, explicitly considering the dynamic phase transition) show a different behaviour: $\chi^{'}$ shows a dip, while $\chi^{''}$ a sharp peak at θ_c. In the following, we will study the AC magnetic susceptibility for the dynamic phase transition and the DC magnetic susceptibility for the thermodynamic phase transition.

5.2.5 Magnetization inversion mechanism

The inversion process of the magnetization follows always three steps:

1. (Nucleation) Under the effect of an external field, a first nucleation of spins is formed, randomly positioned in the lattice.
2. (Growth) The nucleated region expands, by embodying the neighbouring spins.
3. (Coalescence) Growing regions merge together.

The completion of the process determines in which dynamic phase we found the system: if the nucleation is able to spread over all the lattice (or most of them, depending on the equilibrium condition), then the system is in the DDP; on the contrary, if the process has not enough time to complete before the inversion of the external field, the system is in the DOP.
Two behaviours can be noted, depending on the size of the system L and on the amplitude of the applied magnetic field H_0. Right now, we consider the effect of L, assuming a fixed value of H_0. If L is sufficiently big, the nucleation process can start independently in different regions and rapidly spread over all the lattice through coalescence. Conversely, if L is small, the inversion is more often achieved through the growth of one nucleation centre since the system size is appropriate only for hosting one of it. These two behaviours are respectively defined as Multi Droplet (MD) and Single Droplet (SD) inversion mechanism and are represented in fig. 5.10.

This affects the stochasticity of the inversion mechanism: since the nucleation takes place at random in the structure and with a certain probability in time, a single droplet in the structure produces a rather unpredictable behaviour.

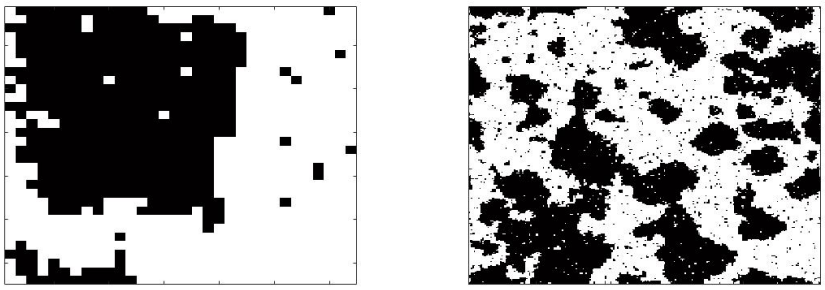

Figure 5.10: Snapshots of two lattices with lateral size of 32 (in the left panel) and 256 (in the right panel) while changing the orientation of the spins from up to down (images taken after the crossing of the $m = 0$ line, following an oscillating field). Black colour represents spins oriented down; white colour represents spins oriented up. We can notice that the smaller system presents only one black region from which the inversion mechanism is proceeding and, therefore, is classified as SD. Differently, the system with a larger dimension shows many inversion points and is classified as MD.

Instead, more nucleation centres reduce variability, due to a sort of averaging effect. While lattices with greater lateral size (in the MD region) show a deterministic behaviour, the smaller ones (in the SD region) produce bursty magnetization cycles. This effect can be clearly seen while following the magnetization in the presence of an oscillating field, as plotted in fig. 5.11.

Droplet theory explains well the dynamic phase transition experienced by the bi-dimensional Ising model. Within this theory, other than the Single Droplet and Multi Droplet regions, Coexistence and Strong Field regions are defined, respectively in the limit of strong field or high system size and weak field or small system size. Fig. 5.12 gives a graphical (not in scale) representation of all the regions and where they are localised in the (H, L) plot. For the scope of this work, only MD and SD will be taken into account. Also, when we consider the deterministic (stochastic) regime, we always refer to the MD (SD) region.

A way to determine if the system is in the SD or the MD regime involves the measurement of the stochasticity of the system time-properties. For example, we can consider the metastable lifetime (τ) already introduced. Its standard

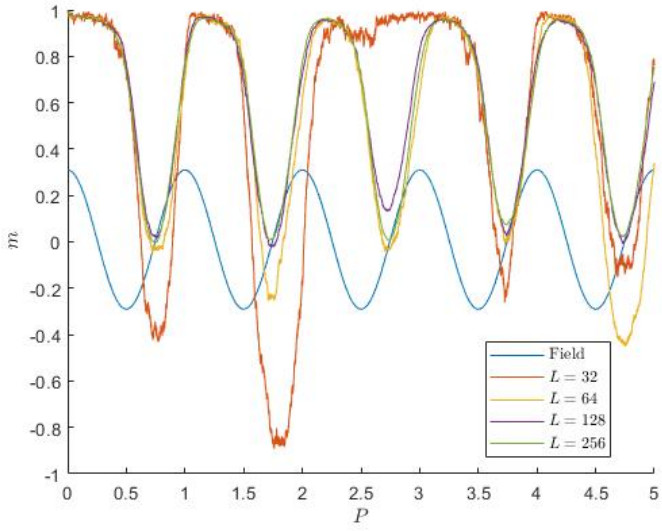

Figure 5.11: Plot of five periods of oscillation for lattices with different lateral sizes. The blue line represents the common magnetic field. For smaller systems, the stochasticity is evident, as much as the deterministic behaviour for the larger ones.

deviation (σ_τ), derived after many measurements, gives a clear indication about the system condition: a high value means that the measurements have high variability and that the system is in the stochastic region; a low value, instead, indicates that the system is in the deterministic region since all the measurements have a similar value. In particular, if:

$$V = \frac{\sigma_\tau}{\langle \tau \rangle} < 0.5 \tag{5.16}$$

then a deterministic behaviour is expected and the system is in the MD regime.
For the metastable lifetime, we consider a static field H. In order to make the analogy to the case in which we are applying an oscillating magnetic field with amplitude H_0 (for the study of DPT), we will have to compare different values of the magnetic field. In particular we will consider the equivalence $H = 1/\sqrt{(2)}H_0$.
Since the metastable lifetime depends on the intensity of the field H and on the lateral system size L, we expect the separation between the MD and the

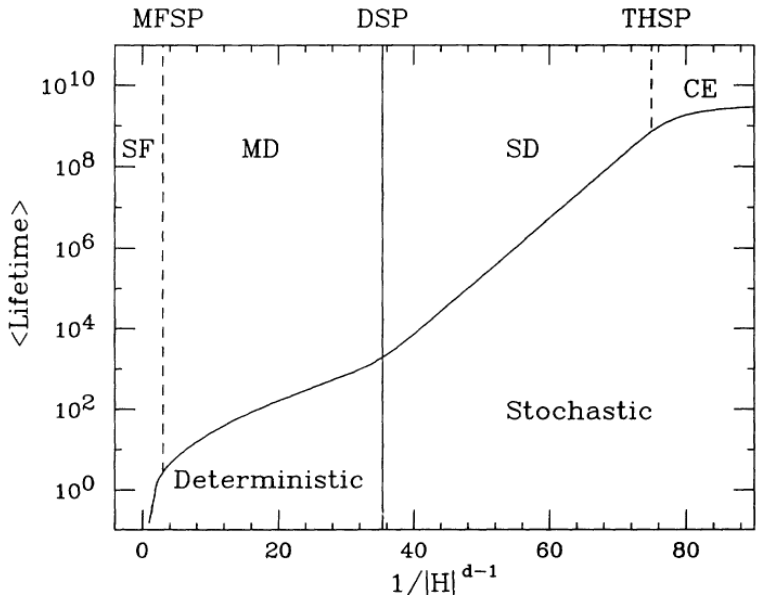

Figure 5.12: Map of the different regions representing the system behaviour, depending on the applied field. The figure is not in scale and is derived for a fixed value of L. In the left part, the deterministic region, in the right part, the stochastic region, separated by the so-called spinodal line. The deterministic region is divided into Strong Field (SF) and Multi Droplet (MD) region; the stochastic region, instead, into the Single Droplet (SD) and the Coexistence (CE). Source .[18].

SD regions to be defined by a line in the (L, H) plane. This line takes the name of "dynamic spinodal line"(or simply spinodal line) and it can be found by imposing $V(H, L) = 0.5$. In practical conditions, imposing $V(H, L) = 0.4$ or $V(H, L) = 0.6$ does not change consistently the position of the spinodal line since the transition from SD to MD regions happens in a narrow range of values.
Rikvold *et al.* [18] derived the following relation describing the spinodal line:

$$H_{DSL} \sim \ln(L)^{-\frac{1}{D-1}} \tag{5.17}$$

in the limit of weak field. Since we are considering a bi-dimensional system, the dimension D is 2 and we expect $H_{DSL} \sim \ln(L)^{-1}$. This result has been derived from droplet theory, which considers the interplay between the different length scale characterising the inversion mechanism: the system size;

the droplet radius; the mean droplet separation (average radius of a droplet before it becomes likely to meet another).

5.2.6 Effect of bias magnetic field

Thus far, no bias field H_b superimposed to the oscillating component has been considered. This allows the system to retain a sort of symmetry, not showing any preferential direction for the magnetization to be. Instead, in the presence of an external bias, the magnetization will modify its behaviour. Let us consider a ferromagnetic system in the DDP and the presence of an oscillating field superimposed to a weak positive bias field. In this condition, the magnetic field is more intense when has positive value and the system, while oscillating, will experience different free energies related to the two magnetized equilibrium state. The positive magnetization condition will be favoured if compared to the negative one. This brings consequences to the behaviour of $\langle Q \rangle$. By deepening the analysis, it can be shown that H_b can be considered the conjugate field of $\langle Q \rangle$ [19]. This was derived by considering the analogy between H_b (bias field over an oscillating one) and H (static field) for the DPT and the TPT near the critical point. They share the same critical exponent $\delta = 3$ when related to the order parameter (respectively $\langle Q \rangle$ and M). As analogous to the temperature in the thermodynamical case, we have to consider the period of oscillation P in the dynamical case.
The analogy between the TPT and the DPT can be discussed comparing the $\langle Q \rangle(P, H_b)$ and $M(T, H)$ plots, as extensively discussed by Reigo *et al.* [20]. Note that we refer to H_b as the bias field superimposed to an oscillating field with amplitude H_0 for the dynamical case; with H to the DC field in the thermodynamical case. Despite at first glance the two behaviours seem to be completely equivalent due to the presence of a critical point separating continuous from discontinuous transition of the order parameter, important differences emerge while comparing the behaviour of $\langle Q \rangle$ and M for $P > P_c$ and $T > T_c$. To further proceed in the analysis one can compare and discuss the fluctuations and the susceptibilities, namely:

$$\sigma_Q = \sqrt{\langle Q^2 \rangle - \langle Q \rangle^2} \tag{5.18}$$

$$\chi_Q = \frac{\partial \langle Q \rangle}{\partial H_b} \tag{5.19}$$

in the dynamical case, and

$$\sigma_M = \sqrt{\langle M^2 \rangle - \langle M \rangle^2} \tag{5.20}$$

$$\chi_M = \frac{\partial \langle M \rangle}{\partial H_b} \tag{5.21}$$

in the thermodynamical case.
It has been shown [20] that above P_c, $\chi_Q(H_b)$ behaves differently from its analogous $\chi_M(H)$ above T_c, especially when $H_0 \to 0$. The former presents side-bands (symmetrical peaks at non-zero value of H_b), the latter only a wide maximum for $H = 0$, as represented in fig. 5.13. This provides a strong argument for the distinction between the two phenomena when moving out of the critical point. What we can still consider is the equivalence of the two phenomena only in the vicinity of the critical point and in absence of external bias, since it was shown that the DPT belongs to the equilibrium Ising universality class [21].

In the following sections we will present the results obtained from our simulations by considering the Lebowitz algorithm with Glauber dynamics. The remaining part of the chapter aims at gaining more insight over the cited theoretical aspects and understand if significant discrepancies can be found once our results are compared to the ones derived considering the standard Metropolis algorithm with Glauber dynamics.

5.3 Critical conditions for the Dynamic Phase Transition

In this chapter, we aim to reproduce the magnetization behaviour in the presence of an external magnetic field in different conditions (DOP and DDP). We start with a qualitative investigation and, then we proceed with a quantitative analysis that could allow us to find agreement or discrepancy about the known behaviour studied with the standard Metropolis algorithm.

As to derive a qualitative indication of the DPT, the following simulation is devised:

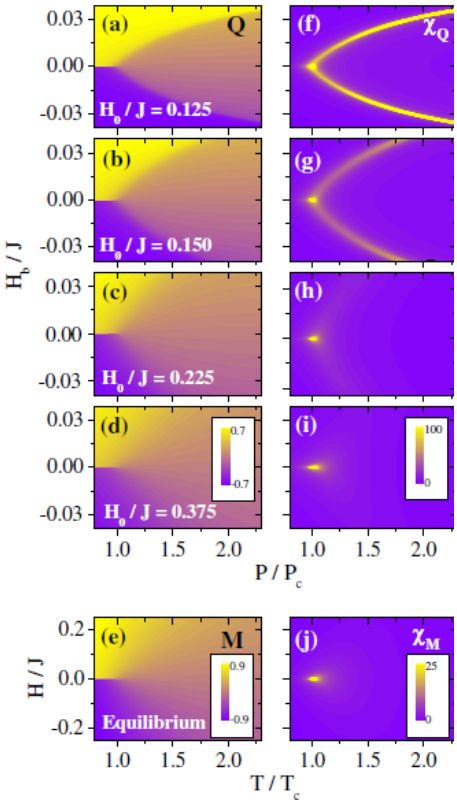

Figure 5.13: Different colours refers to different intensities. In the upper block of subplots $\langle Q \rangle$ on the left and χ_Q on the right are represented, for different intensity of the oscillating field, function of H_b and P. In the bottom row, the behaviour of M and χ_M function of H and T. It can be noted that, while H_0 increases, the condition become equivalent to the equilibrium one. If instead, we consider smaller H_0, χ_Q shows two side-bands originating from the critical point (yellow dot in most of the left column sub-plots) and we lose the equivalence between $\langle Q \rangle$ and M. Source [20].

1. A lattice with random initialisation of the spin orientation is left free to evolve, at fixed T, following a sinusoidal external field with amplitude H_0.

2. The mean magnetization per cycle is derived considering a discrete version of formula (5.3):

$$\hat{Q} = \frac{1}{P} \sum_i m_i \Delta t_i \tag{5.22}$$

   where m_i and Δt_i represent respectively the magnetization and the physical-time increase at the i-th step of the simulation. $\hat{Q}$ is computed for a total of 400 cycles, as to derive a good approximation of $\langle Q \rangle$.

3. Step 2 is repeated, for a fixed T, while H_0 is varied from 1 down to 0 (without re-initialisation of the lattice).

4. Temperature is changed and the lattice is re-initialised completely random.

5. The previous steps are repeated for the temperature range that we want to investigate.

At the end of the simulation, we can derive a qualitatively map representing the conditions in which the system shows a DOP (where $\langle Q \rangle \approx 1$) or a DDP (where $\langle Q \rangle \approx 0$). From it, we can have a clear indication over the critical line in the $(H_{0,c}, T_c)$ plot, for a fixed choice of P. Repeating many times the measurements for different choices of P, we can completely characterise the dynamic phase transition line. For this simulation, a system with lateral size $L = 100$ was chosen, to put the system in the less stochastic MD region. Results for $P = 100$ and $P = 400$ are represented in fig. 5.14. As one can notice, the transition region seems to be well defined. The value of the oscillation period does not influence the critical line for $H_0 \to 0$: as we can expect, even if the field is varied slowly, the system remains magnetized if the field has low intensity. What is affected, is the behaviour at high H_0 and low T: only an oscillating field with low frequency can induce the system to invert magnetization since it gives the system enough time to react; instead, if the temperature is increased, the stable region for the DOP reduces. Thermal fluctuations can induce the system to follow better the magnetic field since

the spins are less reluctant to align against the neighbours and then start the inversion.

Out of curiosity, simulations were run also with the system initialised in the completely magnetized configuration. In this case, in Step 3, H_0 is changed from 0 up to 1, backwards with respect to before. This was done to investigate the properties of the phase transition. Indeed, in the original work over the DPT by Tomé *et al.* [13], it was shown the possibility for the system to have, in a specific region in the (H_0, T) plane, an overlap between the DOP and the DDP, as shown in fig. 5.15.

In this region of the plane, the dynamical phase showed by the system would be related to the initialisation condition: if random, the DDP would appear. If magnetized, DOP.
The simulation was devised such as to favour one of the two phases at a time. If the system is initialised at random, the system will automatically be in the DDP. Starting from $H_0 = 1$ and swinging it back to 0, we hope to preserve DDP as much as possible. Same in the opposite condition. If the system were to show this particular behaviour we would notice a difference between the two maps. Instead, comparing from the simulations, we notice that the two maps completely overlap. This is in accordance with what found in more recent works, where the DPT is demonstrated to be a second order phase transition without any bi-modal regime.

If we want to get quantitative results, we have to consider the Binder cumulant. As said, this technique allows deriving the dynamical critical temperature θ_c for a given pair of values of magnetic field and oscillation period. In our case, mostly for quantitative comparison with known theoretical results, we have decided to derive θ_c for $H_0 = 0.3$ considering both $P = 400$ and $P = 258$. In the simulation, after initialisation of the lattice completely magnetized, a sinusoidal magnetic field is applied for 10000 cycles. Then the temperature is increased and the field is applied again for other 10000 cycles. The whole procedure is repeated for a specific temperature range and different lattice dimensions $L = 64; 128; 192; 256$. From the intersection point between all the Binder cumulant lines, we can estimate θ_c. The results are shown in fig. 5.16. For $P = 258$, we found $\theta_c = 1.812 = 0.798 \cdot T_c$; for $P = 400$, instead, $\theta_c = 1.717 = 0.757 \cdot T_c$. In the second case, the estimation is more complex to derive since there are multiple intersection points in the

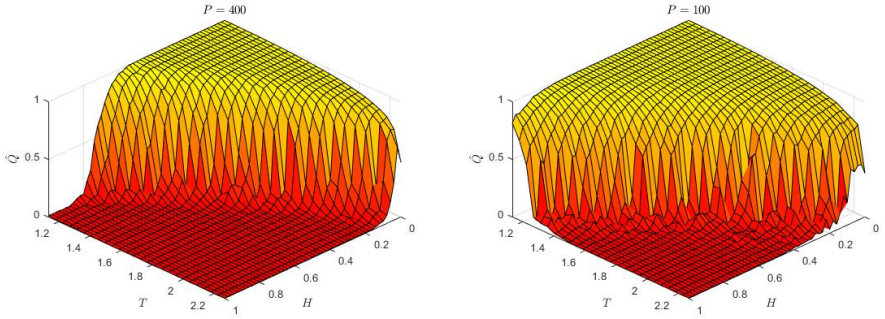

Figure 5.14: Maps representing the conditions (in terms of field intensity and temperature) in which the system shows the DOP or the DDP. In particular, the value of $\hat{Q}$ is calculated. Where $\hat{Q} \approx 0$ (1), the system show a DDP (DOP), which happens for high (low) T and high (low) H_0. In the left panel, $P = 400$. In the right panel $P = 100$.

Binder cumulant lines over a range of 0.02. An average of all the intersection values is considered.

The estimated values happens to be in accordance with what derived from other works ([22] [21]), where $\theta_c \approx 0.8 \cdot T_c$ for $P = 258$. Moreover, also the crossing happens near the theoretically estimated value of $U^* \approx 0.61$ (with more precision in the case of $P = 258$). This demonstrates how the whole approach can give comparable quantitative results to ones derived from the Metropolis algorithm. Even if we are considering a physical-time estimate, instead of the *MCSS*, no relevant differences can be found for $P = 258$.

5.4 Spinodal line: more on magnetization inversion mechanism

As previously anticipated, the spinodal line determines the separation between the MD and the SD region in the (L, H) plane. To understand in which regime the system is before the actual simulation, has a major importance, since it can influence the stochasticity of our results. For this purpose, a simulation can be devised as to derive the spinodal line. It is structured in

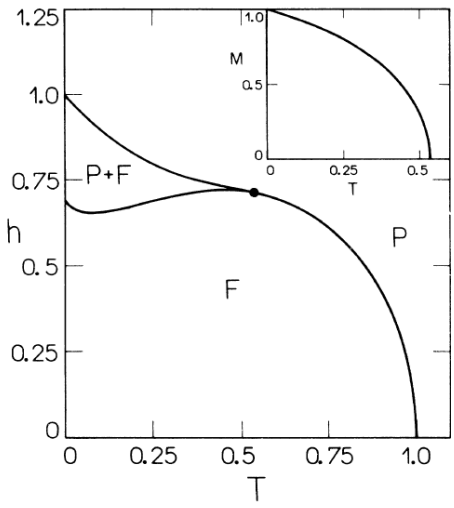

Figure 5.15: Behaviour of the system in the (H_0, T) plane. The "F"label indicates that the system is in the DOP; the "P"label indicates that the system is in the DDP. The mixed region, "P + F"corresponds to a bi-phase region. Depending on the starting conditions, the system remains in DDP or DOP. The map is derived from theoretical calculations. Source [13].

the following way:

1. The system is initialised with a fixed L.
2. $\langle\tau\rangle$ is calculated for 50 repetitions of the experiment. This allows the measurement of its mean and standard deviation and the derivation of the dimensionless parameter V following equation (5.16).
3. Depending on the value of V the lattice size is modified as to approach the value 0.5: if $V < 0.5$, L is decreased; if $V > 0.5$ L is increased.
4. After the crossing of the 0.5 value, the system size for which $V(L^*) = 0.5$ is interpolated considering a linear dependence:

$$L^* = L_{below} - \frac{0.5 - a_1}{a_2 - a_1} \tag{5.23}$$

where L_{below} is the system size just before the crossing of $V = 0.5$ line,

$$V(L_{below}) = a_1$$

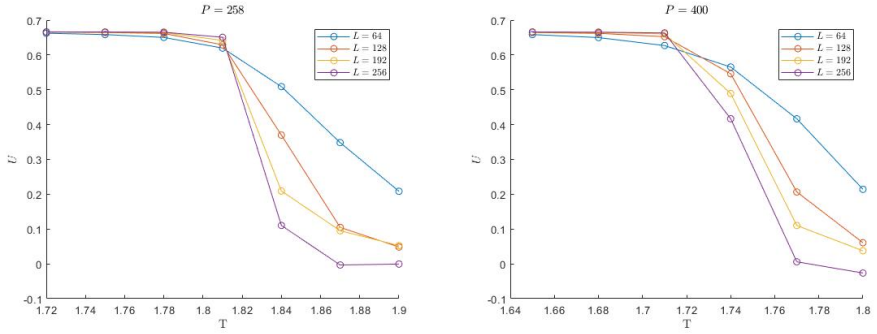

Figure 5.16: Binder cumulant derivation. U is derived for 4 system with different lateral size $L = 64; 128; 192; 256$. In the left panel, $P = 258$. In the left panel, $P = 400$.

and

$$V(L_{below} + 1) = a_2$$

.

5. Points 1-2-3-4 are repeated for different intensities of the applied magnetic field H as to derive the spinodal line for the desired interval.

The derivation of the spinodal line requires the estimation of metastable life time, which is dependent on the particular choice of L and H. τ can be achieved through the following simulation:

1. The system with fixed L is prepared completely magnetized, for a choice of $T < T_c$.
2. For $t = 0$, an external field with reverse sign with respect to the orientation of the system magnetization is applied.
3. The physical-time elapsed before the magnetization crosses the $m = 0.5$ line is taken as the metastable lifetime.

A first investigation has been done with the purpose of determining the effect over τ of the lateral size L of the system and the magnetic field applied H.

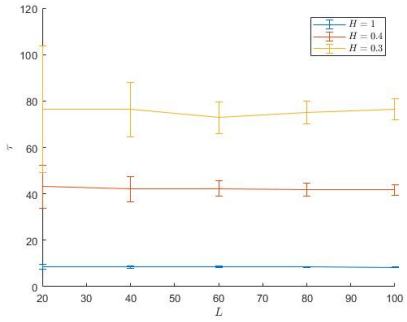

Figure 5.17: Metastable lifetime function of the system lateral size L for different choices of the magnetic field H.

Results of the simulation are reported in the table 5.1. See also fig. 5.17 for a graphical representation for different H.

Metastable Lifetime			
L	$H = 0.3$	$H = 0.4$	$H = 1$
32	74 ± 6	40 ± 2	8.4 ± 0.2
64	73 ± 2	42.5 ± 0.8	8.4 ± 0.1
128	76 ± 1	42.0 ± 0.8	8.40 ± 0.06

Table 5.1: Table for equilibrium Metastable Lifetime.

By looking at the confidence intervals, we can assume τ to be independent from the lattice size. This observation has been also demonstrated by Sides *et al.* [22]. This characteristic becomes particularly helpful while calculating the V parameter for the derivation of the spinodal line. As clearly observable, in accordance with the stochasticity showed by small systems, the standard deviation happens to decrease strongly while increasing the lattice size. This introduces errors in the estimation of the mean value of the metastable time while diminishing L. A way to avoid this problem could be achieved by calculating, for a specific value of H, the mean value of τ for a system with a relatively large size (in our case $L = 256$) to make a more precise estimation. This value is considered as the reference for all the smallest systems.
Finally, following the previous procedure, the spinodal line can be derived. Fig. 5.18 shows the result: below the line, the system is in the SD regime;

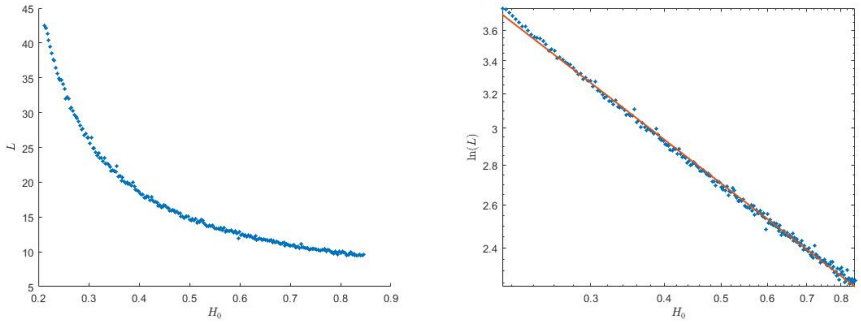

Figure 5.18: Spinodal line, derived by imposing $V(H, L) = 0.5$ and iterating over many values of H. The quantization of L has been broken by considering a linear interpolation as illustrated in equation (5.23). In the left panel, it can be appreciated the separation between the MD and SD regimes in the (L, H) plane. Error bars are of the same size as the marker used for the data representation (not showed). In the right panel, with logarithmic axes, the linear interpolation proving the relation (5.17).

above the line, the system is in the MD regime. As to verify the relation (5.17), a linear regression is performed between $\ln(L)$ and H in a log-log plot. The linear regression suggested good agreement ($R^2 = 0.998$) even though the exponent has been found to be -0.366 instead of -1. Deepen in the reasons for such discrepancy eludes the focus of this thesis, even though could reveal important aspects related to the stochastic-deterministic properties of the bi-dimensional Ising model.
The empirical formula is thus:

$$\ln(L) = 10^q H^m \tag{5.24}$$

where $q = 0.3223 \pm 0.0004$ and $m = -0.366 \pm 0.001$. This formula could help while devising an experiment when a particular regime is desired.
Actually, as said before, when we consider an oscillating field, we have to look at the plane (L, H_0), built from (L, H) considering the relation $H_0 = \sqrt{2}H$.

5.5 Hysteresis loop properties

Simulations running over different values of H_0, T and ω (i.e. P) were devised as to investigate the known results regarding the hysteresis loop properties. All the simulation mainly consist of the following passages:

1. The system with fixed L is prepared coherently with the simulation temperature (if $T < T_c$, complete magnetization, if $T > T_c$ complete randomness).
2. A sinusoidal magnetic field is applied and the magnetization tracked down.
3. After a certain number of periods, to allow the system to reach the steady-state condition, data are taken.

Since the simulations were mainly performed over one decade of values for each parameter, nothing can be said with statistical relevance about the dependencies. Nevertheless, it is interesting seeing the accordance or where the data deviate from the known results, leaving further investigation for future works. The range chosen for all the parameters matches the condition of at least one *MCSS* per cycle if not otherwise specified. Moreover, the lateral size of the system is chosen as to be in the MD regime. In particular, $L = 128$ for all the following paragraphs.

5.5.1 Hysteresis area

The area of the loop can be easily derived from the simulations. The formula considered is the following:

$$A = \sum_{i=2}^{end} m_i(h_i - h_{i-1}) \tag{5.25}$$

This is nothing more than a discretised version of equation (5.7). Here i represents the simulation step running from the second step to the last step

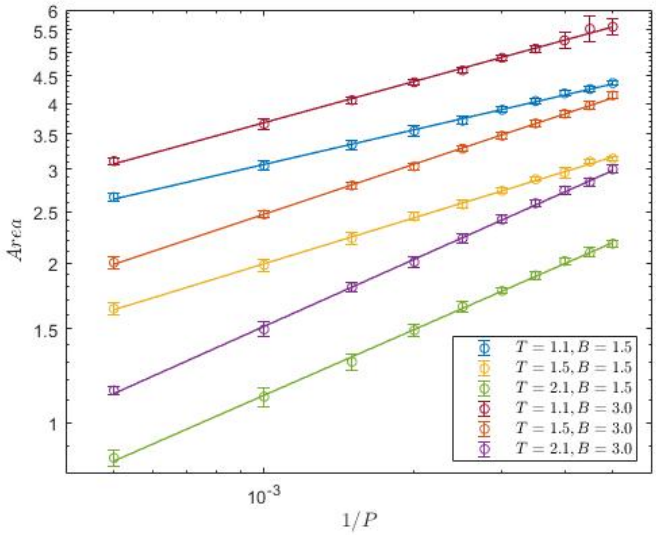

Figure 5.19: Value of the area plotted versus the oscillation frequency. Simulations for different choices of H_0 and T are shown. The plot has both the axes in logarithmic scale to reduce the power-law in a linear relation. Standard errors are superimposed to the markers.

of the simulation; m_i and h_i respectively the values of the magnetization and magnetic field at step i.

The power-law stated in (5.10) is now considered. One at a time, all the possible dependencies are investigated.
Fig. 5.19 shows the results for the frequency dependency. The power-law is followed relatively well ($R^2 > 0.995$ in all the cases). Moreover, the angular coefficient is comparable with the one suggested by previous results with Metropolis algorithm. The values of the b coefficients derived from different pairs of H_0 and T parameters are reported in table 5.2 and is to be compared to the theoretical value $b = 0.36$. The parameters show good agreement, even if a residual dependence of b from the parameters H_0 and T seems to be still embedded.

Fig. 5.20 shows the results for the temperature dependency. In this case also a simple linear dependence $A \sim T$ was tested. The coefficient for the power-law and the angular coefficient for the linear regression are shown in table 5.3.

b coefficient			
H_0	$T = 1.3$	$T = 1.7$	$T = 2.1$
1.5	0.217 ± 0.003	0.288 ± 0.003	0.412 ± 0.005
3	0.258 ± 0.004	0.314 ± 0.003	0.421 ± 0.004

Table 5.2: Table for the frequency exponent.

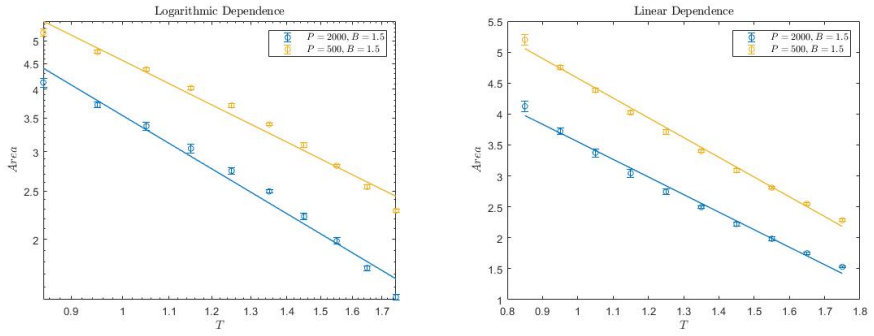

Figure 5.20: Value of the area plotted versus the temperature. Simulations for different choices of P are shown. The plot at the left has both the axes in logarithmic scale as to reduce the power-law in a linear relation. Standard error are superimposed to the markers.

Assuming a logarithmic dependence produces a c constant in good agreement with the one theoretically known of $c = 1.18$, though further investigation is required. The discrepancy from the power-law could be caused by the choice for the temperature range selected for the simulations.

Finally, fig. 5.21 shows the results for the magnetic field dependency. In this case, issues were present while considering too high magnetic field in the low-temperature range, due to insufficient *MCSS* per cycle. For this reason,

	c coefficient	**angular coefficient**
Dependence:	logarithmic	linear
$P = 2000$	1.35 ± 0.07	-2.84 ± 0.10
$P = 500$	1.12 ± 0.06	-3.19 ± 0.09

Table 5.3: Table for the temperature exponent considering an exponential dependence and the angular coefficient considering a linear dependence.

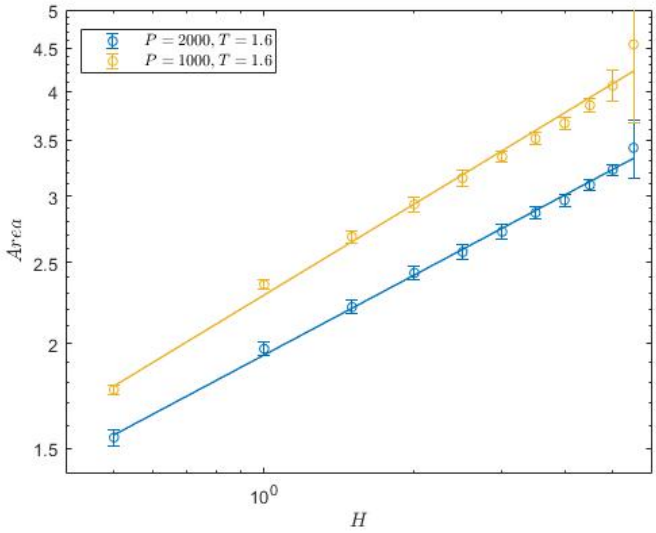

Figure 5.21: Value of the area plotted versus the magnetic field amplitude. Simulations for different choices of P are shown. The plot has both the axes in logarithmic scale as to reduce the power-law in a linear relation. Standard error are superimposed to the markers.

P	**a coefficient**
1000	0.360 ± 0.006
2000	0.32 ± 0.02

Table 5.4: Table for the field amplitude exponent.

only $T = 1.6$ was tested. The derived coefficients are shown in table 5.4 and must be compared to the theoretical value $a = 0.70$. Although the power-law is followed with high accuracy ($R^2 > 0.95$) the exponent is off by a factor of 2.

All the discrepancies with respect to the theoretical values could derive from an investigation in a range too far from the limit $\omega \to 0$. Anyway, since the purpose of this chapter is to give a broad overview of the results obtainable with the Lebowitz algorithm, and simulations with lower ω would require an increasing amount of time, for our purpose this is considered enough.

5.5.2 DC magnetic susceptibility

A different kind of analysis derives from the DC magnetic susceptibility. Thus far, we have only considered a temperature range below T_c. What we analyse now is the behaviour registered for $T > T_c$, where the hysteresis loop should be characterised by a vanishing area and a crossing of the origin in the (H, m) plane. By considering the limit for $H_0 \to 0$, it is possible to exploit the Curie-Weiss (equation (5.12)) relation as to obtain an estimation for T_c. The DC magnetic susceptibility can be obtained by considering the incremental ratio in a relatively small interval around the origin. In particular, the points in the loop between which the incremental ratio is calculated are selected between $m = \pm 0.2$. For simplicity in the derivation of T_c, the inverse of the magnetic susceptibility is calculated.

$$\frac{1}{\chi} \sim \frac{H(m = 0.2) - H(m = -0.2)}{0.4} \tag{5.26}$$

To reduce variability, since every cycle two measures can be derived (one while H rises, one while it decreases), the average between them is considered. Simulations of 100 hysteresis loops are run for different choices of the oscillation period P. Results are shown in fig. 5.22 and the derived T_c in table 5.5. We can identify two regimes, one at low T in which $1/\chi$ is almost constant and one at high T, where $1/\chi$ is linear. This is the theoretically expected behaviour. Moreover, we can see that, for higher T, all the curves have the same linear behaviour. Instead, if we increase the period P, what changes is the delimitation of the two regimes: the high temperature regime widens. Also the constant value of χ changes, decreasing while P increases. The estimated value for T_c is around the theoretical value, even though it does not agree with high accuracy. More reliable techniques are available, e.g. the temperature driven experiments.

P	T_c
500	2.71 ± 0.08
1000	2.75 ± 0.06
2000	2.77 ± 0.06
4000	2.78 ± 0.05

Table 5.5: Table for the estimation of T_c from DC magnetic susceptibility measurements.

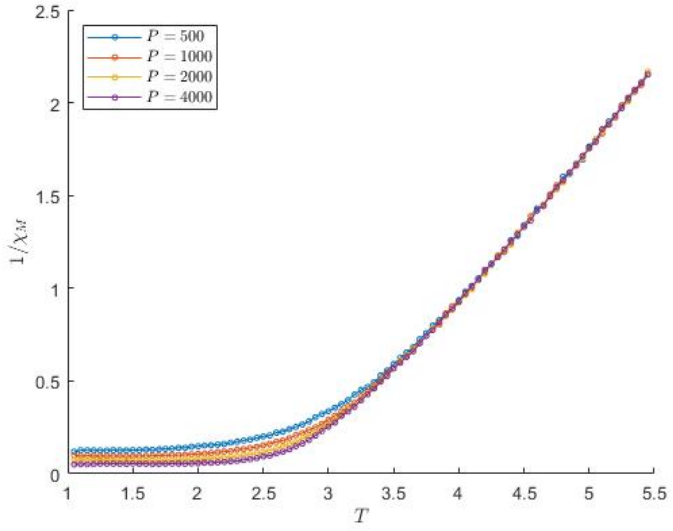

Figure 5.22: Plot of the DC magnetic susceptibility function of temperature for different choices of the period P. Error bars are not shown since are of the same height as the markers. Two different domains can be noticed, one for low temperature with a milder slope and one for high temperature with a steeper angle. The Curie-Weiss low does apply only in the latter case.

5.6 AC magnetic susceptibility

In order to derive the AC magnetic susceptibility, a simulation based on the following steps was devised, for different choices of the period P of the magnetic field oscillation:

1. A system is initialised with random spin orientation in a fixed temperature $T > T_c$.
2. An oscillating field is applied, for a certain number of periods, enough to let the system reach steady-state condition.
3. The average magnetization in a cycle is calculated by averaging $m(t)$ over many cycles and a sinusoidal regression is made. Here the periodicity of the magnetization curve is taken equal to the one of the

P	$\chi^{'}$	$\chi^{''}$
258	1.95 ± 0.05	2.05 ± 0.05
500	1.80 ± 0.05	1.90 ± 0.05
750	1.70 ± 0.05	1.80 ± 0.05

Table 5.6: Table for the estimation of θ_c from the two components of AC magnetic susceptibility measurements.

external field, as to consider only the offset and the amplitude of the magnetization as unknowns.

4. Imaginary and real components of the AC magnetic susceptibility are calculated through equations (5.14) and (5.15).

5. The temperature is decreased and steps 2-3-4-5 are repeated until T is sufficiently low (in our case, $T_{min} = 1$).

Fig. 5.23 shows the results of the simulation from a system with $L = 64$ as lateral size and $H_0 = 0.3$. Before deciding the size of the system, multiple runs were completed varying L from 32 to 100, and no particular differences in the AC magnetic susceptibility were noticed. For this reason, a sufficiently low value for L was chosen, a compromise between a quick enough simulation and the condition of MD regime.
From the analysis of the curve shape the dynamical critical temperature θ_c can be derived. The values are reported in table 5.6, for different choices of the oscillating period. The first simulation was devised as to have $P = 258$, condition already analysed in the previous paragraph for the critical temperature $\theta_c = 0.798 \cdot T_c$. From the analysis of AC magnetic susceptibility, instead, we obtain $\theta_c = 0.88 \cdot T_c$. in both cases we have agreement with the known value.
The thermodynamical critical temperature is instead very difficult to determine due to the wide broadening of $\chi^{'}$ peak. Better methods for its derivation have been previously considered.

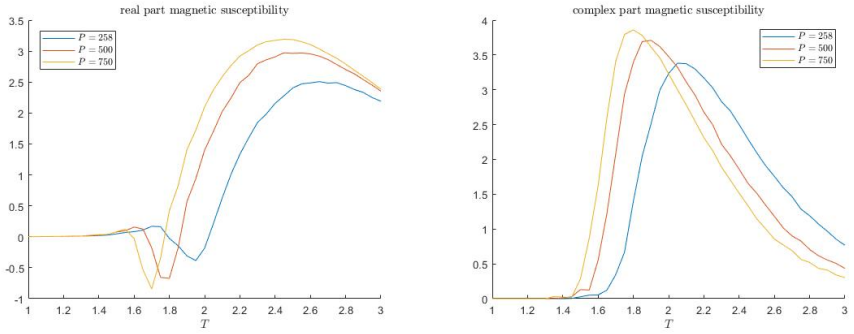

Figure 5.23: Plot of the two components (real on the left and imaginary on the right) of AC magnetic susceptibility function of temperature. Near the dynamical critical temperature (θ_c), the imaginary part shows a peak; the real part shows a dip. Moreover, the real part has a wide peak in proximity of the thermodynamical critical temperature (T_c).

Chapter 6

Thermodynamic and dynamic transitions in systems with defects

The Lebowitz algorithm employed thus far has been shown to be able to reproduce results qualitatively equivalent to those derived with the Metropolis algorithm, once we consider a standard Ising model. Now, we want to simulate the presence of imperfections (or defects) inside the structure. For the Metropolis algorithm, many variations of the Ising model are known (i.e. the Random-Bound Ising Model, Random-Field Ising Model) which allow mimicking the presence of imperfections inside the lattice in different ways. How do we implement the presence of imperfections inside the Lebowitz algorithm? A new approach is devised: the imperfections in the structure can be represented by fixed spins in the lattice, that, once initialised, cannot change orientation. In this way, we create pinned sites that do not participate in the system evolution. This idea has been used before for the Metropolis Algorithm [23], even though it has not developed further.
This chapter is focused on the main implications derived from the previous definition of defects. The results from such investigation span from the determination of a quantitative relation between physical properties and the fraction of defects to the modification of the dynamical and thermodynamical critical conditions as to devise a more suitable material for potential

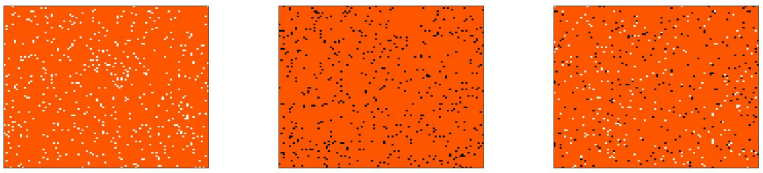

Figure 6.1: The black colour indicates fixed spins with value -1; white colour fixed spin $+1$. Orange colour indicates spins that participate to the system dynamics: they can switch between $+1$ or -1 values along the time evolution. In the first two panel, two ways to define coherently oriented defects (completely up or down). In the right panel, randomly oriented defects. Defects at 5%, over a structure with 100×100 spins.

technological applications.

6.1 Introduction of defects

In this chapter, the term defect is associated with the concept of a spin in the lattice with a fixed orientation, which cannot vary in time nor space. In this work, in case of multiple defects in the structure, they have been arranged in random positions in the lattice. Usually, not more than 5% defects in the whole structure are considered. There are two possible ways to implement defects in the structure: coherently or randomly oriented defects, as represented in fig. 6.1. In this work, only randomly oriented defects are considered.

From a physical point of view, such definition can be associated with the idea of impurities in the structure with very slow dynamics: they display the same interaction with all the neighbours but their motion is characterised by a completely different time scale. Therefore, all the simulations devised are thought to last for a time shorter than it would require the inversion of the spin associated with a defect. This assumption not only gives a physical meaning to the defect but also ensures the validity of the Hamiltonian associated with the lattice. Otherwise, we would not be able to perform reliable Monte Carlo simulations.

Once introduced, it is now time to understand how defects come into play when considering the Lebowitz algorithm. Since they cannot be targeted for a spin-flip event, they can be grouped in an "eleventh"class, which will be invisible while choosing from which class the inverted spin has to come from. In particular, the following steps are being implemented/modified:

1. A "Mask"is initialised, with the structure represented in fig. 6.1: only the position and the orientation of the defects is established, leaving all the non-defects spin undefined.

2. During the building of the auxiliary matrices (CLASS and LOCATION), once a defect from the mask is considered, it is added to the eleventh class and the corresponding position in the LOCATION matrix is substituted with a fictitious value.

3. During the selection of the class for the spin to be inverted, the eleventh class is not taken into consideration.

4. During the change of the nearest neighbours class, if the LOCATION of the considered neighbour has the fictitious value, no change in the class happens.

5. The time of the simulation is updated as in the ideal case:

$$\Delta t = \frac{1}{\text{Q-ARRAY}(10)} \log(R) \tag{6.1}$$

By starting with the following paragraph, various phenomena are analysed. As shown by the Random-Bound Ising Model, the presence of impurities can induce the system to transact in the spin-glass phase. A definition of this phase and a consequent investigation is presented in paragraph 6.2. Even in the ferromagnetic phase, the system characteristics are modified by the defects: dynamical and thermodynamical critical temperatures vary in the presence of defects. The hysteresis loop properties are also being influenced. Finally, the presence of jumps in the hysteresis loops is addressed and the Barkhausen noise is analysed to investigate the power-law in the jump amplitude probability distribution

6.2 The spin-glass transition

The introduction of random fixed-orientation spins within the lattice produces different effects on the system. Firstly, it may cause frustration, intended as the competition between interactions among different spins in the lattice. As an example, consider a chain of spins as follows. Spins 1 and 3 are both defects with opposite orientations.

$$\begin{array}{ccccccccc} & & & 1 & 2 & 3 & & & \\ + & + & + & ? & - & - & - \end{array}$$

The two defects cause indecision in the spin in the middle since both orientations will produce the same interaction energy and therefore could be equally chosen. This configuration is equivalent to the one in which the orientations of the defects are both positive, but the exchange interactions J are opposite in sign, one ferromagnetic like, the other anti-ferromagnetic, which is a more common situation for the Random-Bound Ising Model.
Secondly, the random positioning of defects inside the lattice causes quenched randomness in the structure. Both of these effects (frustration and randomness) represent the basic requirements for the presence of the spin-glass phase in the system. Since this phase changes the general properties of the system it is necessary to investigate which (if any) are the conditions that induce the system to undergo a transition from the ferromagnetic to the spin-glass phase.

6.2.1 Definition of the spin-glass phase

After a brief introduction about what we may expect when increasing the density of the defects, we can now deepen into the topic a little further. We know that frustration and randomness are key elements required to the spin-glass phase to show, but what is, in reality, a spin-glass and how can we recognise it?
The first spin glasses were obtained through magnetic systems composed of spins with interactions randomly chosen as ferro- or antiferromagnetic. In general, below a specific temperature (T_f) there is cooperative freezing of the

spins and the usual long-range order is not shown. This freezing is highly irreversible: after the cooling, the system falls in a metastable frozen state [3]. Further characteristics shared by spin glasses are the following:

- Temperature behaviour: at high temperature, as for all the magnetic systems, all the spins behave individually due to thermal interaction overcoming spin-to-spin interaction. In this condition, the material is in the paramagnetic phase. While cooling the sample, since the interactions between neighbouring magnetic moments become more relevant, many clusters are created. Proceeding with the temperature decrease below a particular value T_f, the system freezes into a stable configuration through a cooperative phase transition. This transition differs from the usual paramagnetic-ferromagnetic phase transition due to the absence of long-range order. The transition can be investigated through the AC magnetic susceptibility, as the imaginary part χ'' shows a sharp peak for $T = T_f$.
- Metastability: there are multiple states in which the system can be found once the condition $T < T_f$ is reached. All of these states share similar energy values and therefore while repeating the heating and cooling of the material several times, we can "jump"from one of them to the others.

6.2.2 Spin-glass identification

Metastability has been investigated to identify and locate the spin-glass transition. If the system is in a ferromagnetic state, starting from many different random configurations (random orientation of the spins) of the lattice and letting the systems evolve freely, only two states will be reached (positive or negative magnetization). If the system is in the spin-glass phase, instead, the number of final states reached will be higher due to metastability.
Now, let us chose two of the many final configurations reached by the system at the end of the simulations (which from now on we will cal simply final configurations) α and β and consider the overlap between them defined as:

$$q_{\alpha,\beta} = \frac{\sum_{i=1}^{N} m_i^{\alpha} m_i^{\beta}}{N} \tag{6.2}$$

where m_i^α and m_i^β represent the average magnetization of the i-th spin, once equilibrium has been reached, in two different replicas α and β. If the system is in the ferromagnetic phase, we will have $q_{\alpha,\beta} \approx \pm 1$ (if we neglect for now thermal fluctuations, which would cause the reduction of the absolute value of the overlap), since the final configurations are or completely equal or completely opposite. If the system is in the spin-glass phase, instead $q_{\alpha,\beta}$ might take also intermediate values in the interval $[-1, +1]$. If the system is in the paramagnetic phase, $q_{\alpha,\beta} \approx 0$, since every final configuration will contain randomly oriented spins. Therefore, if we consider C different initial configurations (randomly oriented spin in the lattice) and we compute the $C(C-1)/2$ possible overlaps $q_{\alpha,\beta}$, we should have a clear indication on where the system can be found: if only ± 1 values are obtained, the system is ferromagnetic; if other values are seen, the system is in the spin-glass phase. If only 0 is obtained, the system is in paramagnetic phase.
For $C \longrightarrow \infty$ the collection of $q_{\alpha,\beta}$ give the probability distribution of q: $P(q)$ which should be symmetric with respect to $q = 0$. From spin-glass theory, it is known that once $P(q)$ is a continuous function in the interval $[-1, +1]$, different from two deltas (showed in the ferromagnetic phase) or a Gaussian function (showed in the paramagnetic phase) the system can be considered in a spin-glass phase. More precisely, we will identify the ferromagnetic phase when $P(0)$ vanishes; the spin-glass phase when $P(q)$ is non-null everywhere, and it is convex in the interval ranging between its two symmetric maxima, placed at $\pm q_{max}$; the paramagnetic phase when the maximum of $P(q)$ is located at $q = 0$.

The following simulation was devised to compute the overlap distribution:

1. C different replicas (lattice with randomly chosen initial orientation of the spins with same location of the defects) of the system with fixed temperature and fraction of defects are initialised.

2. The replicas are left free to evolve for a certain Δt, after which $q_{\alpha,\beta}$ is calculated for all the possible couples (α, β).

3. A histogram is derived representing the distribution of the $\frac{C(C-1)}{2}$ values between $[-1, 1]$.

4. Steps 2 and 3 are repeated until equilibrium is reached for all the replicas. The final histogram is derived.

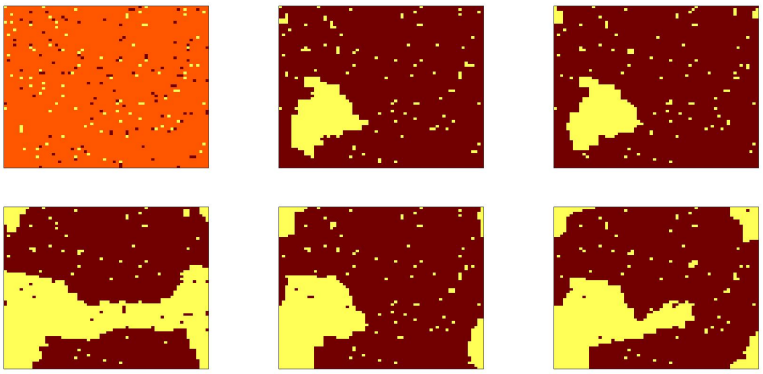

Figure 6.2: First panel indicates the "Mask"used for the defects (position and orientation). The others represent different replicas left free to evolve towards equilibrium after a reasonably long physical-time. In all of them it is possible to recognise a yellow cluster in the bottom-left corner in which the spins have all the same orientation.

The initialisation of the C replicas, although, requires particular attention. For the Random-Bound Ising Model, the system created has spins that are able to fluctuate freely among the two directions. What makes the inversion more or less likely is the strength of the inter-atomic bound. In the current situation, the defects are spins which are not able to invert orientation. This has an effect on the general properties of the previously defined quantities. As an example, $P(q)$ happens to be asymmetric: having defects always in the same location with the same orientation induces formation of clusters (regions of spins all with the same direction) with direction independent from the replica, as shown in fig. 6.2. Therefore, the overlap between these configurations will be affected by a positive bias, taking into account all the clusters that are find more likely in a given direction instead of the opposite one.

As to recover the $P(q)$ symmetry, the initialisation was devised considering defects always in the same position but randomly oriented replica by replica. This completely eliminates the presence of clusters with the same orientation common to all the replicas. The situation is like as if we were considering C replicas of just one configuration of the defects and then we would wait for a sufficiently long time ($\Delta t \longrightarrow \infty$) to observe some of the magnetic

moments with infinite inertia change orientation before the beginning of the simulation.

Since the Lebowitz algorithm allows to study out-of-equilibrium conditions, information regarding the time required before reaching the equilibrium can be derived. For this reason, the overlaps q are calculated at a distance of $\Delta t = 1000$ (in physical-time units). Therefore, $P(q)$ can be expressed function also of time. Moreover, as to understand the vicinity to the equilibrium condition, we define the overlap correlation:

$$G(t) = \sum_q P(q,t)P(q,t+\Delta t) \tag{6.3}$$

At the beginning of the simulation, $P(q,t)$ and $P(q,t+\Delta t)$ are relatively different; instead, near equilibrium, $P(q,t)$ is almost independent from t. Consequently, the overlap correlation will vary with time while the systems move out of equilibrium. Once equilibrium is reached, $G(t)$ will show a plateau.
Results of the simulation over $C = 100$ replicas are represented in fig. 6.3 and 6.4.

By looking at the result of the simulation, one can see the expected behaviour: for lower fraction of defects, the $P(q,t)$ distributions are made of two symmetric deltas near ± 1. Increasing the temperature, the two deltas shift towards the middle. Indeed, the thermal fluctuation of the spins becomes more relevant at higher temperatures and the configurations have less and less spins with same orientation. This causes a decrease in the absolute value of $q_{\alpha,\beta}$ and consequently a change in the $P(q,t)$ distribution. For $D = 2.5\%$, at high temperature, the system is not any longer in the ferromagnetic phase. Instead, the spin-glass phase is shown as $P(0) \neq 0$. For higher values of the defects ($D = 5$), even at lower temperatures, the system is in spin-glass phase. In it, all the replicas show presence of clusters, in different locations and with different orientation.

Other important observations now follow:

- At the beginning of each simulation, $P(q,t)$ presents a sharp peak at $q = 0$. This is due to the initialisation condition with random orientation of the spins. In all the simulations, it rapidly dissolves after few

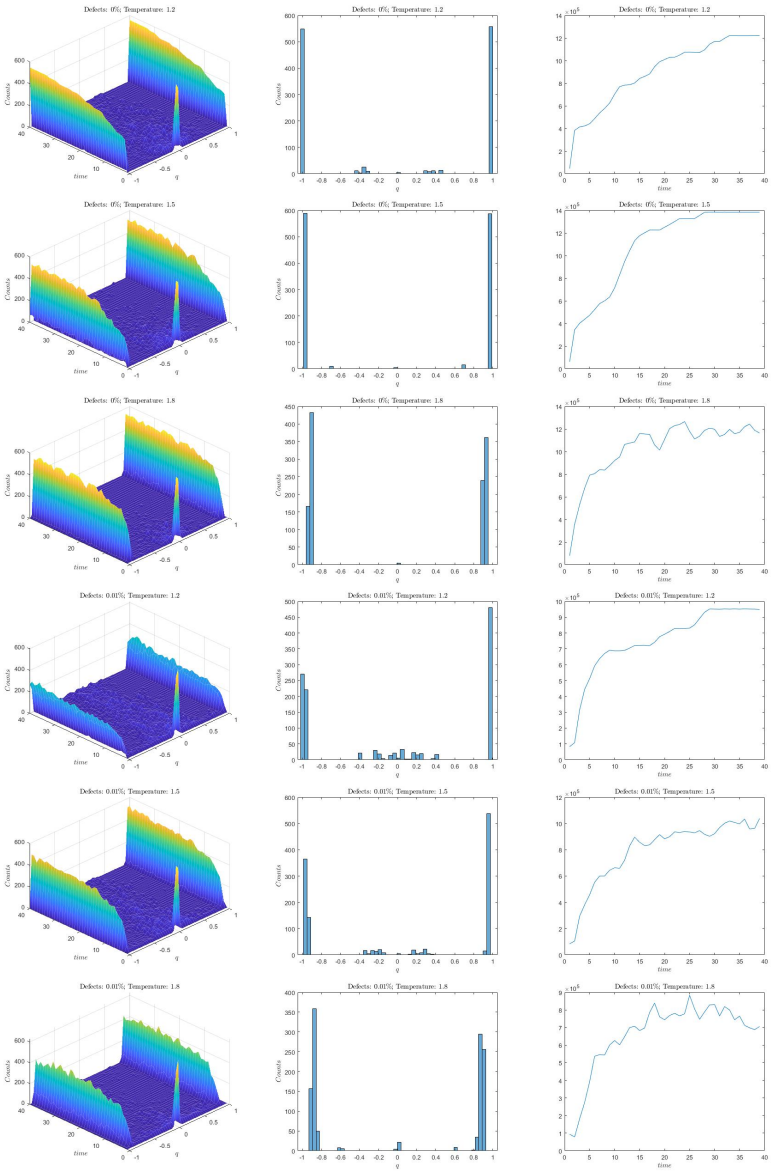

Figure 6.3: In the left column, the time evolution of $P(q,t)$. In the middle column, the histogram plot of the equilibrium $P(q,t)$. In the right column, the tendency to reach the equilibrium. Percentage of defects 0% and 1%; temperatures: 1.2, 1.5 and 1.8. In all the cases, the system behaves as a ferromagnet.

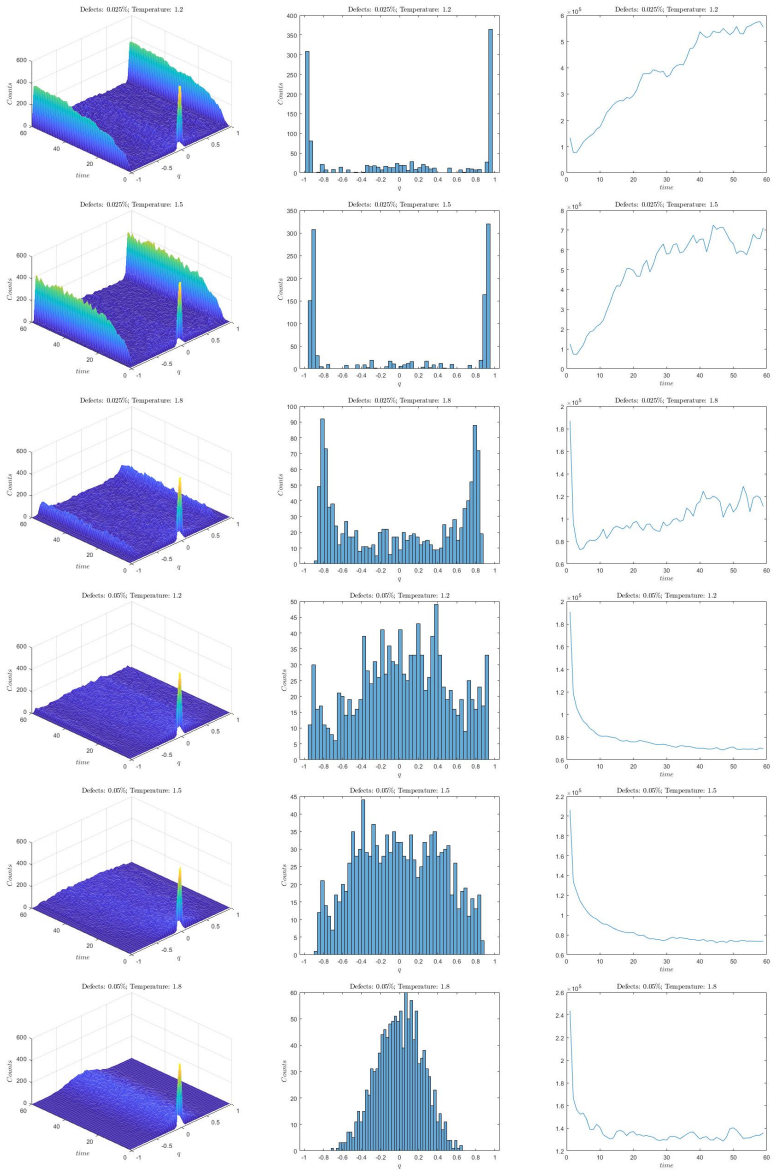

Figure 6.4: In the left column, the time evolution of $P(q,t)$. In the middle column, the histogram plot of the equilibrium $P(q,t)$. In the right column, the tendency to reach the equilibrium. Percentage of defects 2.5% and 5%; temperatures: 1.2, 1.5 and 1.8. In the third row, the system is in the spin-glass phase. In the fourth row, the phase shown is more difficult to be determined. In the last two rows, the system is in the paramagnetic phase.

Δt, in a different way with respect to the one of a paramagnetic system (simulated in fig. 6.5).

- Even in the case of absence of defects, the system takes a considerable amount of time before reaching equilibrium (plateau of $G(t)$). By visually analysing the replicas, it has been noticed the presence of striped configurations (as the one represented in fig. 6.6) which are metastable. These configurations, when overlapped to a magnetized system, give a value of q near 0. Their presence can be detected also by looking at the $G(t)$ plot: the small final jumps before the plateau, are due to dissolving striped configurations (from stripe to magnetized systems). These striped configurations tend to last for a long time before decaying and cause the presence of extra peaks in the histogram plots near $q = 0$. Interestingly, when the temperature is increased, less striped configurations are found. Their metastable lifetime seems to decrease when the system is heated, as we can deduce by considering how fast the plateau of $G(t)$ is reached.

- For $D = 1\%$ the number of replicas showing final striped configuration increases considerably (without cluster formation). This justifies the extra peaks increase, which can be observed around $q = 0$ in the histogram plot for longer times. For what said in the previous point, we can suppose that these extra peaks will decay if the simulation is run for a longer time or if the temperature is increased.

- The simulation with $T = 1.8$ and $D = 2.5\%$ struggles while reaching equilibrium: $G(t)$ doesn't reach any plateau and $P(q, t)$ lacks the presence of the deltas near ± 1.

- The time required for the completion of the simulation increases while increasing the fraction of defects. An explanation now follows. Since the simulation is set to last for a fixed amount of physical-time, the simulation time increase must be related to a decrease in the slope of the linear relation physical-time versus *MCSS*. Recalling what seen in the previous chapters, this means that "near equilibrium"configurations are rarely obtained. This is reasonable: the introduction of defects with different orientation with respect to the one chosen as equilibrium condition doesn't allow their nearest neighbours to fall in the lowest

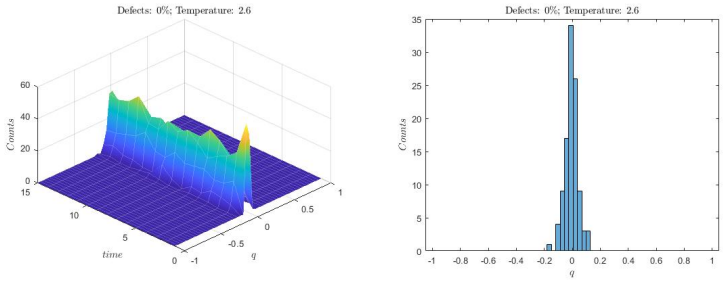

Figure 6.5: Time evolution of a paramagnetic ensembles of replicas ($T > T_c$). In the left column, the time evolution of $P(q,t)$. In the right column, the histogram plot of the equilibrium $P(q,t)$.

energetic class (the one of equilibrium). Rather, as the fraction of defects increases, more spins will occupy higher energetic classes, inducing smaller Δt for each simulation step. As consequence, the physical-time elapses slower for system with high fraction of defects compared to the one without defects and the simulation lasts longer.

- In the last case ($T = 1.8$ and $D = 5\%$), $P(q,t)$ is a Gaussian function centred in 0, resembling the histogram we would obtain for a paramagnetic system. Although the transition spin-glass - paramagnetic phase is not considered, we can infer that for higher temperature and fraction of defects, the paramagnetic phase emerges.

Table 6.1 sums up the results from the simulations.

D	$T = 1.2$	$T = 1.5$	$T = 1.8$
0%	Ferro	Ferro	Ferro
1%	Ferro	Ferro	Ferro
2.5%	Ferro	Ferro	spin-glass
5%	spin-glass/ Para	Para	Para

Table 6.1: Results from the simulations with different temperatures and fraction of defects. Ferro stands for ferromagnetic; Para for paramagnetic.

Therefore, the introduction of defects can induce the spin-glass phase, with formation of clusters and systems that remains trapped in metastable states

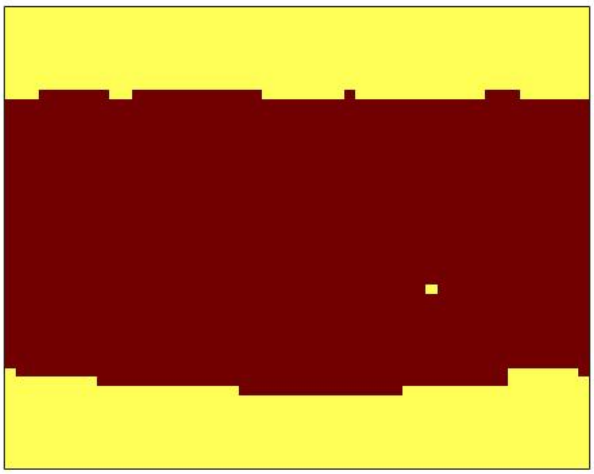

Figure 6.6: Striped configuration showed in a system without defects.

for a long physical-time. The spin-glass phase becomes stable depending on both the temperature and the fraction of defects values.
Later on, we will consider mostly fractions of defects and temperatures for which the spin-glass phase is avoided. Indeed the focus is on how the properties of a ferromagnetic system change with the introduction of a small fraction of defects.

6.3 Effect on the thermodynamical critical temperature

As previously mentioned, the introduction of defects, besides introducing a new phase, modifies the equilibrium among the paramagnetic - ferromagnetic phases. The aim of this chapter is to analyse how the thermodynamical critical temperature changes while modifying the fraction of defects in the structure and possibly gain more insight about the causes for this shift.

We can now proceed by repeating the same kind of analysis done in chapter

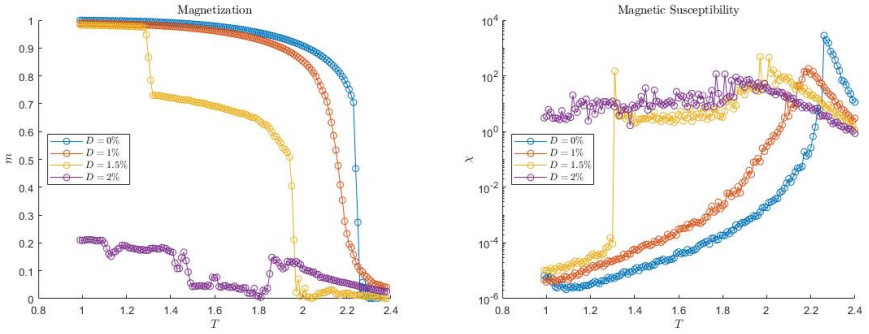

Figure 6.7: In the left panel, the magnetization function of temperature; in the left panel, the magnetic susceptibility function of temperature on a semi-logarithmic plot. Both are derived for different fraction of defects $D = 0\%; 1\%1.5\%; 2\%$.

4.2, with a basic analysis of the magnetic susceptibility. The addiction of defects in the lattice changes partially the initialisation of the lattices: for the analysis of magnetic susceptibility, only one Mask (for the defects initialisation) is considered and T_c is derived simply from the peak in the magnetic susceptibility.

6.3.1 Magnetic susceptibility

For this study, lattices with $L = 128$ were considered. In particular, for each fraction of defects $D = 0\%; 1\%, 1.5\%; 2\%$, the magnetization and the magnetic susceptibility function of the temperature are derived. T is changed from 2.4 to 1. Fig. 6.7 presents the results of the simulation. Notice that the magnetic susceptibility is represented in a semi-logarithmic plot for convenience.

These graphics are full of information. The ideal case, $D = 0\%$, is what we expected: the magnetic lattice shows a spontaneous magnetization after a peak in the magnetic susceptibility, localised at $T = 2.26 \pm 0.01$. When we increase the percentage of defects, $D = 1\%$, the system shows exactly the same behaviour, with only a shift in the value of the critical temperature towards lower values. This is reasonable: the presence of few randomly ori-

ented fixed spins in the structure favours the disordered phase. The ordered phase now requires a lower value of the temperature to be dominant. We can suppose that the presence of defects with the same orientation should cause the opposite behaviour, favouring the ordered phase and shifting T_c up in value.
Notice also a slight decrease in the value of the magnetization when $T \to 1$. This comes from the presence of fixed spins in the opposite direction. In presence of defects randomly oriented (fraction f) the maximum value of the magnetization is $m \approx 1 - f$ for $T \to 0$.
Increasing further the fraction of defects, $m(T)$ starts to change consistently. For $D = 1.5\%$ we have a stair: in the intermediate temperature range, the system is partially magnetized. Only for lower values of T, the system escapes from this metastable state and magnetizes. Also, the magnetic susceptibility has a non-standard behaviour: the peak widens and in the intermediate range it does not decrease as before. For lower temperatures, it has a bump and then shows the same behaviour of the systems with a lower percentage of defects. In the case $D = 2\%$ these characteristics are heightened.
The magnetic susceptibility resembles the behaviour experimentally observed in real spin-glass: a shallow peak with an almost constant behaviour for temperature below the peak. For further agreement with experimental observations, we could investigate the irreversibility property of the magnetic susceptibility, to confirm the transition to spin-glass for $D \geq 1.5\%$ for a system with $L = 128$.
We have found two methods for the determination of the spin-glass transition. The first one relies on the analysis of the $P(q, t)$ distribution; the second one on the analysis of χ_M. The main difference between the two methods is that through $P(q, t)$ we have an indication regarding the phase shown by the system during the evolution toward equilibrium at a fixed temperature; instead, with χ_M, we have to wait for equilibrium and then derive the phase of the system at different temperatures. Depending on the scope of the investigation (out of equilibrium or not), one or the other methods could be better.

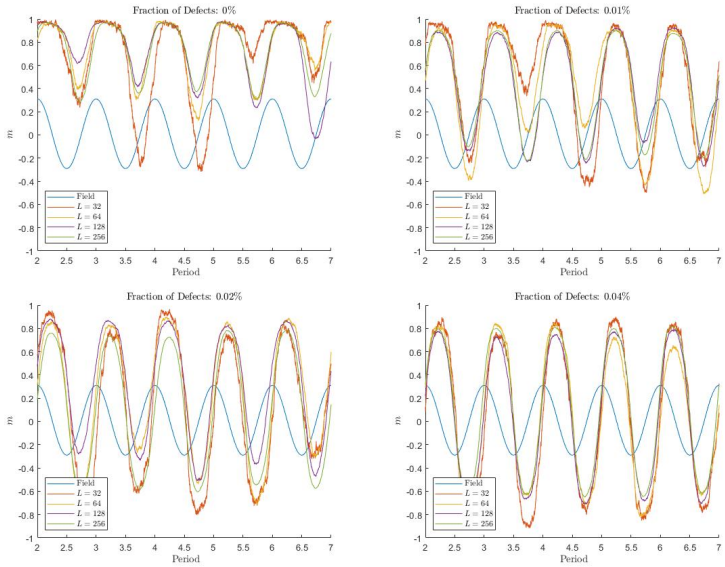

Figure 6.8: Magnetization cycles in presence of an oscillating field for lattices with lateral size $L = 32; 64; 128; 256$. Other simulation values: $P = 250$, $T = 0.8 \cdot T_c$, $H_0 = 0.3$, $H_b = 0.01$.

6.4 Effect of defects on the dynamical critical temperature

We can now focus on the dynamic properties of the system. First observations come from the analysis of the magnetization in the presence of an oscillating field while increasing the fraction of defects. For this purpose, five periods were simulated for systems with different lateral sizes while applying an oscillating field ($H_0 = 0.3$) over a small bias ($H_b = 0.01$, to establish a preferential direction for the magnetization). The results are represented in fig. 6.8.

At first glance, we can observe a reduction in the stochasticity of the inversion mechanism. The smaller system (orange line), in absence of defects inside the SD region, even in presence of a small fraction of defects (1% of defects which with $L = 32$ implies just 10 defects over all the lattice), show a more deterministic behaviour. Indeed, it follows better the inversion of higher-sized systems (purple and green lines) which are in the MD region

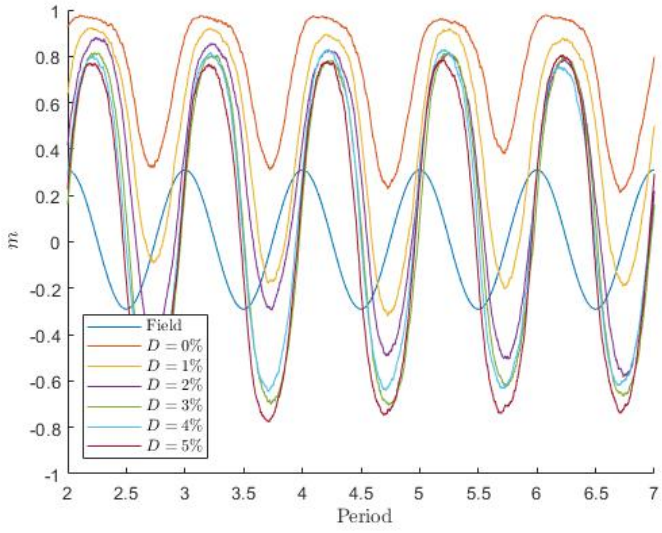

Figure 6.9: Magnetization cycles in presence of an oscillating field for a lattices with increasing fraction of defects $D = 0\%, 1\%, 2\%, 3\%, 4\%, 5\%$. Other simulation values: $L = 128$, $P = 250$, $T = 0.8 \cdot T_c$, $H_0 = 0.3$, $H_b = 0.01$.

and therefore characterized by a deterministic inversion mechanism.
Another important observation regards the expected dynamical phase. In the absence of defects, the systems are in the DOP ($P < P_c$), showing a preferential direction for the magnetization and an average magnetization per cycle $\langle Q \rangle \neq 0$. If we increase the fraction of defects, instead, the magnetization seems to follow better the oscillating field, and $\langle Q \rangle$ approaches zero. Considering fig. 6.9, we can appreciate better the transition from DOP to DDP due to an increasing percentage of defects.

Therefore, we expect a modification of the spinodal line (regulating the transition from MD to SD regime) and a reduction of the critical period P_c while increasing the fraction of defects. The following paragraphs try to verify these observations and give more insights on the topics.

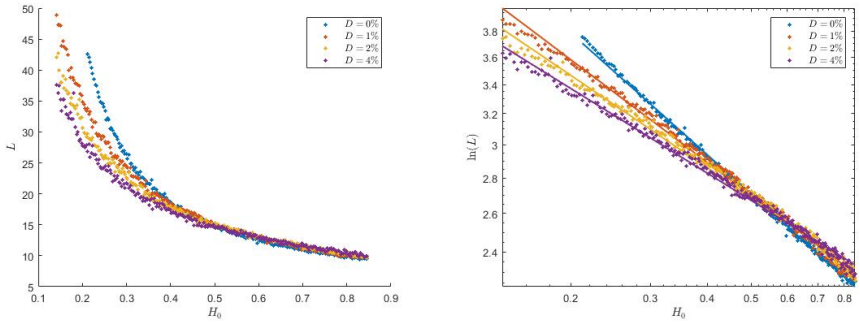

Figure 6.10: In the left panel, the spinodal line for different fraction of defects inside the system. For $D = 0\%$, the line is the same one presented in chapter 5.4. For higher defects concentration, lower values of the magnetic field have been analysed. In the right panel, the linear regression for all four cases (in a log-log plot). The error bars are not displayed since of the same size of the markers.

6.4.1 Spinodal line

To evaluate the effect of defects over the inversion mechanism, the spinodal line is calculated while considering different percentages of randomly oriented defects. The simulation and the methodology is the same adopted in section 5.4, with the only difference that, while calculating the metastable life-time, each repetition has a different defects initialisation. Fig. 6.10 shows the results of the simulations for defects fractions: $D = 0\%; 1\%; 2\%; 4\%$.

For small values of the magnetic field, the fraction of defects strongly influences the spinodal line. The effect is in accordance with the simulations shown in fig. 6.8 and 6.9: while D is increased, systems with smaller lateral size change regime, from stochastic to deterministic.
The theoretical relation $H_{SDL}(L)$ has also been verified in the presence of defects by means of a linear regression (all with $R^2 \approx 0.995$) in a log-log plot, even if some discrepancy can be seen at the extremes of the analysed interval. The coefficients for the relation:

$$\ln(L) = 10^q H^m \tag{6.4}$$

are shown in table 6.2.

Spinodal line coefficients		
D	q	m
1%	-0.3384 ± 0.0005	-0.308 ± 0.001
2%	-0.34568 ± 0.0005	-0.278 ± 0.001
4%	-0.3501 ± 0.0005	-0.254 ± 0.001

Table 6.2: Table for the spinodal line coefficients, for different fractions of defects.

This behaviour follows our expectation: in smaller systems, the inversion mechanism that normally would spread from a single nucleation centre, now begins around the defects with opposite direction. Since the lattice has several of them, even if L is rather small, the inversion mechanism proceeds as the system was in the MD regime and therefore more deterministically.

6.4.2 Critical period

We can now deal with the modification of the critical period. As done in section 5.3 we start by considering a qualitative analysis of the region over the (H_0, T) plane in which DOP (or DDP) is shown by the system. The same simulations are devised and executed over a system of lateral size $L = 128$, with the only difference in the presence of defects. Different fractions of randomly oriented spins are here considered, to investigate how the dynamical critical line changes. Results for $D = 1\%; 2\%$, next to the one from the defect-free system, are shown in fig. 6.11. A small difference can be noticed: in both cases ($P = 100; 400$) the transition line drifts towards smaller fields and temperature, This indicates that the DDP is definitely favoured in presence of defects in the structure, as already supposed previously. Also, if we consider the case $H_0 = 0$, we can notice that for $T \to T_c$ the DDP is not favoured anymore, since the estimated mean magnetization per cycle $\hat{Q} \to 0$. Since the magnetization in absence of field does not oscillate, it means that $m = 0$. No spontaneous magnetization is shown for $T \to T_c$. This is in agreement with the critical temperature shifts towards lower values in presence of defects.

We can now proceed with the quantitative analysis. In particular, as be-

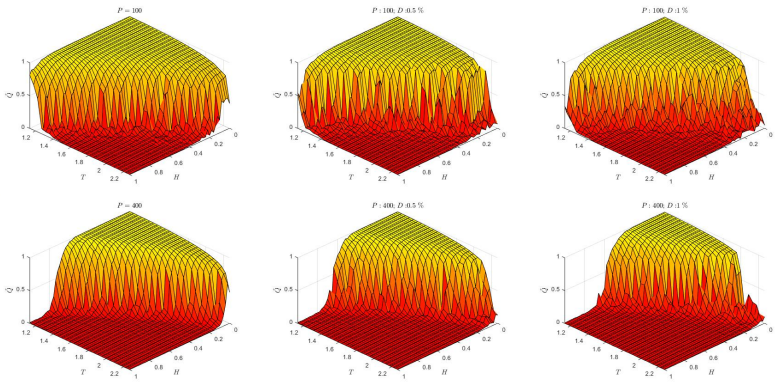

Figure 6.11: Maps representing the conditions (in terms of field intensity and temperature) in which the system shows the DOP or the DDP. In particular, the value of $\hat{Q}$, the estimated mean magnetization per cycle, is calculated. Where $\hat{Q} = 0$ (1), the system show a DDP (DOP), which happens for high (low) T and high (low) H_0. In the upper row, $P = 100$. In the lower row $P = 400$. Each column refers to a different amount of defects, respectively, from left to right: $D = 0\%; 1\%; 2\%$.

fore, we calculate the Binder cumulant for lattices with different fractions of defects. Fig. 6.12 shows the results in the case of $D = 1\%, 2\%$ and $P = 258; 400$.

Clearly, a dynamical temperature cannot be derived in this case. For $L = 64$, the behaviour is the one expected. For larger system lateral sizes, instead, the binder cumulant shows an unpredictable behaviour and no intersection can be derived. A possible interpretation to this effect can be derived considering that what really makes comparable two systems, is not the fraction of defects, but the number of defects inside the structure, at least while we speak of dynamical properties. Indeed, $D = 1\%$ for $L = 64$ means 40 defects in the structure, different from the 655 for the $L = 256$. If this is true, we will be able to observe the intersection between the Binder cumulant lines considering the same number of defects in the lattices. Another possible reason could be the fact that the spin-glass phase could emerge, eliminating the presence of the dynamical critical temperature. This will be investigated in future, for now we limit, once considering the fraction of defects to compare the results between structure of the same lateral size.

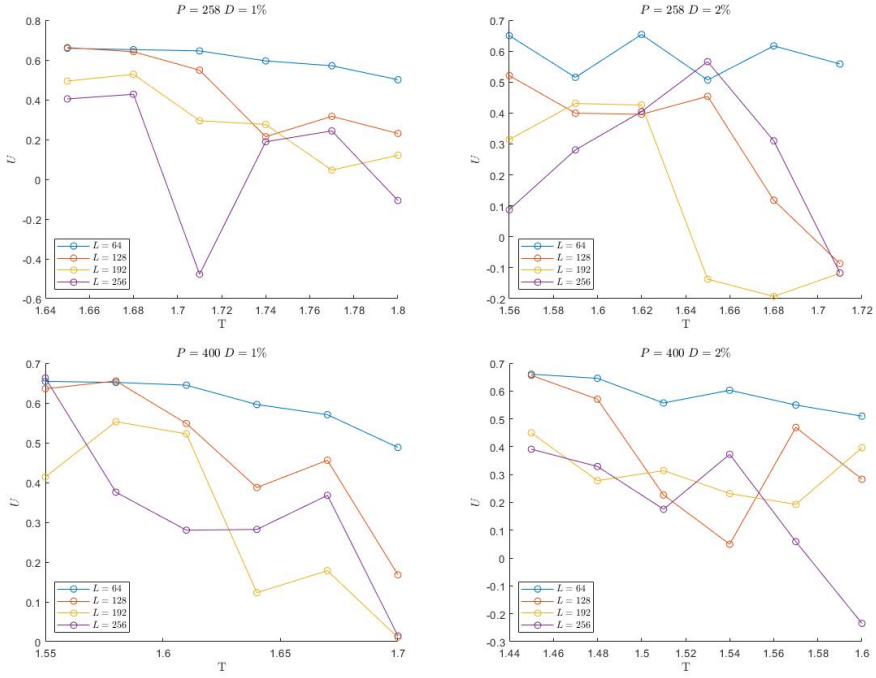

Figure 6.12: Binder cumulant derivation. U is derived for four system with different lateral size $L = 64; 128; 192; 256$. In the upper row, $P = 258$. In the bottom line, $P = 400$. In the bottom row $P = 400$. Left column $D = 1\%$; right column $D = 2\%$.

6.5 Effect of defects on the hysteresis loop

We can now focus the attention over the modification of the hysteresis loop properties in presence of defects. The same simulations of section 5.5 are considered while introducing defects, for a system with $L = 64$. Since data derived from a single fixed configuration of defects could be misleading (in case the defects are unfortunately localised in "particular"positions), all the calculated parameters are averaged over different initialisation of the Mask. The presence of clusters (in the spin-glass phase) has an important role in the hysteresis loop formation. Indeed, while the magnetization inversion takes place and the droplets providing the inversion grow, clusters of different dimensions merge together and expand. Moreover, not all the clusters cooperate cooperate with the external field and could cause important delays before

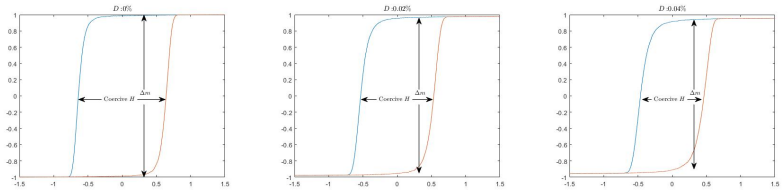

Figure 6.13: Plots of 1 hysteresis cycle. In the left panel, system in absence of defects. In the middle and right panel, system with $D = 2\%$ and 4%. We can notice a shrink in the value of the coercive filed and in the saturation magnetization.

reaching inversion. This could strongly affect the hysteresis properties. For this reason, we will focus our attention over systems both in ferromagnetic and spin-glass phases, i.e. also when the system shows cluster formation.

6.5.1 Hysteresis area

Having spins fixed with a certain orientation has effects on the area of the loop. Roughly speaking, the loop can be approximated with a parallelogram with width double the value of the coercive field and height double the Δm experienced during a semi-cycle, as represented in fig. 6.13. Therefore, the area can be estimated by four times the value of the coercive field.
Since the introduction of defects allows the system to better follow the external magnetic field we expect a reduction on the coercive field value. Also Δm in a semi-cycle will be less than two: some spins remains fixed no matter the intensity of the external field and therefore complete magnetization cannot be reached. We expect the area of the loop to decrease while the defects fraction is increased.

This justifies what can be observed in fig. 6.14, 6.15 and 6.16. Moreover, the power-laws regarding the hysteresis loop area and the magnetic field intensity or frequency are still confirmed even in presence of defects (all R^2 values above 0.995). We are considering log-log plots, as to reduce the power-law to a linear relation. The b coefficient, relating the frequency $\omega = 1/P$ with the loop area, ranges from 0.250 ± 0.002 in the absence of defects up to 0.400 ± 0.005 in case of $D = 6\%$. The a coefficient, instead relating

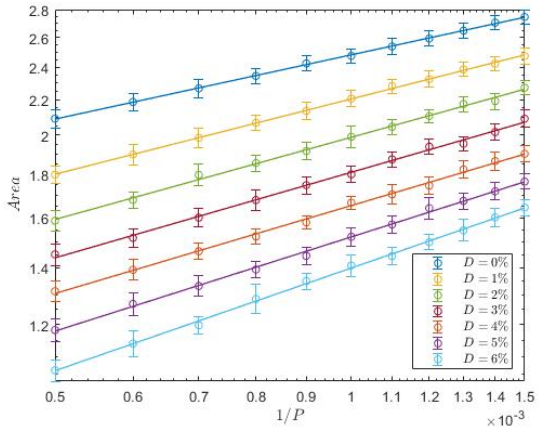

Figure 6.14: Area of the loop versus the oscillating frequency in a logarithmic plot, as to verify the power low suggested. Standard errors are superimposed to the markers.

the intensity of the field with the loop area, ranges from 0.248 ± 0.008 to 0.411 ± 0.004 in case of $D = 4\%$.
In the case of the temperature dependence, the relation $A(T)$ cannot be considered a power-law, probably due to the fact that the power-laws are expected only in the $\omega \to 0$ (or $P \to \infty$) limit, as anticipated in the previous chapter. For this reason, the plot is presented in linear scale, with a linear regression characterised by $R^2 > 0.99$ in all the presented cases. The angular coefficient increases while increasing the the fraction of defects, from -3.11 ± 0.09 in absence of defects to -1.90 ± 0.01 in case of $D = 4\%$.

A better visualisation of the defects effect can be seen while plotting the area function of the fraction of defects, as done in fig. 6.17 for different choices of T and H. As it can be seen, the fraction of defects investigated exceeds the limit we were considering as to remain in the ferromagnetic phase. Percentage greater than 10% will move for sure the system in the spin-glass phase, with cluster formation and losing the ability to show spontaneous magnetization. Nevertheless, out of curiosity, the plot is extended also for higher defects fractions. It was found an exponential dependency from the fraction of defects. In particular:

$$A \sim 10^{d \cdot D} \tag{6.5}$$

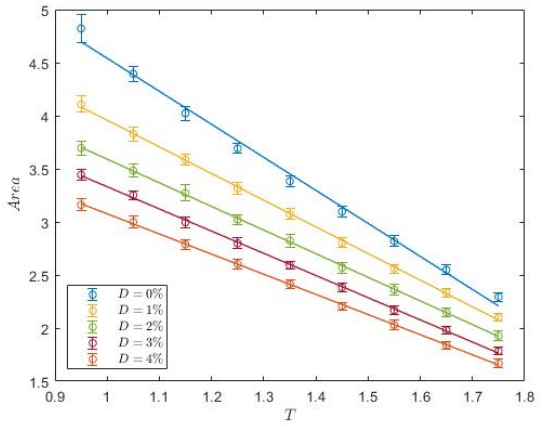

Figure 6.15: Area of the loop versus the temperature in a logarithmic plot, as to verify the power low suggested. Standard errors are superimposed to the markers.

where D is the considered fraction of defects and d is a temperature and magnetic field dependent coefficient. The calculated values in the simulations are presented in table 6.3. All the linear regression in the semi-logarithmic plane showed $R^2 > 0.995$. Finally, in presence of defects, we suggest the following formula describing the dependencies with temperature, field frequency, field intensity and fraction of defects:

$$A \sim h_0^a \omega^b T^c 10^{d \cdot D} \tag{6.6}$$

d coefficient		
	$H = 1.5$	$H = 3$
$T = 1.3$	-3.47 ± 0.07	-3.04 ± 0.06
$T = 1.7$	-3.90 ± 0.03	-3.27 ± 0.03

Table 6.3: Table for the defects dependence coefficient.

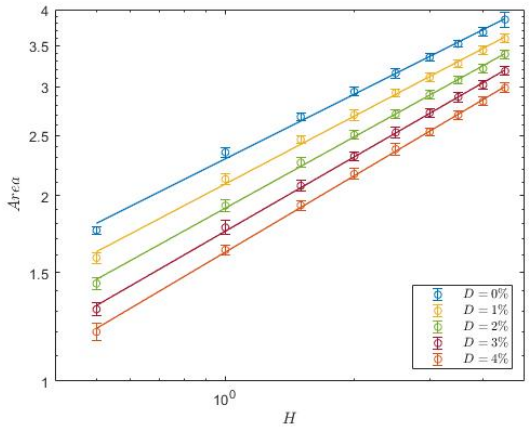

Figure 6.16: Area of the loop versus the field intensity in a logarithmic plot, as to verify the power low suggested. Standard errors are superimposed to the markers.

6.5.2 Magnetic susceptibility

As in the previous chapter, we now analyse the DC magnetic susceptibility coming from the analysis of the hysteresis loop through the Curie-Weiss law. An indication of the behaviour while increasing the fraction of defects would be enough. With the same procedure adopted in the previous chapter, with the only difference that random defects are present and at least 5 replicas considered, the plot represented in fig. 6.18 is derived. Table 6.4 shows instead the estimated value for T_c.

D	T_c
0%	2.75 ± 0.06
1%	2.72 ± 0.06
2%	2.79 ± 0.06
3%	2.65 ± 0.06

Table 6.4: Table for the estimation of T_c from DC magnetic susceptibility measurements for different fraction of defects.

The critical temperature seems to decrease linearly with the fraction of de-

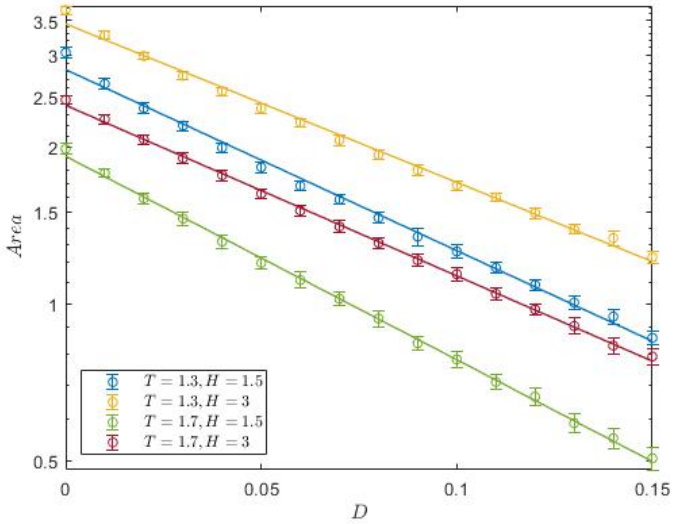

Figure 6.17: Area of the loop versus fraction of defects in a semi-logarithmic plot. Standard errors are superimposed to the markers.

fects, even though the estimated values are not in good agreement with the ones that can be derived considering the static magnetic susceptibility plots, in paragraph 6.3.1. This is expected, since already for the case without defects we obtain an overestimation of the critical temperature.
Moreover, no differences can be seen in the χ_M behaviour when the fraction of defects is high enough to induce the spin-glass-phase (as it should happen in the case $D = 3\%$).

6.6 Statistical analysis of Barkhausen jumps

Thus far, our concern with the hysteresis loop properties has touched only the characteristics over a complete cycle. Nothing has been said about the transition that brings the magnetization to reverse its value. By looking more closely to the transition in real systems, it has been noticed that the magnetization does not proceed smoothly as the magnetic field is applied. Instead, it changes abruptly through discrete jumps with different amplitude.

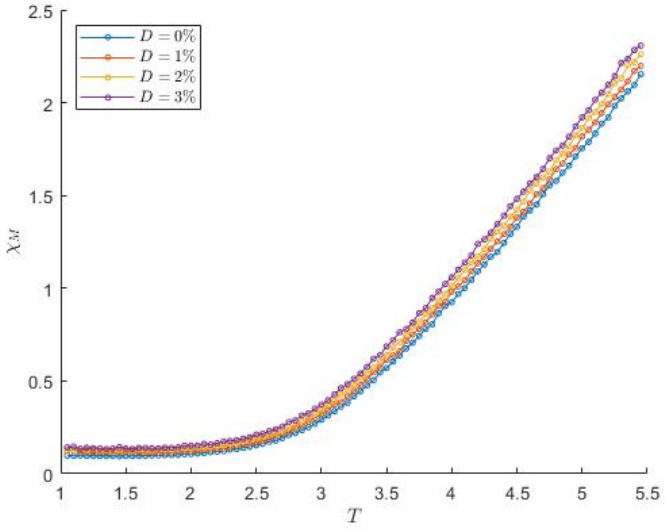

Figure 6.18: Magnetic susceptibility, function of the temperature for different fraction of defects:$D = 0\%; 1\%; 2\%; 3\%$. Error bars are not shown since are of the same dimension of the markers.

This behaviour was first noticed by Barkhausen in 1919 and was named after him as Barkhausen noise. A basic explanation of this phenomenon has been given considering the presence of growing regions in the material characterised by magnetic moments oriented in the same direction of the external magnetic field H. Indeed, while H is increased, these energetically favoured regions start to grow inside the material. Once they reach a defect in the structure, they suddenly stop their motion and remain stuck with the defect until the magnetic field is sufficiently high to unpin them. This procedure repeats until the material has been completely magnetized or the external magnetic field is reversed.
After the unpinning of a growing region, the magnetization experiences a jump with a certain amplitude (Δm). If many amplitudes are collected over multiple loop cycles their probability distribution can be derived $P(\Delta m)$. Puppin and Zani [24] [25] investigated over this topic and found a power-law emerging in real systems between Δm and $P(\Delta m)$:

$$P(\Delta m) = \Delta m^{\tau} \tag{6.7}$$

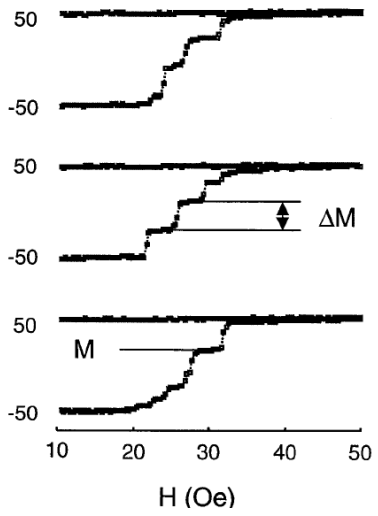

Figure 6.19: ΔM represents a magnetization jump associated to the reversal of the magnetization inside a material while a magnetic field is applied. Source [25].

for both positive (Δm with same sign of the applied magnetic field) and negative jumps (Δm with opposite sign of the applied magnetic field). Equilibrium Monte Carlo simulations were devised as to reproduce such power-laws, giving good agreement [26]. In this paragraph, we try to extend such investigation in out-of-equilibrium systems with the Lebowitz algorithm which could be a more appropriate approach considering the out equilibrium nature of hysteresis loops.

Before proceeding with the statistical analysis an important clarification must be done. What do we take as a magnetization jump? In the real physical world, a jump can be easily identified as the magnetization difference between two metastable levels, as can be seen in fig. 6.19. In the Equilibrium Monte Carlo simulation, instead, a jump is defined as the Δm before and after the magnetic field is increased/decreased of a fixed amount dH, following the procedure illustrated at the beginning of chapter 4. In the dynamic Monte Carlo defining a jump is less straightforward. We cannot rely over the Δm between metastable states, since it is rather complex to locate them. If one looks closely enough, the magnetization varies at each simulation step by a tiny amount $\Delta m = \pm 2/L^2$ and it is not possible understand if a fluctuation

is simply an effect due to the simulation that requires a modification of the magnetization at each step or if it is due to the system stuck in a metastable state. Moreover, measuring every fixed amount of *MCSS*, as to resemble the method done for the Equilibrium Monte Carlo simulation, doesn't have physical sense, since the magnetic field is related to the physical-time instead of the *MCSS* and we would end up measuring every now and then depending on the relation physical-time versus *MCSS*.
Two practical ways can be considered:

1. We take as a jump the Δm between the magnetizations sampled at time distance of a fixed quantity Δt (in physical-time).
2. We consider the previous definition, but we group together the consecutive jumps with same sign, as to alternate a positive with a negative jump.

In the following the former methodology has been considered. Attention must be paid while choosing the Δt value. Indeed we want to ensure that the system has enough time to perform at least the same number of spin updates as the number of spin of the system. This set a minimum threshold in the Δt value, which can be quantified considering the external parameters of the simulation (T, L, P, ...) and the plots in fig. 5.3 and 5.4. Moreover, if we choose a too high Δt, we may miss to register smaller jumps and consider them as one bigger. Also negative jumps become more difficult to catch. This, instead, set an upper level for Δt, which cannot be easily calculated. For this reason, Δt was taken as small as possible, equal to the physical-time equivalent to few *MCSS*.

We have to remember that we can properly speak about hysteresis jumps only in presence of defects. Indeed, if the external magnetic field is slowly varied in absence of defects, the system experiences a sudden reversal magnetization when H becomes equal to the coercive field. In order to understand the right choice for Δt, we have also to look at the percentage of defects inside the lattice. With this aim, the plots represented in fig. 6.20 were derived.

As we can see, the fraction of defects does not strongly influence the relation physical-time versus *MCSS* far from equilibrium. Near equilibrium, the situation changes and the fraction of defects must be considered while

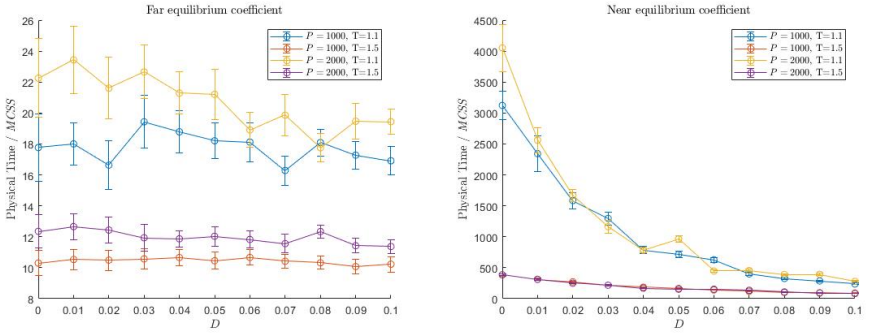

Figure 6.20: L fixed at 50. In the right panel the ratio between the physical-time and the *MCSS* in near equilibrium conditions; in the left panel the same ratio in far from equilibrium conditions for different values of the defects concentration D. Simulations done for different initialisation temperatures T and magnetic field periods P. H fixed at 1.

deciding the appropriate Δt. Moreover, if we fix a particular Δt, it may happen that the appropriate number of *MCSS* are spent in the near equilibrium condition but not for the far equilibrium condition and vice versa, since the proportionality coefficients have different order of magnitudes for the two cases.

As to have a reliable statistic, at least three order of magnitudes for the jump amplitudes (Δm) were considered. This sets a condition over the lateral size of the system. Indeed, the maximum jumps that can be measured are of the order of $5 \cdot 10^{-1}$. Therefore, we want to be able to detect jumps of the order from 10^{-1} to 10^{-5}. Since the minimum detectable Δm is $2/L^2$, we must have at least $L \geq 200$.

The following simulation is devised:

1. A lattice with $L = 200$ is initialised completely negatively magnetized, with fixed temperature $T < T_c$.

2. Random defects are added to the lattice, in fixed positions and orientation.

3. A sinusoidal magnetic field is superimposed with fixed amplitude $H_0 =$

0.5. The period for the oscillation is chosen as to leave enough time to the system to vary the magnetization. in particular, $P = 10^6$

4. Every Δt, the magnetization is sampled and Δm is derived. The measurement are repeated along all the cycle and for a fixed number of cycles.

5. The precedent steps are repeated many times as to have a considerable amount of data derived from multiple initialisation of defects.

We have proceeded with the analysis regarding positive and negative jumps separately, both in the cases near equilibrium and far from equilibrium. As to distinguish between the vicinity to equilibrium, we have considered all the jumps when $|m| > 0.9$ as near equilibrium jumps. Otherwise, as far from equilibrium jumps. The power low is interpolated beginning from the peak in $P(\Delta m)$ up to $\Delta m \longrightarrow 1$. The fraction of defects is chosen to be 3%, which, dependently on the value of the temperature could cause the system to fall in the spin-glass phase. For this reason, we expect worse results for higher temperatures. Results from the simulation while the temperature of the system is varied are presented in fig. 6.21.

As predicted, increasing the temperature, the linear regression worsens. By looking at the plot of the hysteresis cycles, for $T = 1.8$ the system seems to approach the paramagnetic behaviour in which the area of the loop approaches zero. Another problem can derive from the failure in the identification of the metastable states and therefore in the identification of the incorrect jumps (and a worse $P(\Delta m)$ statistics). Indeed, in the considered approach, a transition between metastable states could be decomposed in many intermediate steps if the time the system takes to move from two metastable states is lower then Δt. Indication of this behaviour can be seen in the absence of jumps in the order of magnitude of 10^{-1} for all temperatures, which sounds a little strange considering the hysteresis plots. Moreover, as can be better seen in the second simulation for $T = 1.6$, the overall jump statistics has a shallow peak towards higher Δm. What makes inaccurate the estimate is the "far equilibrium"jumps, for which no power-law seems to be found.

A significant improvement is obtained if we group together all the consecutive jumps with same sign. In this way, we obtain an alternation between

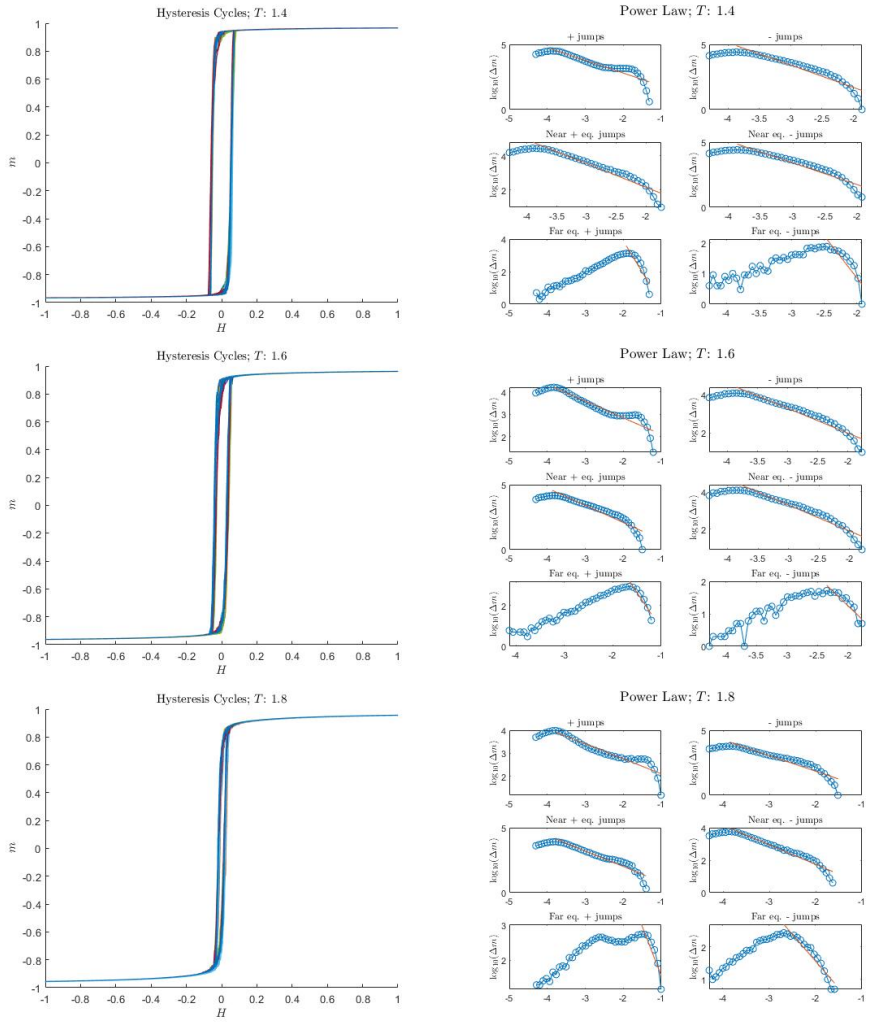

Figure 6.21: In the left panel, the hysteresis loops from which the jump statistic is derived. In the right panel, the $P(\Delta m)$ calculated for positive ("+") and negative jumps ("-") far from equilibrium, near equilibrium and total. The scale is logarithmic as to reduce the power-law in a linear regression. Parameters of the simulation: field period $P = 5 \cdot 10^5$; field amplitude $H_0 = 1$; fraction of defects $D = 3\%$; Number of replicas: 8; Number of hysteresis cycles: 4; Lateral Size: $L = 200$.

positive and negative jumps and we do not risk to separate a unique jump in multiple smaller ones. Fig. 6.22 shows the derived jumps statistical analysis. As we can observe, the positive jumps statistics improves. Instead, the negative jumps statistic does not seem to improve, especially for the "far from equilibrium"jumps. This behaviour is expected. Indeed, in the"far equilibrium"condition, the system undergoes a magnetization reversal.

Finally, the coefficients for the power-law are derived. Results are reported in table 6.5. The coefficients found are in reasonable agreement with what experimentally observed by Puppin [25] and Zani et al. [24]: in the overall statistic, the experimental power-law coefficients were found to be $\tau = -1.1$ in case of positive jumps and $\tau = -1.6$ for negative jumps.

T	τ		R^2	
1.4	-0.95	-1.56	0.962	0.921
	-1.33	-1.62	0.995	0.914
	-0.49	-1.80	0.563	0.843
1.6	-0.88	-1.30	0.956	0.931
	-1.22	-1.37	0.979	0.920
	-0.44	-2.25	0.421	0.801
1.8	-0.90	-1.18	0.926	0.870
	-1.08	-1.21	0.974	0.947
	-0.65	-1.73	0.720	0.856

Table 6.5: Table for the jump statistics. In each sub-table, the coefficient and the R^2 refers to the corresponding statistic in the sub-plot of fig. 6.22. The statistic for the overall near plus far equilibrium jumps are in the 1^{st}, 4^{th} and 7^{th} row, for each temperature value considered.

As final remark, also simulations for $D = 4\%$ were considered and the statistics derived. No major differences in the power-law coefficient could be found. The defect concentration seems not to influence significantly the critical exponent associated with the jumps statistics. What we expect is that the fraction of defects could influence the range over which we can found a power-law. Indeed, in $D \longrightarrow 0$ we cannot consider a statistic since the magnetic reversal happens in just one jump.

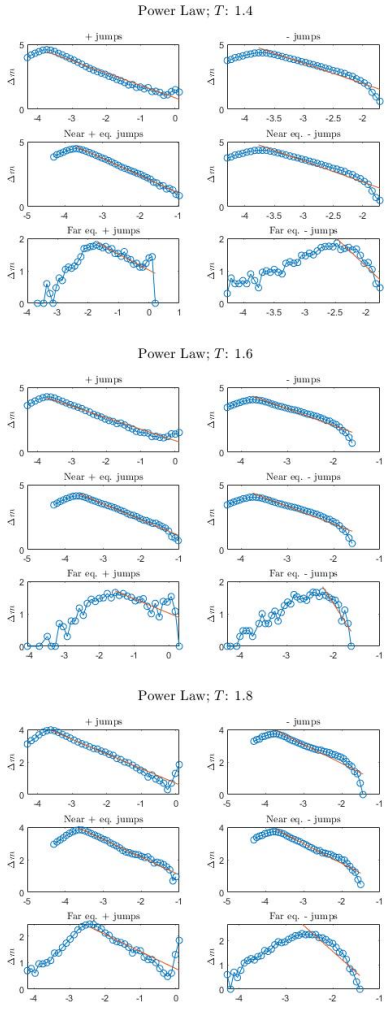

Figure 6.22: In the figure, the $P(\Delta m)$ calculated for positive ("+") and negative jumps ("-") far from equilibrium, near equilibrium and total. The scale is logarithmic as to reduce the power-law in a linear regression. Parameters of the simulation: field period $P = 5 \cdot 10^5$; field amplitude $H_0 = 1$; fraction of defects $D = 3\%$; Number of replicas: 8; Number of hysteresis cycles: 4; Lateral Size: $L = 200$.

Chapter 7

Application to opinion formation in human dynamics

Thus far, we have extensively described the behaviour of magnetic systems out or in equilibrium conditions. This could misleadingly induce to think the Ising Model as describing "merely"physical systems. This is not the case. What happens if we try to apply the Ising Model to a completely different field of study? Its relatively simple structure, decomposed to its essence, describes the interplay between many actors, characterised by a binary behaviour (i.e. yes or no, spin up or spin down, ...) and with the ability to influence whoever is near them. Possibly, it accounts for the effect of a "noise"(in the physical system interpreted by a non-zero temperature) that brings disorder into the structure.
In this final chapter we will investigate one of the possible extensions and applications of the Ising Model to non-magnetic systems. More precisely, we will analyse the ability of the model to describe the process of opinion formation in human society, when the opinion is characterised by only two levels. The parallelism is almost straightforward: individuals take the place of magnetic moments in the structure; binary opinion replaces spin direction (accounting for "vote yes"or "vote no"; "vote A"or "vote B"in a bicameral type of government,...) and the interaction is represented by opinion exchange in all kind of conditions. The effect of temperature over the system can be interpreted as the possibility that individuals can change their opinion

without any influence, counterbalancing the opinion exchange process.
This type of application finds place into the realm of the sociophysics, which considers mathematical techniques ad tools in order to derive information regarding the behaviour of human crowds.
Once clarified how the Ising Model could be extended out of the magnetic applications, we can ask ourselves on which occasion we can perform Monte Carlo simulations. This is a delicate issue. Indeed, the convergence to equilibrium of the Monte-Carlo simulations is ensured in the presence of a Hamiltonian, which is something that, depending on the type of the model, cannot be always easily assigned.
initial part of this chapter, we present an opinion formation model known as Sznajd Model (SM). Then, we consider the issue of making it Hamiltonian, by implementing a minimal number of modifications on the original SM. We devise Monte Carlo simulations to validate the similarity between the two models, and, finally, we describe the effect of "social temperature".

7.1 Sznajd model

The Sznajd Model was introduced in 2001 [27] with the aim of describing the formation and evolution of democratic decisions inside society. After its appearance, it received a lot of attention and was further extended to describe more complex systems ([28] [29] [30]). In its simplest form, it considers a society modelled as a linear chain of N spins with either opinion "yes"or "no", i.e. orientation $+1$ or -1. The interaction between two individuals produces the spreading of opinions to their neighbours. This process repeats again and again until a steady-state condition is reached. From a practical point of view, the algorithm consists of the following steps:

1. Selection: a spin in the chain is randomly selected (S_i).
2. Dynamical rule:
    - (First dynamical rule): if S_i and S_{i+1} share the same opinion, they extend it to their neighbours. $S_{i+2} = S_{i-1} = S_i$

- (Second dynamical rule): if the S_i and S_{i+1} have different opinion, then their neighbours S_{i+2} and S_{i-1} take opposite opinion. In particular, $S_{i+2} = S_i$ and $S_{i+1} = S_{i-1}$.

3. Repeat: step 1-2 are repeated until an equilibrium condition is reached.

The algorithm is explicitly devised to let the system evolve towards one of the following equilibrium configurations:

- Dictatorship: all the individuals share the same opinion (either "yes"or "no")
- Stalemate: indecision rules. All the individuals have opposite opinion with respect to their neighbours. "Yes"and "no"are equally shared among the whole population.

In the first publication [27], it was found that these configurations emerge with different probabilities depending on the initialisation condition. In particular, it depends on the initial fraction of individuals voting "yes"(or, if one prefers, "no"), as shown in fig. 7.1.

Extensions to this simple model were proposed within the same paper. In particular, since in reality the decision formation does not come from the mere contact between people but also requires some sort of persuasion, it was introduced the possibility to not follow the deterministic algorithm. In practical terms, a neighbour can decide to behave randomly with probability p ($p < 1$) instead of being updated following the dynamical rules. This modification emulates a sort of information noise, which affects are similar to the ones brought by thermal noise. This topic will be analysed in the last paragraph of this chapter.

In subsequent publications, another interesting modification to the SM has been proposed. In particular, the second dynamical rule was modified as follows:

- if spins S_i and S_{i+1} have different opinion, then with probability $p < 1$ their neighbours S_{i+2} and S_{i-1} take opposite opinion $S_{i+2} = S_i$ and $S_{i+1} = S_{i-1}$, with probability $1 - p$ nothing happens.

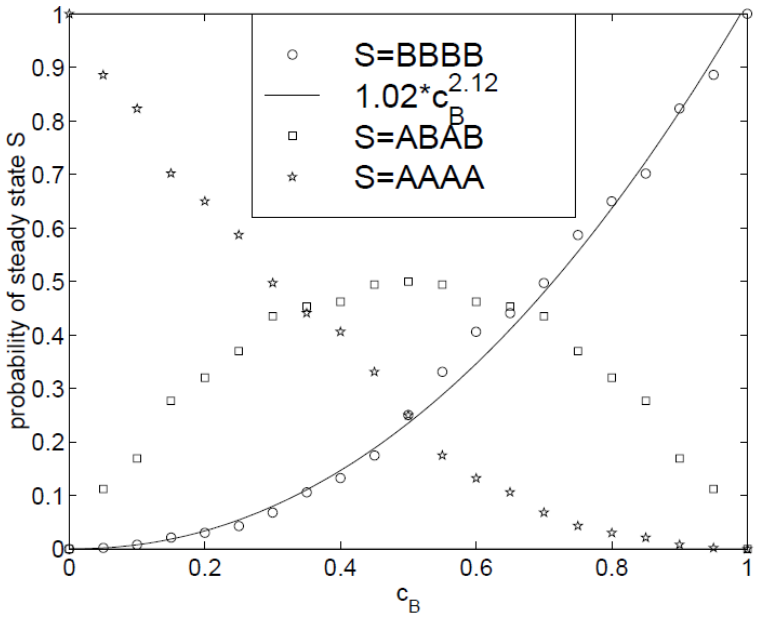

Figure 7.1: Achieved final configuration at equilibrium. The three equilibrium condition are here indicated with $BBBB$ and $AAAA$ as dictatorship and $ABAB$ as stalemate. c_B is the fraction of individuals voting B for an election. Source [27].

For their peculiarity, some SMs with particular choices of p have been defined: $p = 1$ is named "*United we Stand, Divided we Fall*"$(USDF)$ which is the standard algorithm; $p = 0.5$ is named "*if you Don't Know what to do, just Do Whatever*"$(DKDW)$; $p = 0$ is named "*if you Don't Know what to do, just Do Nothing*"$(DKDN)$. These three possibilities lead to a different spectrum of results, depending also on the initialised fraction of voting "yes". A practical representation is offered in fig. 7.2, where the 3 conditions over p are simulated with different choice of the initial fraction of individuals voting "yes"$(c = 0.25; 0.5; 0.75)$.

The developed model is a very elegant way of describing the formation of opinions inside a society. But, to derive a Hamiltonian from the rules stated is not a simple task. If we want to introduce Monte Carlo simulations, we have to find a way to express the system Hamiltonian, possibly with a slight modification of the dynamical rule. In the following paragraph, we present a slightly different model that tries to emulate the behaviour of the SM, char-

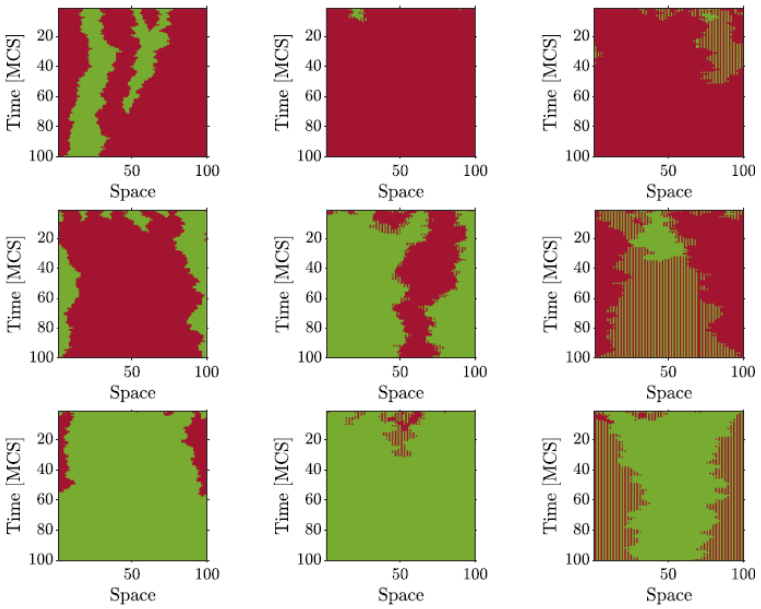

Figure 7.2: Evolution of the different SMs (left column, $p = 0$: *if you Don't Know what to do, Do Nothing*; middle column, $p = 0.5$: *if you Don't Know what to do, Do Whatever*; right column, $p = 1$: *United we Stand, Divided we Fall*) for different fraction c. Each row correspond to the 1D chain at a different *MCSS*. In each subplot, time flows from top to bottom row. Source [31].

acterised by an explicit Hamiltonian. We will consider this model a possible alternative to the SM only if we are able to reproduce the same steady-state behaviour (probability of final configurations appearance function of the initial fraction of people voting "yes") and the same properties.

7.2 A Hamiltonian for the Sznajd Model

To find a suitable Hamiltonian for an opinion formation model, we can start considering the SM dynamics and then introduce some modifications. Firstly, for convenience, when we pick a spin in the structure, instead of extending its opinion to its neighbours, we would like to question its opinion and therefore

decide whether to flip it or not. Secondly, we would like that the chosen spin checks its first and second neighbours and then it decides based on the majority of them. This means that only if three of the four nearest neighbours are equally oriented (i.e. there's at least a couple of consecutive spins with the same orientation) it becomes convenient for a spin to flip. This should modele the first dynamical rule of the SM, in which couples of consecutive individuals with the same opinion produce the spreading of their opinion. Moreover, another feature of the SM is reproduced: indecision. To understand it, we can use the following case:

$$\begin{array}{ccccc} 1 & 2 & 3 & 4 & 5 \\ + & + & - & - & - \end{array} \tag{7.1}$$

Depending on which couples 1 & 2 or 4 & 5 is selected in the standard SM, the spin 3 should be oriented as + or -. Our approach also considers indecision since there is no clear majority in the neighbours of spin 3 and both orientations are accepted.

And for the second dynamical rule? In reality, it is not well reproduced. As an example, consider the following case:

$$\begin{array}{ccccc} 1 & 2 & 3 & 4 & 5 \\ + & - & - & - & + \end{array} \tag{7.2}$$

If one of the two couples 1 & 2 or 4 & 5 is selected in the SM, the spin 3 should be oriented as +. In our approach, instead, spin 3 shows indecision and there is not a preferable orientation. A possible solution for this indecision could be consider a different value for the interactions between first and second neighbours, even though it will not be implemented and analysed in this work. For this reason, we expect some differences between the two models.

From the two initial requests, considering a linear chain, we can consider the following Hamiltonian:

$$H_{SM} = -\sum_i (s_i)(s_{i-2} + s_{i-1} + s_{i+1} + s_{i+2}) \tag{7.3}$$

with $s_i = \pm 1$. Here, we have considered equal the exchange integrals between first and second neighbours, $J_1 = J_2 = 1$, since in the SM spin 1 has the same interaction over 3 as 2. Once the majority of the neighbours share the same direction, s_i minimises the total energy by choosing the same orientation of its neighbours, as desired. Equation (7.3) is simply equivalent to the second-neighbour Ising Model Hamiltonian. Indeed:

$$H_{SM} = -\sum_i (s_i s_{i-2} + s_i s_{i-1} + s_i s_{i+1} + s_i s_{i+2}) = -\sum_{\langle i,j \rangle^2} (s_i s_j) = H_{2N}^{1D} \quad (7.4)$$

in which $\langle i, j \rangle^2$ denotes the sum over all the first and second neighbours.

Once found a suitable Hamiltonian model emulating the Sznajd dynamics, we can now focus on what is still missing before proceeding with actual simulations. Both the Glauber dynamics and the Lebowitz algorithm must be adapted. And, each one of them requires a little discussion.

7.2.1 Adapting the Glauber dynamics

Thus far, the Glauber dynamics has been used in the transition probabilities expression ($w_i(s_i)$), representing the probability of a transition between states characterised by the reversal of the i-th spin. The deterministic nature of the SM (i.e. the presence of an algorithm following which we arrive at equilibrium) induces us to pick a $T = 0$ model. What does it happen to the transition probabilities in such a critical condition? If we simply take $T \longrightarrow 0$, we obtain:

$$\lim_{T \to 0} w_i(s_i) = \lim_{T \to 0} \left[\frac{1}{2} \left(1 - s_i \tanh\left(\frac{\Delta E_i}{k_B T} \right) \right) \right] = \begin{cases} 0, & \text{if } \Delta E_i > 0 \\ 0.5, & \text{if } \Delta E_i = 0 \\ 1, & \text{if } \Delta E_i < 0 \end{cases} \quad (7.5)$$

where ΔE_i represents the energy gain the system has upon inversion of spin i. In other words, the transition into a state with the i-th spin inverted has a transition rate equal to 1 if during the process the total energy lowers ($\Delta E_i < 0$), equal to 0 if the total energy increases ($\Delta E_i > 0$), equal to 0.5 if the total energy remains constant($\Delta E_i = 0$). This is the behaviour we would expect at zero temperature: the transition into states with higher energy is

now not allowed since the thermal energy is null. Before any other possible observation, it could be helpful analysing also the modifications required in the Lebowitz algorithm.

7.2.2 Adapting the Lebowitz algorithm

Differently from the previous version of the Lebowitz algorithm used for a bi-dimensional, first nearest-neighbours Ising Model, we now consider a chain of spins and the interaction with the second nearest neighbours. As seen in chapter 2 (Methods), the Lebowitz algorithm requires as many classes as the number of different ΔE that a spin-flip could bring into the system energy. If we assume equal interactions ($J_1 = J_2 = 1$) between first and second neighbours, the total number of classes is, fortunately, 10: it coincides with the one we had for the bi-dimensional system. This is reasonable if one considers that, provided that both J_1 and J_2 are equals, nothing changes in terms of energy between the cross and the line configurations.

$$\begin{array}{ccc} & + & \\ + & - & + \\ & + & \end{array} \quad \Longleftrightarrow \quad + \; + \; - \; + \; + \tag{7.6}$$

Continuing with the analogies, during a spin-flip event, the selected spin changes the class of ± 5. Its first and second neighbours change classes by ± 1. Everything remains equal to the previous version of the algorithm, except the structure of the variables Location and Class. They will be turned into an array instead of a matrix, reflecting the system's mono-dimensionality. Table 7.1 sums up all the characteristics of the classes.

Starting from a random disposition of the opinions in the chain, at the beginning of the simulation classes 3 and 8 will be more occupied; classes 1-5-6-10 less occupied. Once started, we will observe a progressive emptying of the 3-4-5-6-7-8 classes and the consequently filling of the 1-2-9-10 classes. This may take a consistent amount of simulation steps. Indeed, it could happen that the 1D analogous of the striped configurations encountered in chapters 4 and 5 emerge (shown in fig. 7.3). In these configurations, almost the totality of spins are in classes 1 and 10 and classes 2-3-8-9 are all populated by 1

class	opinion	# of +1 neighbours	ΔE_i	w_i
1	+1	4	+4	0
2	+1	3	+2	0
3	+1	2	0	0.5
4	+1	1	-2	1
5	+1	0	-4	1
6	−1	4	-4	1
7	−1	3	-2	1
8	−1	2	0	0.5
9	−1	1	+2	0
10	−1	0	+4	0

Table 7.1: 10 Classes for the 2 nearest neighbours Lebowitz algorithm. The second column represent the opinion of the spin in a particular class. The third column, the number of spins with orientation +1 considering all the first and second neighbours. Fourth column represents the change in the total system energy that the inversion of a spin in a particular class would bring. Fifth column the transition probability related to the spin in a particular class.

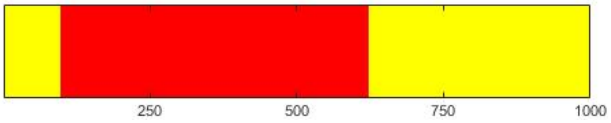

Figure 7.3: 1D analogous of a stripe configuration. It is possible to recognise 2 clusters with opposite opinions.

spin. This metastable state can dissolve only if one of the two equally oriented regions shrinks to the point that it consists of only 1 spin. Then it will be reversed the next step. And then? Actually, this is a big problem from the point of view of the simulation with the Lebowitz algorithm: the algorithm will fail in the identification of the next spin to invert. From the point of view of the model, once dictatorship is reached (all individuals share the same opinion), we can say that an equilibrium condition has been reached and nothing will happen again, forever and ever, since we are at $T = 0$. Therefore, it makes complete sense that the simulation stops running.

In the following, the created model will be referred to as Hamiltonian Sznajd

Model (HSM), even if one of the basic dynamical rules of SM has been slightly modified. We can now proceed with the analysis of the results coming from the HSM and compare them with the ones from SM.

7.3 Zero-temperature models analysis

Before presenting the results coming from simulations over the HSM, we have to clarify with which SM we should compare them. We have defined three possible SMs, depending on the value p chosen for accepting or not the second dynamical rule. We can consider the following cases. For simplicity, as done in the previous paragraph, we switch for just a few lines to the Metropolis Algorithm instead of the Lebowitz Algorithm, speaking of a posteriori inversion instead of a priori. This should not harm the argumentation.

- $++-++$: the spin in the middle has transition probability (w) equal to $+1$. Therefore, if selected, it will be flipped.
- $++--+$: the spin in the middle has also $w = 1$. If selected it will be flipped.
- $+-++-$: the spin in the middle is characterised by $w = 0.5$. Its selection does not lead unequivocally to the inversion: there's 50% chance.
- $+----$: the spin in the middle has $w = 0$. It will not change orientation.
- $-----$: the spin in the middle has $w = 0$. It will not change orientation.

The third case is the one we are interested in since it resembles the condition in which the second dynamical rule of SM applies (i.e. indecision condition). Since here we have $w = 0.5$, we will consider the SM with $p = 0.5$, which corresponds to the *If you Don't Know what to do, just do whatever* ($DKDW$) for the comparison.

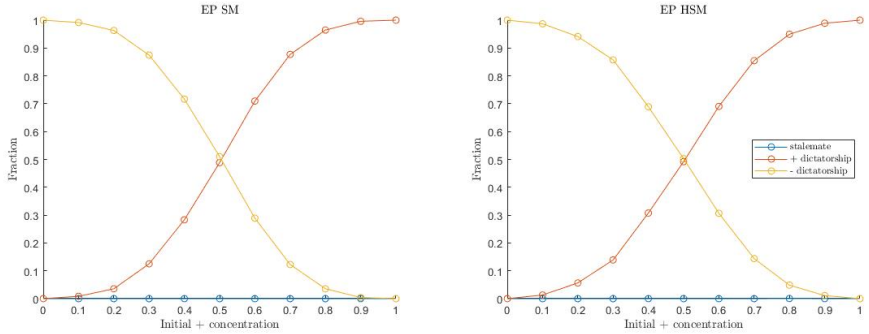

Figure 7.4: EP after 2000 *MCSS* considering SM (DKDW) in the left panel and HSM in the right panel. Each line correspond to one of the possible equilibrium configuration: dictatorship positive red line, dictatorship negative yellow line, stalemate blue line.

Now, we aim to compare the results of the simulations obtained from the two models (SM and HSM). In particular, we are interested in the Exit Probabilities (EP), defined as the probability that a chain will evolve reaching a specific equilibrium configuration. Since we have three possible equilibrium configurations, we will have three different EPs. Every single EP depends on the initial fraction c of spins $+1$. As an example, starting from a small fraction c, it is more likely to obtain the negative dictatorship as equilibrium configuration.
Fig. 7.4 shows the EPs, function of the initial fraction c of spins $+1$, obtained from a simulation over 2000 chains with size $N = 100$, considering the SM ($DKDW$) and HSM. Before the system reaches one of the possible equilibrium configurations, a certain amount of simulation steps are required (here expressed as the usual $MCSS$). For these simulations, 2000 $MCSS$ were waited. Only 0.2% of the chains did not reach one of the possible equilibrium configurations, as they had not enough simulation steps to reach them and were discarded.

As it is possible to observe, no major differences between the equilibrium configurations are showed. Moreover, in both cases, we have a clear indication that the stalemate is an unstable equilibrium configuration since it has not been reached even once. As one expects, the dictatorship configurations are symmetric with respect to $c = 0$.

We can now analyse how fast a chain approaches equilibrium for both models. Since the final configurations are characterised by spins equally oriented, how fast they will be reached depends on the fraction of initialised spins up c. For this purpose 2000 chains with $N = 100$ were considered. Simulations with different values of c were run for 200; 400; 800 *MCSS* for both models. The number of chains that did not reach one of the possible equilibrium configurations at the end of the simulation was derived and it is plotted in fig. 7.5. As one can expect, the number of configurations that do not reach equilibrium is higher when c is near 0.5: reaching the equilibrium requires a longer time if the system has equally oriented spins up or down. If we now compare the results, we notice that the HSM, with the Lebowitz algorithm, proceeds towards equilibrium in less *MCSS*. Indeed, all the chains reached equilibrium, even when the simulation was run for the shorter amount of *MCSS*.

What found is reasonable. This is a feature of the Lebowitz algorithm that, when the temperature approaches 0, proceeds rapidly towards equilibrium. For a better understanding, consider the particular case in which a simple $N = 10$ chain has only one spin -1 aside from all the others (actually, this configuration, or one of the possible permutations, is very likely to happen in the simulation before positive dictatorship is reached):

$$+ \quad + \quad + \quad + \quad + \quad - \quad + \quad + \quad + \quad + \tag{7.7}$$

By applying the Sznajd algorithm 5/10 spin choices do not modify anything in the structure. The simulation step in which no modification happens is defined as "wasted step". The number of these "wasted steps"in the Sznajd algorithm reasonably increases if we increase the dimensionality of the chain. Instead, with the Lebowitz algorithm, since the chosen spin will be reversed no matter what, no "wasted steps"can happen. This explains why the Lebowitz algorithm could be a better choice describing opinion formation while considering large systems.

It may be interesting also comparing how the transition towards equilibrium happens in both models. With this purpose, the same chain was left free to evolve following first the standard SM and then the HSM. Fig. 7.5 shows, row by row the chain after a *MCSS*. In this case, to test different initial

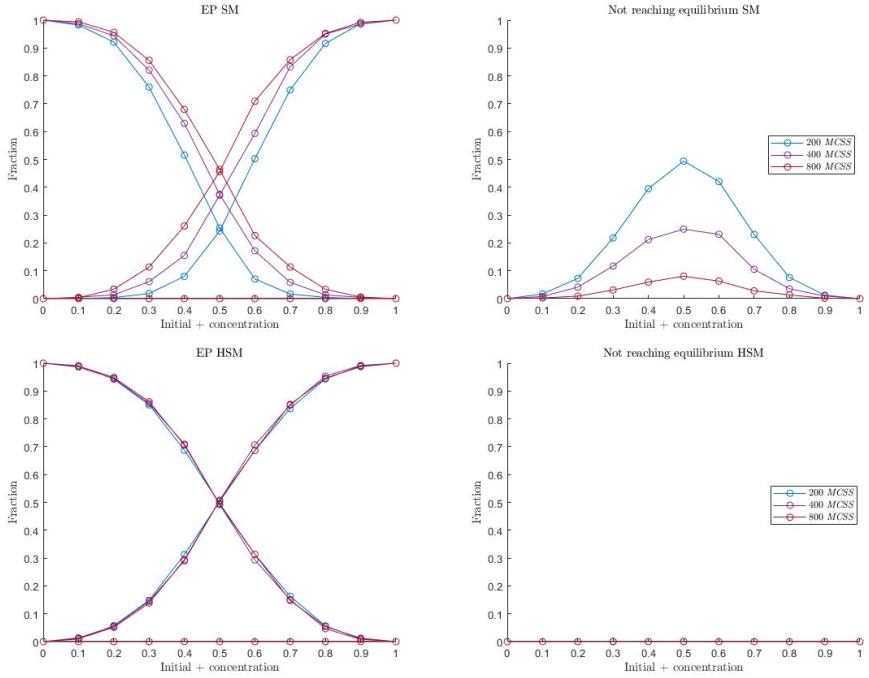

Figure 7.5: Results of the simulations considering SM in the first row, HSM in the second row. On the left, the EPs, function of the fraction c. On the right, the number of configurations that did not reach one of the equilibrium configurations, function of the fraction c. In both models, the simulations were run for a different amount of steps: 200; 400; 800 *MCSS*.

conditions, three chains with $c = 0.25; 0.5; 0.75$ were considered.
It is possible to understand better the difference between the *MCSS* of the two models. For SM, minor modifications differentiate one step from the following. For HSM, instead, changes in the chain happen faster. Moreover, looking at the case $c = 0.5$, we can observe the formation of regions equally oriented quite differently following the two models. Therefore the transition towards equilibrium is not comparable.

Inside the simulation, an individual may change his/her opinion multiple times. We define the time occurring before an opinion change as "time of stubbornness" and we refer to it as τ. In the original work [27], it was analysed the statistic coming from the time of stubbornness applied to the SM with (*USDF*) and it was found a power-law relating τ with its probability $P(\tau)$,

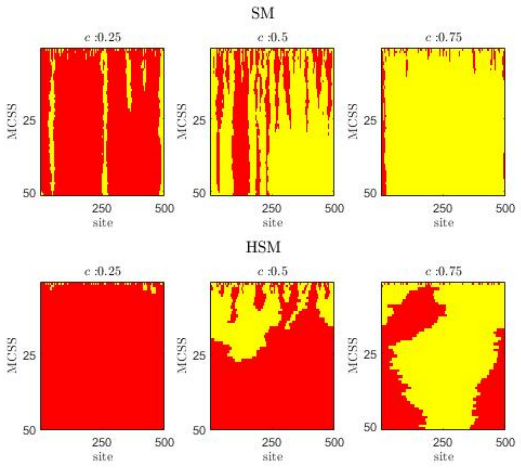

Figure 7.6: Transition towards equilibrium. Each row of each square represents the chain at a fixed *MCSS*. For each model, $c = 0.25$ (left); $c = 0.5$ (middle); $c = 0.75$ (left). SM on the top. HSM on the bottom.

with exponent -1.5. By analysing the SM ($DKDW$) (and even $DKDN$), the power-law happens to be still verified. Now we want to understand if it does apply to the new model (HSM).
It is necessary now a clarification. The time of stubbornness, for the SM (in all three cases), is calculated following a fictitious time t^* that follows the opinion change: it increases only when someone in the chain changes opinion. Practically speaking, t^* is quite similar to the *MCSS* in the HSM. For this reason, the comparison between the results from SM and HSM is reliable. Additionally, for the HSM we can measure the time of stubbornness considering the physical-time. Fig. 7.7 investigates the power-law coming from the time of stubbornness, calculated considering 100 chains of $N = 100$ that reached equilibrium, and 7.3 reports the values of the exponential and R^2 for the linear regressions, considering logarithmic plots.

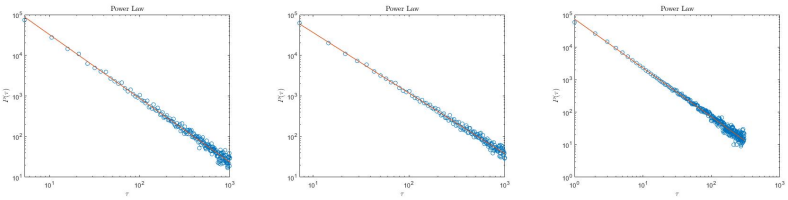

Figure 7.7: Power-law. Left panel: SM ($p = 0.5$). Middle panel: HSM considering *MCSS*. Right panel: HSM considering the physical-time. For both systems, data from 100 simulations over chains of size $N = 100$ were collected and analysed. Only simulations in which the equilibrium configuration is reached were considered. Linear regression was performed only over the interval $[1, 10^3]$ for the simulations in *MCSS* and $[10^-3, 3 * 10^2]$ for the simulations as to reduce the noise deriving from high times of stubbornness with very low frequency.

Model	α	R^2
SM ($p = 0.5$)	-1.57 ± 0.01	0.99
HSM (*MCSS*)	-1.49 ± 0.01	0.99
HSM (physical-time)	-1.50 ± 0.01	0.98

Table 7.2: Power-law information estimation. The exponents (α) are presented with the R^2 of linear regression in the logarithmic plot $P(\tau)$, τ.

As a final remark, we can conclude that, an alternative to the Sznajd Model of the type *Don't Know what to do, just Do Whatever*, could be the Hamiltonian Sznajd Model with the Lebowitz algorithm, even though the transition is not comparable. Every other important aspect as the Exit Probability and the power-law statistic from the time of stubbornness does not show particular discrepancies depending on the considered model.

7.4 Noise for opinion formation

As said at the beginning of the chapter, it is possible to consider the presence of a "social temperature"defined as the possibility that an individual does

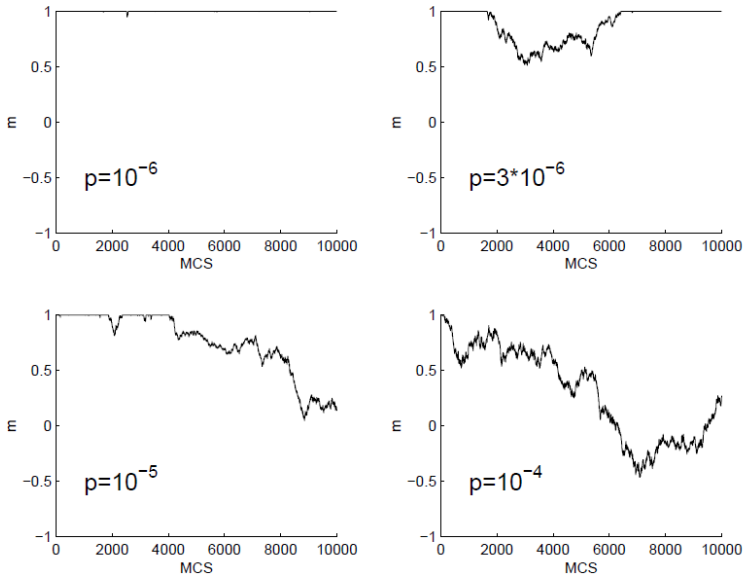

Figure 7.8: Magnetization evolution for a chain with $N = 1000$, considering SM ($USDF$), with noise. For $p < 3 \cdot 10^{-6}$ the system is able to maintain the equilibrium configuration. Instead, for lower values of p, it drifts away from it. Source [27].

not follow the dynamical rule with probability p. In this case, in the original paper, it was found that for $p > 10^{-6}$ the representative Ising chain is not able to reach equilibrium and has a magnetization that fluctuates around $m = 0$, as shown in fig. 7.8.

How can we reproduce such "social temperature" for the HSM? A possibility could be to consider a $T \neq 0$ model. In our case, we simply rewrite the Lebowitz algorithm considering the transition probabilities for $T \neq 0$. The critical temperature determines the transition from an ordered to a disordered chain and therefore we can think that for $T < T_c$ dictatorship can be reached, instead for $T > T_c$ the chain will fluctuate without reaching a unanimous decision. It must be noted that, considering the thermodynamical limit ($L \longrightarrow \infty$), the second neighbours Ising model has been found to have $T_c = 0$ [32]. Therefore, dictatorship seems to be a rather unrealistic equilibrium condition for a society with a large population, modelled with a 1D second-neighbours Ising model, even with a tiny presence of "social temperature". Our model suggests a quite philosophical conclusion: a dic-

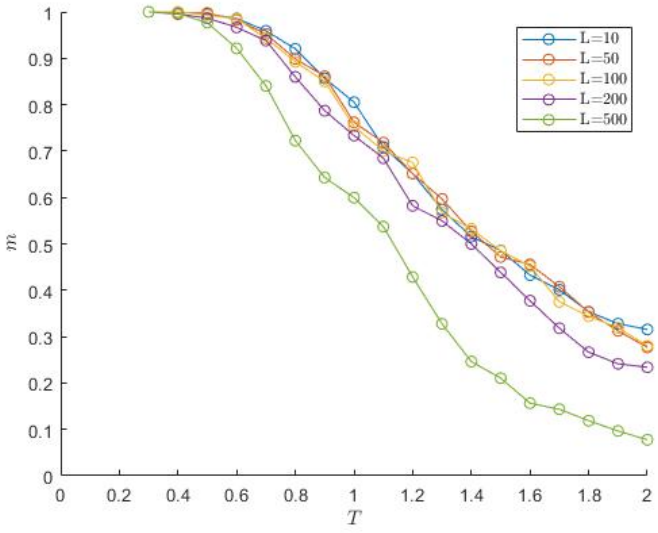

Figure 7.9: Mean "opinion"function of temperature, obtained from simulations over chains with different sizes $L = 10; 50; 100; 200; 500$. It is possible to notice a trend in the critical temperature: it decreases while increasing the system size, indicating that the thermodynamical phase transition is only a finite size scaling consequence.

tatorship has not long life if in the society there's even just one individual that is able to think by him/her-self, change opinion and transmit it to other peoples. Sooner or later, the interaction with individuals will make this seed grow until an avalanche will be created which will overthrow the dictatorship.

Let us come back to our Ising system. The previous conclusion is valid only in the thermodynamical limit. If one considers a finite system, as we do with our simulations, T_c moves away from 0, as one can observe in fig. 7.9. Here the mean "opinion"over 50 chains is derived function of the system temperature. We can observe the finite-size system showing the spontaneous formation of an overall "opinion"below a certain temperature which seems to depend on the system size.

We now focus on what happens in terms of time of stubbornness τ. In the original paper, the power-law was found to drift away from its behaviour at $T = 0$ for the SM ($USDF$) in presence of noise p, as shown in fig. 7.10. This

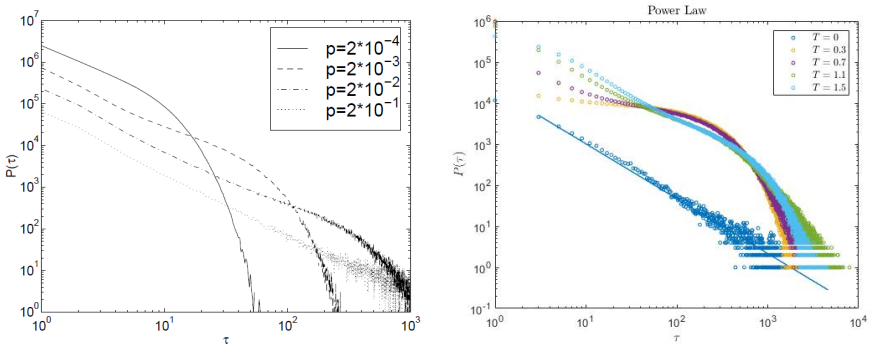

Figure 7.10: Modification of the power-law in presence of noise. For $\tau > \tau^*$ we have an exponential behaviour. For $\tau < \tau^*$ a power-law. In the left panel, the SM (*USDF*), source [27]. In the right panel, the HSM.

behaviour is also observed for the SM (*DKDW*).
In particular, there is a value $\tau^*(p)$ for which in the range $\tau > \tau^*$, $P(\tau)$ has an exponential behaviour with τ. Instead in the range $\tau < \tau^*$ the power-law is still confirmed. The position of τ^* tends to shift towards infinite in case $n \longrightarrow 1$. With HSM something similar still happens. Instead of increasing the noise, we increase the temperature and the $P(\tau)$ changes in the same way. This analogy sets a further argument in favour of the analogy between social temperature p and the actual temperature of the Lebowitz algorithm.

7.5 Further implementations and final remarks

Thus far, the HSM has been developed and compared to the known SM. Since it has a Hamiltonian, we can perform Monte Carlo simulations and derive conclusions over its transition towards equilibrium. For completeness, ideas for future implementations that did not found space for further investigation in this work are now presented:

- Mono-dimensional Ising systems were only considered. Instead, also bi-dimensional (or generally multidimensional systems) can give interest-

ing results. Several studies have been published on the bi-dimensional Sznajd Model, with an appropriate extension of the dynamical rule. Also, the Lebowitz algorithm could be adapted for this dimensionality upgrade. In particular, since it must be a second-neighbours model, we will have an increase of the number of ΔE deriving from a spin-flip inversion and consequently an increase in the number of classes involved in the algorithm. A possibility is to consider as second neighbours all the spins that touch the first neighbours. In this case, each spin will be interacting with 12 neighbours, in which 4 of them will have a double interaction with the central spin and the remaining 8 a single interaction. This model will require a 34 class Lebowitz algorithm. An alternative, instead, comes from considering as second neighbours the nearest in terms of distance, i.e. the ones on the vertex of the 3×3 square surrounding the considered spin. In this case, the interacting spins will be 8. In this case, an 18 class Lebowitz algorithm would be required.

- Inside our model, we can consider the presence of "stubborn"people who could be reluctant to change opinion. They cannot be selected in the selection step (or have transition probability $w = 0$), resembling what we have defined as defects in the previous chapter.

What seen in this chapter is one of the potential applications of the Ising Model. For sure, opinion formation in society is a rather complex topic and cannot be entirely described by such a simple model. However, if we focus on the essential characteristics of a society (interaction between individuals, exchange of opinions, presence of "social temperature", ...) and we implement them in the algorithm, good results can be derived.
Within this chapter, we explore the similarity between the Lebowitz algorithm and the Sznajd dynamics. This allowed us to derive a $T = 0$ second neighbour model that is able to reproduce the same exit probabilities and power-law obtained by the Sznajd model (in the case $p = 0.5$, *if you Do not Know what to do, just Do Whatever*) and on which we can perform Monte Carlo simulations. Therefore, we think that this approach can be considered a valuable alternative describing the formation and motion towards equilibrium.
Now we present a final remark: since the Lebowitz algorithm does not consider "wasted steps", it reduces heavily the computational time required to

reach equilibrium. if compared to the Sznajd model. This could allow faster simulations or extend the investigation over larger systems.

Chapter 8

Conclusions

We now recall some of the most important results derived within this work.

8.1 Lebowitz vs. Metropolis

We have demonstrated the efficacy of the Lebowitz algorithm, able to reproduce the same results deriving from the Metropolis approach and allowing a saving in the computational time due to the absence of rejected steps. In particular, the Lebowitz algorithm is appropriate to describe all the critical phenomena (thermodynamical and dynamical), allowing to derive their critical temperature: 2.27 ± 0.01 for the thermodynamical case; $0.798 \cdot T_c$ for the dynamical case, for the particular choices of $H_0 = 0.3$ and $P = 258$.

8.2 System with defects with Lebowitz algorithm

Here we have presented a different approach to the problem of modeling defects in magnetic materials. We have considered defects as frozen spins in the structure, which allows us to reproduce the same results of the Random-

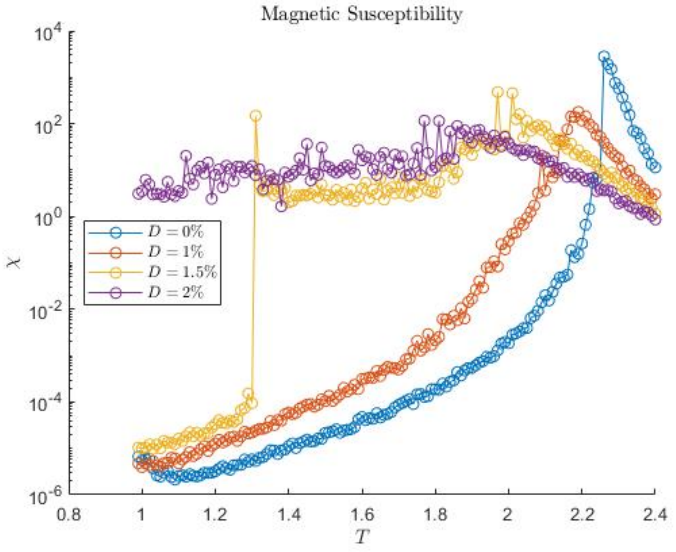

Figure 8.1: Static magnetic susceptibility for a lattice with lateral size $L = 128$ with increasing percentage of defects.

Bond Ising Model. In particular, this new approach reveals the presence of spin-glass phase transition at a specific fraction of defects, as can be seen in fig. 8.1 by the analysis of the static magnetic susceptibility. Indeed, the broadening of the peak below T_c and the discrepancy in the behaviour for $T \to 0$ are key characteristics of the spin-glass phase.

Moreover, the experimental Barkhausen noise statistic is confirmed also by the considered approach, supporting the idea of defects in the structure as the main cause of the Barkhausen noise (fig. 8.2). In particular, it was found a temperature dependency, milder in the case of positive jumps. Another observation regards the difference between the near and the out of equilibrium power-law exponents. For all the investigated temperatures, the negative Barkhausen jumps showed a decrease in the exponent while considering far from equilibrium condition. On the contrary, for positive Barkhausen jumps, in the far from equilibrium condition, the exponents are higher. Further investigation is required.

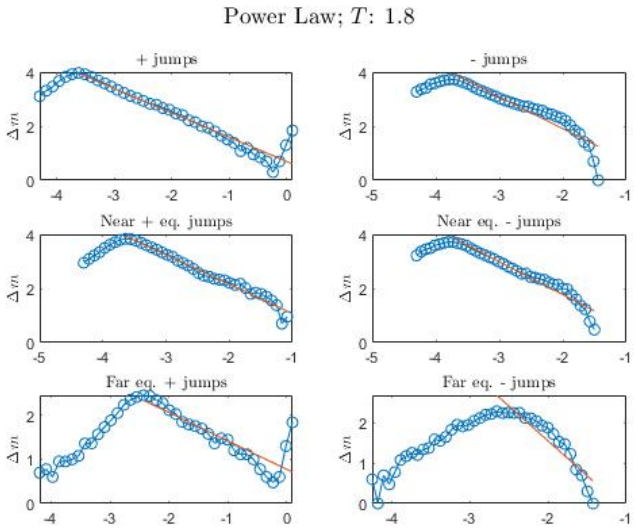

Figure 8.2: In the figure, the $P(\Delta m)$ calculated for positive ("+") and negative jumps ("-") far from equilibrium, near equilibrium and total (in the top row). The scale is logarithmic as to reduce the power law in a linear regression. Parameters of the simulation: field period $P = 5 \cdot 10^5$; field amplitude $H_0 = 1$; fraction of defects $D = 3\%$; Number of replicas: 8; Number of hysteresis cycles: 4; Lateral Size: $L = 200$.

8.3 Modification of the DPT due to defects

The introduction of few defects in the structure produces a modification in the DPT phenomenon. The system magnetization is able to follow more precisely the variation of the external field, showing also a more deterministic behaviour with respect to the case with no defects, as shown in fig. 8.3. The more deterministic behaviour is caused by just few defects in the structure, even lower then 1%. This opens new possible applications for magnetic materials with a small percentage of defects, able to induce ferromagnetic system to faster time response but still maintaining the ferromagnetic nature.

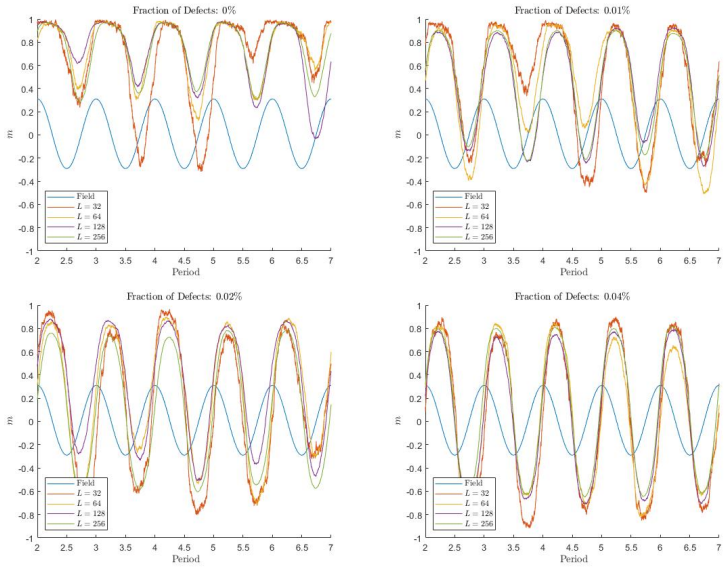

Figure 8.3: Magnetization cycles in presence of an oscillating field for lattices with lateral size $L = 32; 64; 128; 256$. Other simulation values: $P = 250$, $T = 0.8 \cdot T_c$, $H_0 = 0.3$, $H_b = 0.01$.

8.4 Application to opinion formation

The Lebowitz algorithm was adapted to reproduce the behaviour of the Sznajd model, describing opinion formation in society. Very similar exit probabilities were found (as represented in fig. 8.4), as the same power law related to the time of stubbornness.

A proper Monte Carlo simulation can be considered with the developed approach, since a Hamiltonian has been structured. Moreover, by setting the temperature $T > 0$ we are able to simulate the effect of indecision in the society. $T > 0$ has been found to be analogous to the concept of noise in the Sznajd model. The main result is that no dictatorship can develop in a society in which individuals can change opinions by their own and influence others.

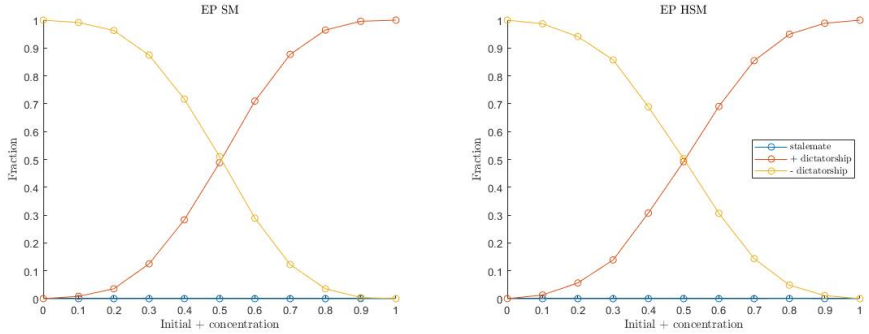

Figure 8.4: Exit Probabilities after 2000 *MCSS* considering Sznajd model (DKDW) in the left panel and the Hamiltonian Sznajd model with Lebowitz algorithm in the right panel. Each line correspond to one of the possible equilibrium configuration: dictatorship positive red line, dictatorship negative yellow line, stalemate blue line.

8.5 Future works

As future development, we suggest continuing by further deepen the investigation over the finite-size scaling properties of the system in presence of defects, as a complete understanding of the phenomenon still lacks. Moreover, it could be studied an optimal configuration of defects inside the structure as to provide a more deterministic behaviour of the magnetic system but still retaining the same ferromagnetic nature, even when the lattice has a smaller size.
The Lebowitz algorithm could be adapted to follow not only time-varying parameters but also space-varying parameters. As a possible example, one can consider applying a uniform magnetic field over just half of the system or the central part of the system and study how the system behaves in these conditions. From the point of view of the algorithm, it would double the number of classes: from 10 to 20, considering 10 classes for the part of the system without a field and the other 10 for the part with a field. This implementation could be considered to reproduce the behaviour of a magnetic system over which a laser (an electromagnetic wave source) is applied.

Bibliography

[1] Alfred Bortz, M. Kalos, and Joel Lebowitz. "A New Algorithm for Monte Carlo Simulation of King Spin Systems". In: *J. Comput. Phys.* 17 (Jan. 1975), p. 10. DOI: 10.1016/0021-9991(75)90060-1.

[2] Roy Glauber. "Time-Dependent Statistics of the Ising Model". In: *Journal of Mathematical Physics* 4 (Feb. 1963), pp. 294–307. DOI: 10.1063/1.1703954.

[3] Stephen Blundell and David Thouless. "Magnetism in Condensed Matter". In: *American Journal of Physics - AMER J PHYS* 71 (Jan. 2003), pp. 94–95. DOI: 10.1119/1.1522704.

[4] Roberto Piazza. *Statistical Physics. A Prelude and Fugue for Engineers*. Springer International Publishing, 2017. ISBN: 978-3-319-44536-6.

[5] Pierre Weiss. "A New Algorithm for Monte Carlo Simulation of King Spin Systems". In: *Compte Rendus (in French)* 143 (1906), pp. 1136–1149.

[6] Heinrich Barkhausen. "Zwei mit Hilfe der neuen Verstärker entdeckte Erscheinungen". In: *Physik Z.* 20 (1919), pp. 401–403.

[7] The free Dictionary. *Barkhausen Effect*. 1999. URL: https://encyclopedia2.thefreedictionary.com/Barkhausen+Effect (visited on 09/07/2021).

[8] Ernst Ising. "Beitrag zur Theorie des Ferromagnetismus". In: *Zeitschrift für Physik* 31 (Feb. 1925), pp. 253–258. DOI: 10.1007/BF02980577.

[9] Lars Onsager. "Crystal Statistics. I. A Two-Dimensional Model with an Order-Disorder Transition". In: *prv* 65 (Jan. 1944), pp. 117–. DOI: 10.1103/PhysRev.65.117.

[10] M. Newman and Gerard Barkema. "Monte Carlo Methods in Statistical Physics". In: (Jan. 1999).

[11] H. Stanley and H. Eugene. "Introduction to Phase Transitions and Critical Phenomena". In: *Physics Today* 26 (Jan. 1973). DOI: 10.1063/1.3127900.

[12] Alan M. Ferrenberg and D. P. Landau. "Critical behavior of the three-dimensional Ising model: A high-resolution Monte Carlo study". In: *Phys. Rev. B* 44 (10 Sept. 1991), pp. 5081–5091. DOI: 10.1103/PhysRevB.44.5081. URL: https://link.aps.org/doi/10.1103/PhysRevB.44.5081.

[13] Tânia Tomé and Mário de Oliveira. "Dynamic phase transition in the kinetic Ising model under a time-dependent oscillating field". In: *Physical review. A* 41 (May 1990), pp. 4251–4254. DOI: 10.1103/PhysRevA.41.4251.

[14] Gyorgy Korniss, Per Arne Rikvold, and MA Novotny. "Absence of first-order transition and tricritical point in the dynamic phase diagram of a spatially extended bistable system in an oscillating field". In: *Physical Review E* 66 (Nov. 2002), p. 056127. DOI: 10.1103/PhysRevE.66.056127.

[15] Sourav Chattopadhyay and S. Santra. "Kinetic Ising model under sinusoidal oscillating external magnetic field: hysteresis and dynamic phase transition". In: *The European Physical Journal B* 94 (Mar. 2021). DOI: 10.1140/epjb/s10051-021-00081-3.

[16] Hyunhang Park and Michel Pleimling. "Dynamic phase transition in the three-dimensional kinetic Ising model in an oscillating field". In: *Physical Review E* 87 (Mar. 2013). DOI: 10.1103/PhysRevE.87.032145.

[17] Muktish Acharyya and Bikas Chakrabarti. "Response of Ising systems to oscillating and pulsed fields: Hysteresis, ac, and pulse susceptibility". In: *Physical review. B, Condensed matter* 52 (Oct. 1995), pp. 6550–6568. DOI: 10.1103/PhysRevB.52.6550.

[18] Per Arne Rikvold et al. "Metastable lifetimes in a kinetic Ising model: Dependence on field and system size". In: *Physical review. E, Statistical physics, plasmas, fluids, and related interdisciplinary topics* 49 (Jan. 1994). DOI: 10.1103/PhysRevE.49.5080.

[19] Rodolfo Gallardo et al. “Analytical derivation of critical exponents of the dynamic phase transition in the mean-field approximation”. In: *Physical Review E* 86 (Nov. 2012), p. 051101. DOI: 10.1103/PhysRevE.86.051101.

[20] Patricia Riego, Paolo Vavassori, and A. Berger. “Metamagnetic Anomalies near Dynamic Phase Transitions”. In: *Physical Review Letters* 118 (Mar. 2017). DOI: 10.1103/PhysRevLett.118.117202.

[21] G. Buendia and Per Arne Rikvold. “Fluctuations in a model ferromagnetic film driven by a slowly oscillating field with a constant bias”. In: *Physical Review B* 96 (July 2017). DOI: 10.1103/PhysRevB.96.134306.

[22] S. Sides, Per Arne Rikvold, and MA Novotny. “Kinetic Ising model in an oscillating field: Avrami theory for the hysteretic response and finite-size scaling for the dynamic phase transition”. In: *Physical Review E* 59 (Sept. 1998). DOI: 10.1103/PhysRevE.59.2710.

[23] A. Labarta et al. “Phase transition in the Ising ferromagnetic model with fixed spins”. In: *Physical review. B, Condensed matter* 38 (Aug. 1988). DOI: 10.1103/PhysRevB.38.500.

[24] Maurizio Zani and Ezio Puppin. “Negative Barkhausen jumps in amorphous ribbons of Fe63B14Si8Ni15”. In: *Journal of Applied Physics* 94 (Nov. 2003), p. 5901. DOI: 10.1063/1.1616994.

[25] Ezio Puppin. “Statistical Properties of Barkhausen Noise in Thin Fe Films”. In: *Physical review letters* 84 (June 2000), pp. 5415–8. DOI: 10.1103/PhysRevLett.84.5415.

[26] Filippo Perani. “Cluster Monte-Carlo for Random-Bond Ising Model”. Master thesis. Politecnico di Milano, 2020.

[27] Katarzyna Sznajd-Weron and Jozef Sznajd. “Opinion Evolution in Closed Community”. In: *International Journal of Modern Physics C* 11 (Jan. 2001). DOI: 10.1142/S0129183100000936.

[28] D. Stauffer, Adriano Sousa, and S. Oliveira. “Generalization to Square Lattice of Sznajd Sociophysics Model”. In: *International Journal of Modern Physics C - IJMPC* 11 (Sept. 2000), pp. 1239–1245. DOI: 10.1142/S012918310000105X.

[29] Dietrich Stauffer. "Better being third than second in a search for a majority opinion". In: *Advances in Complex Systems (ACS)* 05 (Mar. 2002), pp. 97–100. DOI: 10.1142/S0219525902000511.

[30] Americo Bernardes, D. Stauffer, and János Kertész. "Election results and the Sznajd model on Barabasi network". In: *Physics of Condensed Matter* 25 (Jan. 2002), pp. 123–127. DOI: 10.1140/e10051-002-0013-y.

[31] Katarzyna Sznajd-Weron, Józef Sznajd, and Tomasz Weron. "A review on the Sznajd model — 20 years after". In: *Physica A: Statistical Mechanics and its Applications* 565 (Mar. 2021), p. 125537. DOI: 10.1016/j.physa.2020.125537.

[32] Kassan-ogly A. "One-dimensional Ising model with next-nearest-neighbour interaction in magnetic field". In: *Phase Transitions: A Multinational Journal* 74 (Dec. 2001), pp. 353–365. DOI: 10.1080/01411590108227581.